International Committee for Future Accelerators

Sponsored by the Particles and Fields Commission of IUPAP

Beam Dynamics Newsletter

No. 41

Issue Editor:
I. Hofmann

Editor in Chief:
W. Chou

December 2006

Contents

1 Foreword

1.1 From the Chair

Weiren Chou, Fermilab
mail to: chou@fnal.gov

The Internet is revolutionizing every corner of our life. One corner that is of particular interest and importance to us is scientific publishing. The traditional way of publishing, namely, readers purchasing printed books or subscribing to journals from book stores or online, is gradually being replaced by e-publishing. A new development for the latter is the Open Access (OA) Publishing. The name is self explanatory. There was a recent report titled "*Report of the task force on open access publishing in particle physics*" (http://doc.cern.ch//archive/electronic/other/generic/public/cer-002632247.pdf) According to this report, six major journals in our field (*Physical Review D, PRST-AB, JHEP, JCAP, JINST* and *European Physical Journal C*) are OA-ready. During the period 2000-2005, these journals covered about 60% of the total number of papers published by all the journals in particle physics (theoretical, experimental and instrumentation). In my view, OA represents the future of scientific publishing. This initiative is still at an early stage and, understandably, a number of publishers are hesitant to join at this moment before they learn more about how the transition from traditional publishing to OA publishing will be embraced by the authors, readers and funding agencies. A viable financing system must be established in order to keep the publishing institutions functioning. This, however, does not suggest that one should wait. In fact, one of the major journals in our field, *Physical Review Special Topics – Accelerators and Beams (PRST-AB)* is a pioneer in OA publishing. Instead of subscription, all PRST-AB articles can be viewed and downloaded from the web free of charge. Financial support comes from several institutions. The ICFA will discuss this matter at its meeting in February in Beijing. I hope our community will play a leadership role to help speed the transition.

The first *International Accelerator School for Linear Colliders* held last May in Sokendai, Japan was a great success. (http://www.linearcollider.org/school/) Based on the demands from the community, the ILC GDE, ILCSC and ICFA Beam Dynamics Panel decided to organize a second school in Europe. It will take place from October 1st to 10th, 2007 in Erice, Italy. Details will appear in the next issue of the newsletter.

The Editor of this issue is Prof. Ingo Hofmann, a panel member from the GSI, Germany. He is an internationally well-known expert in the study of collective effects and has collected a number of well-written articles in the theme section of *Recent Work on Benchmarking of Simulation Codes*. I'd like to express my gratitude to Ingo for this well-organized and high quality Newsletter.

1.2 From the Editor

Ingo Hofmann, GSI, 64291 Darmstadt, Germany
mail to i.hofmann@gsi.de

The special theme of this issue is dedicated to the subject of **simulation code "benchmarking"**, with emphasis on beam dynamics of high intensity or high phase space density beams. This topic has been of concern to the ICFA beam dynamics panel for several years. The panel chairman and several panel members have been stimulating work on this topic. In a number of ICFA workshops and mini-workshops there were presentations and working groups, where progress was presented and discussed. The driving force for the excellent progress achieved in this field has obviously been due to the existence of the large accelerator projects, under construction or in planning stages, where high intensity or high phase space density is of importance.

Therefore it seemed appropriate to use an ICFA Beam Dynamics Newsletter as an opportunity to ask specialists in the field to present the status of their work. The presented work is far from comprehensive or complete. It clearly calls for continuation and coordination using new experimental data and projects.

2 International Linear Collider (ILC)

2.1 Beam Position Monitoring with Cavity Higher Order Modes in the Superconducting Linac FLASH*

Nicoleta Baboi[1], Stephen Molloy[2], Nathan Eddy[3], Josef Frisch[2], Linda Hendrickson[2], Olaf Hensler[1], Doug McCormick[2], Justin May[2], Sergei Nagaitsev[3], Olivier Napoly[4], Rita Paparella[4], Lyudvig Petrosyan[1], Luciano Piccolli[3], Ron Rechenmacher[3], Marc Ross[2], Claire Simon[4], Tonee Smith[2], Ken Watanabe[5] and Manfred Wendt[3]

[1]DESY, MDI Group, Notkestr. 85, 22607 Hamburg, Germany, [2]SLAC, Menlo Park, CA, U.S.A., [3]FNAL, Batavia, IL, U.S.A., [4]CEA, DSM/DAPNIA, Gif-sur-Yvette, France, [5]KEK, Tsukuba, Japan

mail to: nicoleta.baboi@desy.de

2.1.1 Introduction

FLASH (Free Electron Laser in Hamburg§) is a user facility for a high intensity VUV-light source [1]. The radiation wavelength is tunable in the range from about 40 to

*Work supported in part by the US Department of Energy Contract DE-AC02-76SF00515 and by the European Community FP6 "Structuring the European Research Area" programme (CARE, contract number RII3-CT-2003-506395)

§The accelerator was known until recently as the VUV-FEL (VUV Free Electron Laser) and TTF2 (TESLA Test Facility – Phase 2)

13 nm by changing the electron beam energy from 450 to 700 MeV. The accelerator is also a test facility for the European XFEL (X-ray Free Electron Laser) to be built in Hamburg [2] and the project study ILC (International Linear Collider) [3]. The superconducting TESLA technology is tested at this facility, together with other accelerator components.

2.1.1.1 The TESLA cavity

The TESLA cavities are used for acceleration in FLASH and the XFEL. The ILC will have similar accelerating structures. The TESLA cavities are superconducting 9-cell 1 m long structures (see Figure 1). A 1.3 GHz wave is input through a power coupler. Two HOM (Higher Order Modes) couplers extract energy from the resonant fields excited by the electron beams [4].

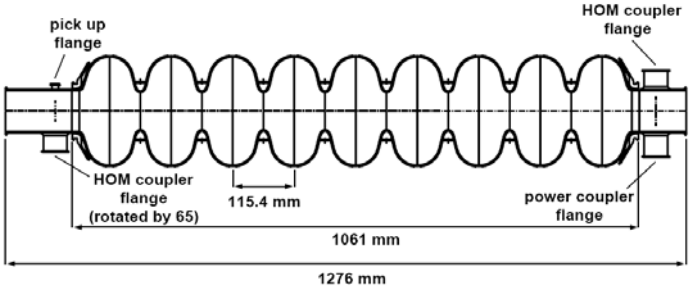

Figure 1: The TESLA cavity.

The HOMs are fields excited by the beam, which act back on the beam and can degrade its quality, e.g. the transverse emittance. Therefore it is important to damp them with the HOM couplers. Also, the amplitude of the excited transverse field increases with the beam offset from the cavity axis, therefore centering the beam reduces them.

Eight cavities are installed in a cryo-module and cooled at about 2 K. At the moment 5 cryo-modules have been installed at FLASH.

2.1.1.2 Dipole modes as position monitors

The HOM spectrum of a cavity contains passbands, each with 9 modes with similar field pattern [5]. Out of these, the dipole passbands are of highest concern since they are the main cause of multi-bunch transverse emittance growth. These are fields with two nodes on the azimuthal direction. Their amplitude is proportional to the offset of the exciting beam from the cavity axis. The linear dependence of the dipole modes on the beam offset makes them suitable to be used as BPMs (beam position monitors), similarly to cavity BPMs. Cavity monitors have a potential for very low resolution in comparison to other BPM types [6].

However, there are significant differences of the dipole modes in the TESLA cavities and the cavity BPMs. Each mode has two orthogonal directions, or two polarizations. In the BPM case these are horizontal and vertical, fixed by the pickup position. A pure horizontal or vertical beam offset will cause only one of these polarizations to be excited. For the accelerating cavities the field directions are rotated so that a pure horizontal offset will excite both polarizations. Another difference to the cavity BPMs consists in the split in the frequencies of the two polarizations. Moreover

the polarization directions and frequencies are different from cavity to cavity. A more complicated calibration method is therefore necessary.

2.1.2 Preliminary Studies

Figure 2 shows the setup for studies on the use of the dipole modes as BPMs. The single-bunch beam is deflected to various transverse positions and angles in an accelerating module containing 8 cavities by two pairs of magnetic steerers. A dipole mode is chosen from the spectrum for a given cavity and measured with a spectrum analyzer. One conventional BPM at each side of the module is used to measure the beam position.

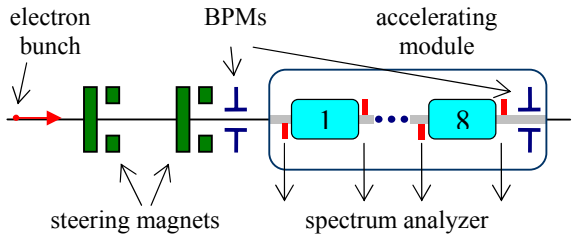

Figure 2: Measurement setup.

A mode in the first dipole passband of the first cavity of the first FLASH cryo-module is shown in Figure 3. One can distinguish the two polarizations with different frequencies. The first polarization has been found to respond to vertical beam movement, while the second is rather a "horizontal" mode.

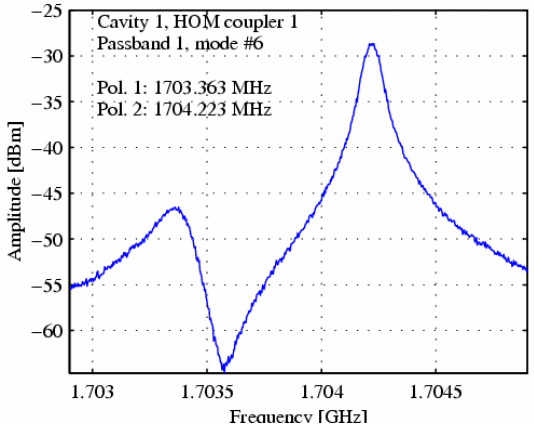

Figure 3: Dipole mode.

Horizontal and vertical position and angle scans have been made alternatively. The first polarization has been used for vertical scans, and the second for horizontal ones. Figure 4 shows a scan in each of the four transverse dimensions. The linear response of the modes amplitude to beam movement can clearly be seen. The deviation from linearity corresponds to beam jitter at the time of the measurement.

With alternative scans we could find the axis of the cavity, i.e. the beam trajectory for which a minimum in this dipole mode amplitude is obtained. Please note that the axis of other modes may be different, as already previously observed [7].

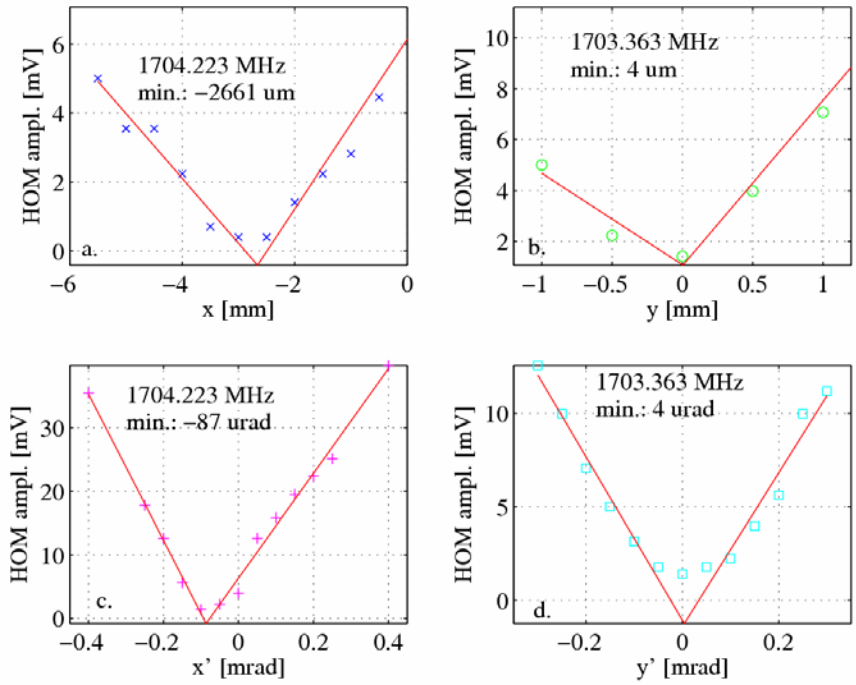

Figure 4: Scan of beam position in the 4D space.

2.1.3 The HOM-BPMs

2.1.3.1 The HOM electronics

Electronics has been designed and built for processing of one dipole mode from the HOM spectrum, similar to BPM-electronics. The principle of the electronics is shown in Figure 5 [8]. A bandpass filter selects from the spectrum a dipole mode at about 1.7 GHz. The signal is down-converted to about 20 MHz by mixing with a 1.68 GHz reference signal. The signal is then digitized.

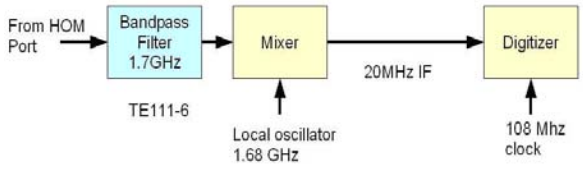

Figure 5: Principle of the HOM electronics.

Electronics modules have been installed at both couplers of all 40 cavities at FLASH. An example of a typical output signal from this electronics is shown in Figure 6. One can see the beating of the frequencies of the two polarizations of the dipole mode. For the first part of the signal the digitizers are saturated, due to a large beam offset.

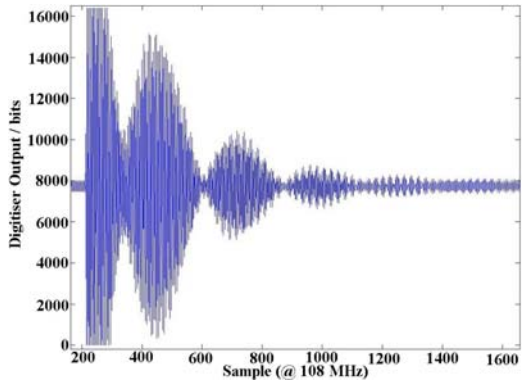

Figure 6: Output example of the HOM-BPM electronics.

This electronics should allow for the fast, simultaneous data collection from all HOM couplers. Moreover, it also provides information about the signal-phase, which allows us to distinguish between negative and positive beam offsets, and also to get information about the beam angle.

2.1.3.2 Calibration

In order to calibrate the HOM signals into beam position, the beam has been steered to various offsets and angles with a similar setup as the one in Figure 2. The HOMs have been recorded for each scan step, together with the setting of the steerers and the reading of the BPMs. Care has been taken to make scans large enough to include the axis of the mode.

As mentioned earlier, the calibration of the HOM-BPMs is somewhat more complicated than in the case of cavity BPMs. A method based on Singular Value Decomposition (SVD) is used. This method allow for analysis of large data sets, without the need of a model for the accelerator. An orthonormal basis for the data from one 4D scan is found with the SVD. The amplitudes of the strongest basis modes are used. The cavity modes are then combinations of these basis modes. Linear regression correlates then the modes to the beam position at the cavity location as predicted by the conventional BPMs [8,9,10].

First estimations of the resolution achieved with the new calibration in a few cavities showed values of 5-10 μm rms [11]. Figure 7 shows a histogram of the residual between the position reading at one cavity and the prediction of the beam position at that cavity from the position measured in the two adjacent cavities. A resolution of 5 μm is obtained in this case. Theoretically, a much better resolution is achievable. A resolution of 1.5 μm has been previously observed [10]. Work is going on in order to improve the electronics and improve the calibration.

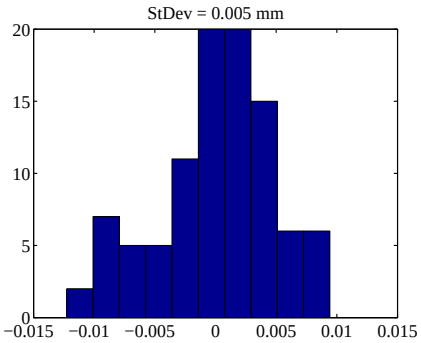

Figure 7: Histogram of the residual (in mm) of the beam position measured in one cavity against the prediction from two adjacent cavities.

2.1.3.3 Integration of the HOM-BPM signals in the control system

The calibration matrices have been used in the past for off-line beam position measurement tests. Currently work is being made to integrate the beam position measurement into the control system of FLASH: the Distributed Object Oriented Control System (DOOCS) [12]. A new server has been written for this purpose. The consistency of this server will be checked in 2007.

2.1.4 Summary and Outlook

The proof-of-principle for the use of HOMs as BPMs has been made. Electronics has been installed for monitoring one dipole mode in each of the 40 cavities at FLASH. Their calibration and the integration in the accelerator control system are under going. A resolution of 5-10 μm rms has been observed and 1 μm is thought possible through improvement of the electronics. After commissioning of the single-bunch calibration, multi-bunch signals will be studied.

Apart for measuring the beam position, the HOM-BPMs have been used to measure the relative position of the 8 cavities inside the cryo-module [9,10]. Also, by minimizing the raw dipole signals one can reduce the HOMs and therefore their effect on the beam.

The installation of such HOM-BPMs at cavities in the ILC may relax the requirements of the conventional BPMs in the main linac or even reduce their number and cost. Also it can help to control better the emittance growth.

2.1.5 References

1. V. Ayvazyan et al., Eur. Phys. J. D37, 297 (2006); http://flash.desy.de/
2. http://xfel.desy.de/tdr/index_eng.html
3. http://www.linearcollider.org/cms/
4. J. Sekutowicz, DESY-TESLA-94-07, 1994.
5. R. Wanzenberg, TESLA 2001-33, 2001.
6. S. Walston et al., EPAC 2006.
7. N. Baboi et al., LINAC 2004, Lübeck, Germany.
8. J. Frisch et al, BIW 2006, Chicago, IL, U.S.A.
9. S. Molloy et al., to be published in Phys. Rev. ST-AB, 2006.

10. J. Frisch, et al., EPAC 2006, Edinburgh, UK.
11. S. Molloy et al., LINAC 2006, Knoxville, TN, U.S.A.
12. http://tesla.desy.de/doocs/doocs.html.

3 Recent Work on Benchmarking of Simulation Codes

3.1 Remarks on the Challenge of Simulation Code "Benchmarking"

Ingo Hofmann, GSI, Darmstadt, Germany
mail to: i.hofmann@gsi.de

3.1.1 Introduction

The need for developing advanced tools of simulation in beam dynamics has been increasingly emphasized in view of the new frontiers in high intensity and high phase space density, in combination with enhanced needs to store such beams under the conditions of tolerable beam loss and beam quality degradation. Since the late 1990's several workshops have addressed the matter of how reliable code predictions are, in particular in connection with the US Spallation Neutron Source; followed by the Snowmass Workshop on the Future of High Energy Physics in 2001; three ICFA workshops on high intensity and high phase space density beams in 2002 (Fermilab), 2004 (Bensheim) and 2006 (Tsukuba); in connection with electron clouds a series of ECLOUD workshops since 2002; an ICFA workshop on halos in 2003 (Long Island) and an ICFA mini-workshop on space charge issues also in 2003 (Oxford).

Since simulation codes have become important tools in predicting performance limitations and in verifying the design of several new projects, the need for verification of these codes and their validation by real experiments became an issue. The present compilation of such efforts – far from being comprehensive or even complete - tries to reflect the status of such a code "benchmarking", to use a term adopted by a number of authors in the beam simulation community. The challenge to the community is to define – and agree upon – a set of benchmarks, which helps to obtain an increasing confidence in the way simulation codes are expected to describe beams in the real world.

3.1.2 General Features

Simulation and experiments are complementary approaches to study the behaviour of beams. Both suffer from their own limitations:

- Simulations are usually based on imperfect models missing part of the real behaviour; but they give high flexibility, where particular interactions (particle-particle, particle-mean field, beam-beam, beam-wall, beam-rest gas, beam-electron clouds etc.) or boundary or initial conditions can be turned on/off and parameters can be varied. This allows identification of phenomena with particular physical effects. Diagnostics is "perfect" in the sense that unconstrained information can be extracted at any time.

- Experiments have an underlying "perfect" model, but the complexity of interactions in accelerators makes it often impossible to disentangle the main sources of influence, and parameters can be varied only over a limited range. Diagnostics is usually quite imperfect and limited in resolution.

This complementary situation suggests that the process of "benchmarking" cannot be one of simply verifying codes through experiments (or vice versa). The real task is one where both, simulation and experiment, are developed hand in hand. Progress in simulation requires the definition of new or refined experiments or measurements and vice versa. Ideally experimentalists should be sufficiently familiar with developments on the theoretical/numerical side and theorist should participate in experiments and understand their constraints.

3.1.3 Steps

A more precise description of the "benchmarking" task requires breaking it up into a number of steps. The first "trivial" step is that of "debugging", making sure the code does what it is written for. Thereafter we may distinguish between three steps, which should be carried out in sequence[1]:

- **Verification:** The task is to prove that a computerized model of a beam in a well-defined environment agrees with a theoretical model, for which assured analytical solutions exist. Hence verification is a quite precisely defined task and a test within the framework of the underlying model, and not under most general conditions as would occur in real beams. The problems here are largely of mathematical or numerical nature due to algorithms, time steps, grids, and convergence problems and similar.
- **Comparison:** A comparison with other (already tested) codes gives enhanced assurance. Often codes are not too rigorously comparable, especially if the underlying concepts differ, and one needs to learn where discrepancies might stem from.
- **Validation:** Comparing code results with experimental data is crucial, but limited. A realistic goal cannot be to validate a code as such, which is practically impossible. Validation is always more vague – due to the limited representation of real beams and environments - and limited to a particular problem and its modelling. Therefore validation is more a (possibly open ended) process and not a unique task.

3.1.4 Examples of Application

As illustrated above code "benchmarking" cannot be a unique procedure for whatever accelerator application. Given the large complexity of real world accelerators in terms of what types of beams, time scales, boundary conditions, electromagnetic fields, rest gas interactions etc., and the necessary model simplifications, such "benchmarking" efforts will have to be specific for different types of accelerators and applications.

---

[1] M. Furman and J. Wei have interchanged the role of "verification" and "validation".

The following papers give a good cross section of efforts that have been taken under quite different boundary conditions. The first three papers deal with linac and transport codes, followed by ring codes and a concluding with a summary of Jie Wei from HB2006, which gives a survey ... see also Chin's report (Section 5.1).

3.2 Linac Code Benchmarking for the HIPPI project

A. Franchi, W. Bayer, G. Franchetti, L. Groening, I. Hofmann, A. Orzhekhovskaya, S. Yaramyshev, X. Yin , GSI, Darmstadt, Germany
A. Sauer, R. Tiede, G. Clemente, IAP, Frankfurt am Main, Germany
R. Duperrier, D. Uriot, CEA, Saclay, France
G. Bellodi, F. Gerigk, A. Lombardi, T. Mütze, CERN, Geneva, Switzerland

mail to: andrea.franchi@cern.ch

3.2.1 Introduction

One of the main tasks of the beam dynamics working package of the European network "High Intensity Pulsed Proton Injector" (HIPPI) is the comparison and validation of 3D linac codes in the high current regime. Several codes are available and currently run for such simulations. The Alvarez DTL section of UNILAC (five tanks, $L \approx 55$ m) is used as reference lattice, as a dedicated machine experiment will be carried out in order to measure the three phase space projections (x-x'), (y-y') and ($\delta\phi$-$\delta W/W$) at both ends of the section under various space-charge and mismatch conditions. The initial measured phase space projections will be used to generate the input particle distributions to be tracked using the codes. The final measured phase space projections will be then compared with the numerical predictions.

Different space-charge and lattice modelling may pose severe problems in understanding the source of discrepancies, when tracking simulations at high current and in presence of mismatch are run. For this reason, in preparation of the experimental validation, the code benchmarking has been divided in three steps.

1. The first is a static benchmarking of the space-charge routines: common ensembles of particles are given in input to the different space-charge solvers; the resulting space-charge electric fields are then compared with the analytical solutions against different numerical parameters and boundary conditions (for PIC codes). To investigate the effects of numerical errors on the single particle dynamics, the single particle depressed tune is inferred using the electric fields previously calculated, and is compared again with an analytical solution. Both tests require modifications in the source codes (that usually do not print out the space-charge electric field) and have been performed on codes with source code available only.
2. The second step consists of tracking simulations with a zero-current beam and a common input distribution. Scope of this test is twofold: first, the preparation of the input files for all the codes, checking carefully that they describe the same structure; second, the understanding of discrepancies arising from the different representation of physical elements implemented in the codes, especially for the RF.

3. In the last step, tracking simulations are run under the same conditions of the experiments planned for 2006/077 and the results will be compared among the codes. Here the scope is to investigate how space charge and nonlinear RF effects couple in the codes and to establish the most suitable numerical parameters to be used when simulating the experiment conditions.

This letter is organized as follow. In Sec. 1.2 the work organization is outlined, while in Sec. 1.3 the codes that we have been running are briefly described and the main features are compared. In Sec. 1.4 the main results obtained form the benchmarking of the space-charge routine as well as the comparison of tracking simulations are presented. For a detailed discussion on both the lattice modelling and the proper comparison of RMS quantities we refer to the HIPPI code benchmarking web page [1] and CARE note [2].

3.2.2 Organization

Coordinator: I. Hofmann (GSI)

- **GSI Darmstadt**
  1. Tools for benchmarking the space-charge solvers (G. Franchetti, A. Orzhekhovskaya, A. Franchi)
  2. UNILAC modelling (L. Groening, W. Barth, W. Bayer, S. Yaramyshev)
  3. run IMPACT, HALODYN and PATH (A. Franchi)
  4. run DYNAMION (S. Yaramyshev, W. Bayer)
  5. run PARMILA and TRACE-3D (X. Yin)
  6. Alvarez DTL matching (L. Groening, W. Bayer, X. Yin)
  7. collecting material and web page editing (A. Franchi)
- **IAP Frankfurt**
  1. update and run LORASR (R. Tiede. G. Clemente, J. Dietrich)
  2. run SUPERFISH for RF UNILAC modelling of (A. Sauer)
  3. run PARMILA (A. Sauer)
  4. help running TRACE-3D (A. Sauer)
- **CEA Saclay**
  1. run TOUTATIS for Poisson solver test (R. Duperier)
  2. run PARTRAN (D. Uriot)
  3. improving the UNILAC modelling (D. Uriot)
- **CERN Geneva**
  1. update and support running PATH (T. Mütze, A. Lombardi, G. Bellodi)
  2. support running IMPACT (F. Gerigk)
- **External Support**
  1. J. Qiang (LBNL): support running IMPACT
  2. J. Billen (LANL), H. Takeda : update and support running PARMILA
  3. S. Rambaldi, G. Turchetti (Bologna Univ.): update HALODYN

3.2.3 The Codes

In this section a review of the main features of the codes involved in the benchmarking is given. Particles are tracked in the 6D space, whereas the space-charge solver is 2D *r-z* or 3D depending on the code. Most of the solvers have PIC algorithm

implemented, the charge distribution being deposited onto a grid and the Poisson equation solved on the grid. The space-charge electric field at any position is then computed via interpolation. A brief description of each code follows (in alphabetic order).

- **DYNAMION** [3] is a scalar code developed in ITEP Moscow and GSI Darmstadt. The space-charge routine is a 3D particle-particle integrator with a hard-sphere cut-off, introduced to avoid artificial short-range collisions. The RF description is based on the expansion of the RF voltage, whose coefficients are computed in pre-processing (solving the Laplace equation with boundary conditions defined by the 3D DTL geometry) [5].
- **HALODYN** [5] is a parallel code developed in the University of Bologna. The space-charge routine is based on a scalar 3D PIC spectral Poisson solver (FFT with inversion of a linear system) with closed boundary conditions defined on a rectangular pipe [6]. The RF is modelled using the thin lens approximation and an expansion in terms of Bessel functions.
- **IMPACT** [7] is a parallel code developed in Los Alamos (LANL) and Berkeley (LBNL). The space-charge routine is based on a parallel 3D PIC spectral Poisson solver (Green function with convolution) with several boundary conditions (open, closed and periodic) on both rectangular and elliptical pipes. The RF description is inferred from the on-axis electric field with either a linear or a nonlinear Lorentz integrator.
- **LORASR** [8] is a scalar code with GUI developed in IAP, J.W. Goethe University, Frankfurt am Main. The space-charge routine is based on a scalar 3D PIC Poisson spectral solver (FFT with inversion of a linear system) with closed boundary conditions defined on a rectangular pipe. The RF description is inferred from the radial (on- and off-axis) electric field.
- **PARMILA** [9] is a scalar code developed in Los Alamos (LANL). The user can choose either a 2D *r-z* (SCHEFF) or a 3D (PICNIC) PIC Poisson solver with open boundary conditions. The RF is modelled making use of either the transit-time-factor (TTF) table generated by SUPERFISH or a nonlinear thin kick.
- **PARTRAN** [10] is a scalar code developed in CEA, Saclay. The space-charge routine is a 3D PIC (PICNIC [11]) Poisson solver with open boundary conditions. The RF is modelled either by importing an electro-magnetic field map (1D, 2D or 3D) or using a nonlinear thin kick.
- **PATH** [12] is a scalar code with GUI developed in CERN. The user can choose either a 2D *r-z* (SCHEFF) Poisson solver with open boundary conditions or a 3D particle-particle integrator. The RF is described either by importing a 3D electro-magnetic field map or by using a nonlinear thin kick.
- **TOUTATIS** [13] is a scalar code for RFQ developed in CEA, Saclay. The space-charge routine is a 3D PIC multi-grid Poisson solver with either open or periodic boundary conditions on an arbitrary geometry. The RF is modelled making use of a 3D electromagnetic field map.

In Table1 the main general features are listed together with an indication of the requested CPU time. The latter one has been obtained running the codes on the same Linux node and a hardware-equivalent Windows PC with the number of macro-particles indicated in the fifth column. The parallel codes have been run using one CPU only.

While the CPU time for the fully parallel code IMPACT scales with the number of CPUs, the partially-parallel code HALODYN distributes over all the available nodes the tracking only, being the Poisson solver serial and run by the master node only. The grid resolution of PIC codes is of 64^3 for IMPACT, $64^2 \times 256$ for HALODYN, 20×40 for the 2D solver SCHEFF (PARMILA and PATH) and 48^3 for the 3D solver PICNIC (PARMILA and PARTRAN). The number of space-charge calculations per DTL cell can be chosen by the user not in all the codes: it varies from 200 of DYNAMION, 80 for IMPACT, ≈60 for HALODYN, 40 for PATH, ≈15 for LORASR, 3 in PARTRAN. Due to the different algorithms it was not possible to fix the same integration step and grid resolutions for all the codes. In case of DYNAMION and IMPACT in fact the choice of a large number of steps is necessary in order to avoid artificial collision (DYNAMION) and numerical problems when using the Lorentz integrator (IMPACT). The number of step in PARTRAN has been chosen by taking the emittance curve obtained with a high-resolution simulation and by lowering the number of integration steps: the optimal choice is the one providing the same emittance curve with the minimum number of integration steps. The CPU time has been found dependent on the choice of boundary conditions in IMPACT: selecting the closed boundary condition on the rectangular pipe (the same of HALODYN) the requested CPU time is reduced of about 40%.

Table 1: Summary table with an indication of the requested CPU time for different choice of solvers and boundary conditions. See text for the choice of the number of macro-particles, integration step and grid resolution. All the codes having a post-processor for the graphical analysis are labeled with "post" in the GUI entry.

code (a.o.)	***platform***	***GUI***	***parallel***	***particles***	***s. c. solver***	***boundary conditions***	***CPU time***
DYNAMION	Windows (Li)Unix	no	no	5×10^3	3D p-p		1.3 days 2.5 days
HALODYN	(Li)Unix	post	yes	1×10^6	3D PIC	closed	1.0 day
IMPACT	(Li)Unix	no	yes	1×10^6	3D PIC	open closed	4.0 days 2.5 days
LORASR	Windows	yes	no	1×10^6	3D PIC	closed	N.A.
PARMILA	Windows	post	no	1×10^5	2D PIC 3D PIC	open	1.5 days 7.0 days
PARTRAN	Windows	post	no	1×10^5	3D PIC	open	6.0 days
PATH	Windows	yes	no	1×10^5 2×10^4	2D PIC 3D p-p	open	1.5 days 1.5 days

3.2.4 Benchmarking and Comparison

3.2.4.1 Space charge electric field test

A common particle distribution was used to compute the space-charge electric field *E*. We modified the codes in such a way to print on file *E* at the position of each particle. The latter is then compared with a semi-analytical solution (assuming open boundary conditions) obtained with an algorithm described in [14]. As figure of merit we use the relative error δE/E defined in [2] and plot it against the distance from the beam axis. Figure 1 shows the results for DYNAMION and the PIC codes with a grid resolution of 128^3 (or 129^3 according to the algorithm). The relative error shows for all codes an exponential drop within the bunch core, whereas some differences appear outside: while the IMPACT (open boundary conditions) error keeps converging to zero, it remains on the ~1% level for DYNAMION, TOUTATIS and IMPACT (closed boundary conditions) and it increases up to 10% in HALODYN and LORASR. We interpret the 100% error at the bunch centre for all the codes as follows: with the electric field E going linearly to zero as $r \to 0$, the same is true for the error δE.

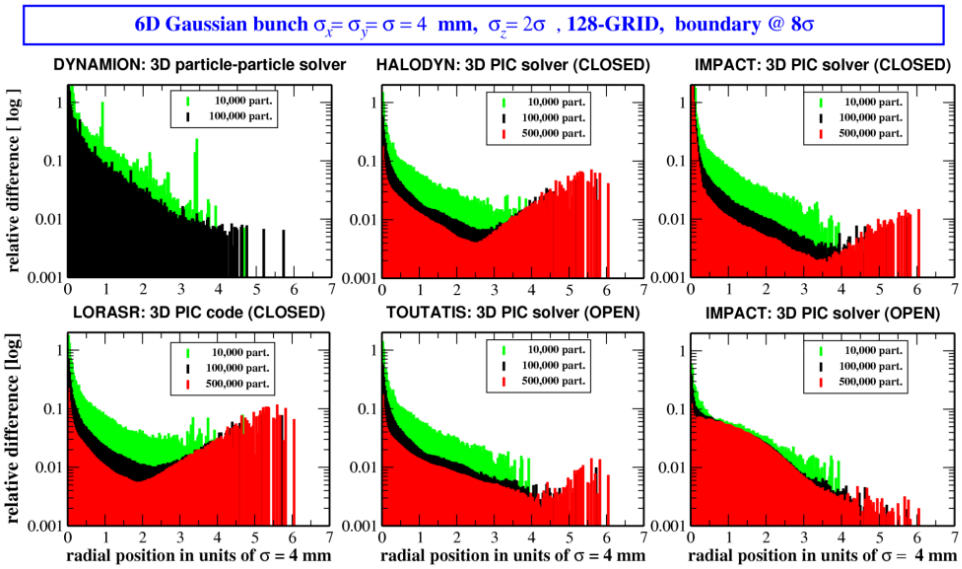

Figure 1 Field error δ**E**/**E** for DYNAMION and PIC codes with a grid resolution of 128^3 (129^3)

3.2.4.2 Single particle tune test

Even if the quality of the space charge electric field is a clear figure of merit of a solver, its error does not provide an estimation of the induced error in the beam dynamics. Resonant halo and resonance trapping and de-trapping are both mechanisms of interest in high intensity regimes. A correct description of these phenomena passes through the correct representation of the single particle dynamics, which in turn is characterized by the single particle tune (SPT) and the crossing of a resonance condition. Space charge depresses the tune due to its intrinsic defocusing characteristics. Errors in the electric field computation result therefore in wrong

depressed SPT. In [2,15] a scaling law was proposed in order to represent the error in the SPT computation as a function of the number of macro-particles *Np* and the grid resolution Δx:

$$\delta q = K_1 \left(\frac{K_2(f_n, Vol_b)}{\sqrt{\Delta x^3 N_p}} + K_3(Vol_G, Vol_b)\Delta x^{\alpha} \right) ,$$

where K_1 is a constant. K_2 has a statistical origin and introduces a numerical "tune spread", whereas K_3 is originated by the limited spatial resolution of the solver (Δx) and introduces a numerical "tune shift". By using the same numerical and beam parameters, the PIC solvers can be compared by looking at the coefficients of this law: the smaller they are, the higher is the solver quality. In Figure 2 the dependence of both the "spread" and the "shift" on the numerical parameters is plotted. K_2 and K_3 are inferred by fitting the curves and appear to have almost the same value for all the PIC solvers here tested. The solver of LORASR shows a higher resolution (lower "tune shift"), although it appears to be the noisiest (larger "tune spread").

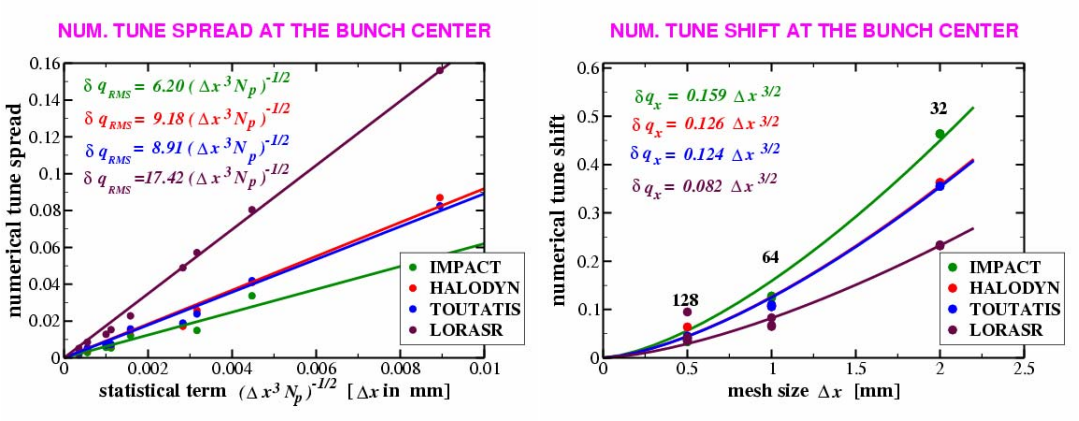

Figure 2: Numerical "tune spread" (left) and "tune shift" (right) at the bunch centre and corresponding constant K_2, K_3 .

3.2.4.3 UNILAC tracking

Preliminary tracking simulations of the UNILAC DTL section have been run using a zero-current $^{238}U^{+28}$ beam. SUPERFISH has been used to generate the TTF table for PARMILA and the RF (nonlinear) maps for IMPACT. DYNAMION models the RF solving the Laplace equation in the region between two drift tubes, whereas HALODYN applies a thin kick at the gap centre. PATH and PARTRAN can import a 3D electro-magnetic field map, although for convenience the same modelling of HALODYN was used. LORASR imports the radial RF electric field computed by MICROWAVE-STUDIOLAB. The transverse sizes and emittances (not shown here) agree within 1% (the initial beam distribution is an ensemble of 10^4 macro-particles). The behaviour of the longitudinal beam size and emittance is also good, although at some locations larger differences of about 10% appear in few codes (Fig. 3).

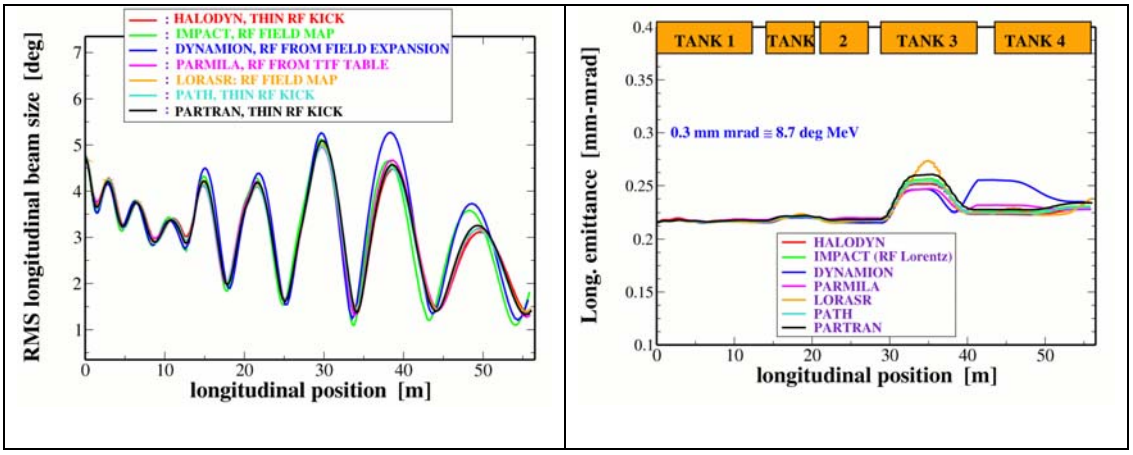

Figure 3: RMS longitudinal phase and emittance computed by all the codes and plotted along the DTL.

The next step is to include the space charge forces by setting the bunch current to I=37.5 mA, which is the reference value for high-intensity UNILAC operations. In order to investigate two different regimes, we ran two groups of simulations: one with a short bunch driving a severe longitudinal tune depression δ_z=0.35 (CASE 1), a second with a longer bunch leading to a weak depression δ_z=0.88 (CASE 2). In both cases the transverse tune depression is $\delta_r \approx 0.6$. Space charge dominates in CASE 1, whereas in CASE 2 it is coupled with the nonlinearities arising from the proximity of the bunch core to the longitudinal separatrix.

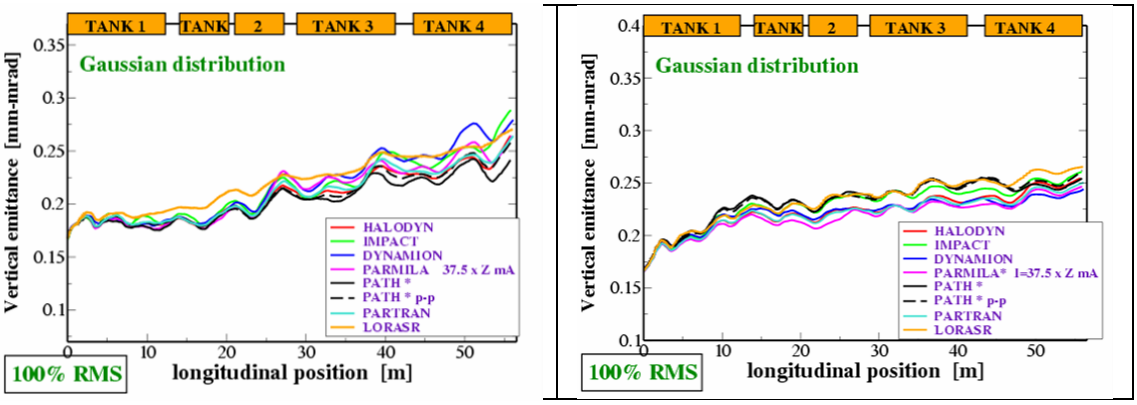

Figure 4: Vertical RMS emittance computed by all the codes and plotted along the DTL for CASE 1 (left) and CASE 2 (right).

In both cases the final horizontal (RMS normalized) emittance presents a large spread of about ±15% among the codes, whereas in the vertical plane the discrepancies remain confined to ±5%, besides the different transverse boundary conditions (see Fig. 4). In Fig. 5 the longitudinal RMS emittance computed by all the codes is plotted along the DTL. The emittance growth is related exclusively to space charge in CASE 1 (left plot), as the beam remains entirely within the separatrix. The picture changes completely in CASE 2 (right plot), where the longer bunch makes part of the beam to approach and to get trapped into the separatrix; in this case the emittance growth is mostly driven by the RF nonlinear fields. At the entrance of tank 3 ($L \approx 30$ m) the

synchronous phase jumps from -30° to -25°, reducing the bucket area and introducing an additional growth. In the longitudinal plane the agreement among the codes for a space charge dominated beam is within few percents, with the exception of DYNAMION that predicts a lower growth. The situation is different for CASE 2 where the general agreement among the codes is rather poor after tank 3. The results here shown were obtained after a series of code debugging and adjustments. In some codes bugs (mostly related to the charge state $Z \neq 1$) have been found and fixed. It was also observed that PIC codes with closed longitudinal boundary conditions underestimate the longitudinal emittance growth if the mesh box is too close to the beam. Very important for CASE 2 was the definition of "longitudinal beam loss". As the latter one turned out to be highly code dependent, we forced the codes to reject all the particles whose distance from the synchronous particle was larger than π.

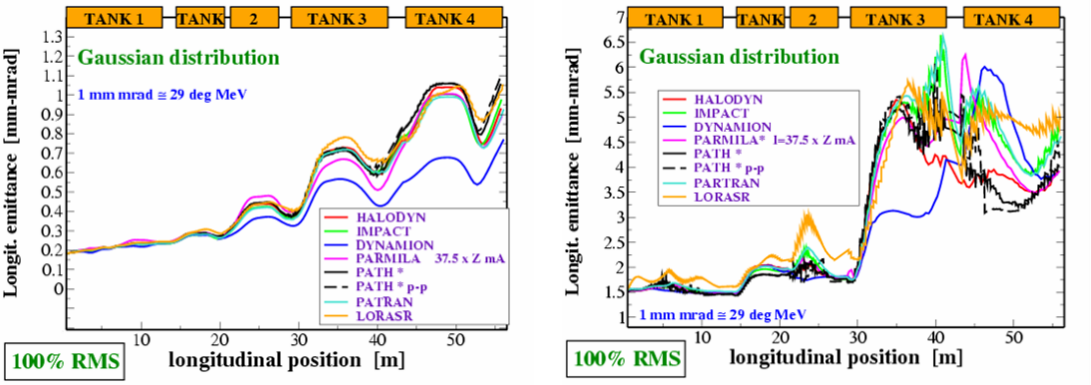

Figure 5: Longitudinal RMS emittance computed by all the codes and plotted along the DTL for CASE 1 (left) and CASE 2 (right).

3.2.5 Acknowledgements

We acknowledge the support of the European Community-Research Infrastructure Activity under the FP6 "Structuring the European Research Area" programme (CARE, contract number RII3-CT-2003-506395)

3.2.6 References

1. http://www-linux.gsi.de/~franchi/HIPPI/code_benchmarking.html
2. CARE-Note-2006-011-HIPPI: http://www-dapnia.cea.fr/Documentation/Care/care-note-hippi-index-2006.php
3. A.Kolomiets et al. , DYNAMION - The Code for Beam Dynamics Simulation in High Current Ion Linac, Proc. EPAC-98, pp. 1201-03.
4. S. Yaramishev et al, Development of the versatile multi-particle code DYNAMION, Nucl. Intr.& Meth. A, Vol 558/1 pp 90-94, (2005).
5. A. Franchi et al. , A 3D Poisson-Vlasov Code to Simulate the Space-Charge Effects in the High Intensity TRASCO Linac, Proc. LINAC-02, pp. 653-655
6. G. Turchetti et al., Accuracy analysis of a spectral Poisson solver, Nucl. Intr.& Meth. A, vol. 561 Issue 2 (2006), pp. 223-229.
7. J. Qiang et al., An Object Oriented Parallel Particle- In-Cell Code for Beam Dynamics Simulation in Linear Accelerator, Jo. of Comp. Phys., 163, 2000, pp. 434{45.

8. R. Tiede et al., LORASR code developement, Proc. EPAC06.
9. J. H. Billen, PARMILA, LA-UR-98-4478, 2001.
10. R. Duperrier, N. Pichoff, and D. Uriot, in Proceedings of the International Conference Computational Science: ICCS 2002, Amsterdam, the Netherlands, 2002 (Springer-Verlag, Berlin, 2002).
11. N. Pichoff et al., in Proceedings of the International LINAC Conference, Chicago, IL, 1998(Argonne National Lab., Chicago, 1998), p. 141.
12. http://tmuetze.home.cern.ch/tmuetze/
13. R. Duperrier, TOUTATIS: A radio frequency quadrupole code, Phys. Rev. STAB, 3, 2000, p.124201-06.
14. A. Orzhekhovskaya et al., A space-charge algorithm for ellipsoidal bunches with arbitrary beam size and particle distribution, Proc. EPAC-04, pp. 1972-74
15. G. Turchetti et al., Proc. ICAP-02, (15-18 October 2002, East Lansing, USA)

3.3 Semi-Lagrangian Vlasov Codes for the Transport of Intense Particle Beams in the 4D transverse phase-space

Nicolas Crouseilles[1], Guillaume Latu[2], Jean-Louis Lemaire[3], Eric Sonnendrücker[4]

[1]IECN and CALVI-INRIA Lorraine, Nancy
[2] LABRI - INRIA Futurs, Bordeaux
[3]CEA/DAM/DIF, Bruyères-Le-Châtel
[4]IRMA and CALVI-INRIA Lorraine, Strasbourg

mail to: crouseil@math.u-strasbg.fr

3.3.1 Introduction

Particle In Cell (PIC) simulations have proven very efficient for the simulation of particle beams in accelerators, in particular for low intensity beams. However, for very intense beams as those needed e.g. for heavy ion fusion, their inherent noise and slow convergence when the number of particles increases might not make them the most efficient tool. We have been investigating for several years now, direct Vlasov solvers using a grid of phase space, based on the semi-Lagrangian method. This method consists in following the particle trajectories backward from each grid point and interpolating at the origin to update the particle distribution on the phase space grid [4]. Other types of eulerian Vlasov solvers have been investigated in [5] in the context of plasma physics. Simulation of the whole six dimensional phase space is not accessible yet with this approach. However interesting physics can be obtained using the paraxial model [3,7], to study the evolution of the 4D transverse phase space of a beam. The particle distribution function $f(z, \mathbf{x}, \mathbf{v})$, depending on longitudinal position z, transverse position $\mathbf{x}=(x, y)$ and transverse velocity $\mathbf{v}=(v_x, v_y)$, then obeys the paraxial Vlasov equation:

$$\frac{\partial f}{\partial z} + \frac{v}{v_b} \cdot \nabla_x f + \frac{q}{\gamma_b m v_b} (E + v \times B) \cdot \nabla_v f = 0, \qquad (1)$$

where $\gamma_b = (1-(v_b/c)^2)^{-1/2}$, v_b is the velocity of the beam, c is the velocity of light in free space, m the mass of the considered particles and q their charge. Moreover the force term F is given by

$$F = E + (\mathbf{v}, v_b)^T \times B,$$

where $E=(E_x,E_y)$ solves the 2D Poisson equation

$$E = -\nabla\phi, \qquad -\Delta_x\phi = \frac{q}{\varepsilon_0}\int f(z,\mathbf{x},\mathbf{v})d\mathbf{v},$$

and B is the magnetic focusing field, of the form $\mathbf{B} = (-\frac{1}{2}B'(z)x, -\frac{1}{2}B'(z)y, B(z))$ for periodic solenoidal focusing and of the form $\mathbf{B} = (\kappa(z)y, \kappa(z)x, 0)$ for magnetic quadrupole focusing.

Recently we have been improving the parallel efficiency of our previous 2D code based on a uniform grid [10] and extending our 1D axis-symmetric adaptive solver [8, 9] to 2D (i.e. 4D phase space). This letter is devoted to the assessment of these new solvers on a relevant test case. In the sequel, we shall recall the features of these solvers and then we shall assess their performance for the transport of a beam in a magnetic quadrupole channel.

3.3.2 Description of the Codes

Eulerian methods have proven their efficiency on uniform meshes in two dimensional phase space, but when the dimensionality increases, since a minimum number of points per direction is required to accurately describe the physics, the total number of points on a grid becomes very important. Hence one issue to overcome this problem can be the efficient use of parallel computing. On the other side, for inhomogeneously populated systems, many of the grid points are wasted (where no particles are present). This is especially the case for beam simulations, where the beam moves rapidly through phase space (due to alternating-gradient focusing forces, for example). For this reason, in order to handle the 4D phase space problems we are interested in, new methodologies had to be developed. First for codes based on a uniform grid, a parallel method with good scalability on hundreds of processors was developed and then in order to obtain en efficient adaptive solver a specific effort on sparse data structures was needed.

Our previous Eulerian Vlasov Solvers where based either on global cubic spline interpolation [4], or on flux exchanges with polynomial reconstruction [11]. The latter is more dissipative and thus less adequate for beam transport over many lattice periods as it is smearing out the fine structures more for the same grid resolution. On the other hand the cubic spline solver has the drawback of needing a full transpose of the distribution function at each split step. Even with specific implementation efforts like the overlapping of computation and communications as much as possible, this does not scale well over 100 processors. For this reason we developed a new version of the code based on a novel local spline interpolation designed to give results identical up to numerical accuracy to those of the global spline interpolation [2]. Indeed, the phase space computational domain is decomposed into patches; each patch is devoted to a processor and computes its own cubic spline coefficients by solving reduced linear systems. Finally, some boundary conditions are imposed at the boundary of the patches

to get a C^1 global solution. This new code, LOSS (LOcal Spline Simulator), shows very good scalability properties as expected.

Another aspect needed to handle a 4D phase space with Eulerian methods is grid adaptivity. To this aim we developed an adaptive method based on wavelet interpolation for 2D phase space [8,9]. The distribution function is decomposed on a wavelet basis at different levels such that the coefficients called details are small where the function does not vary a lot. Then, according to a prediction and a thresholding procedure, only the significant details are computed. The distribution function can then be determined on the corresponding adaptive grid. Even though the mathematical method can be generalized to arbitrarily high dimensions, already for 4 dimensions, the amount of data that need to be handled requires adequate optimized data structures [12]. The remaining ot this letter is devoted to benchmarking and comparisons between the two new Vlasov solvers: the uniform and massively parallel solver LOSS [2] and the adaptive solver based on interpolating wavelets OBIWAN [12].

3.3.3 The Benchmark Test

We consider the transport of a transverse of a semi-Gaussian proton beam in a magnetic quadrupole lattice using the paraxial Vlasov equation described in the introduction. The magnetic focusing field is of the form $\mathbf{B} = (\kappa(z)y, \kappa(z)x, 0)$. The initial distribution function for the semi-Gaussian beam is:

$$f_0(x,v) = e^{-(v_x^2+v_y^2)/2} \text{ if } x^2 + y^2 < 1 \text{ and 0 elsewhere.}$$

The beam parameters for all the simulations are the following: the energy of the beam is equal to *6.7 MeV*, the beam current *I* is *0.3 A*, the emittance is $3\ 10^6\ \pi$ *mm mrad*. The length of the period is equal to *0.4196 m*. These values give a tune depression of *0.56*. The beam is RMS matched to the focusing channel.

3.3.4 Simulation Results

3.3.4.1 Code based on uniform mesh

We ran the LOSS code on a $64^2 \times 128^2$ mesh for 26 periods and on a 128^4 mesh for 6 periods. RMS values as well as phase spaces plots are displayed in Figures 1 to 5. The numerical diffusion which amount to a loss of particles at the boundaries is kept to less than 1 % over 26 periods as shown in Figure 1 and has no influence on the final results. This can be still improved when the grid is refined. However, there is a limitation due to memory requirements and computing time on a given computer. The phase spaces snapshots come from LOSS but look very similar for the OBIWAN code (not represented).

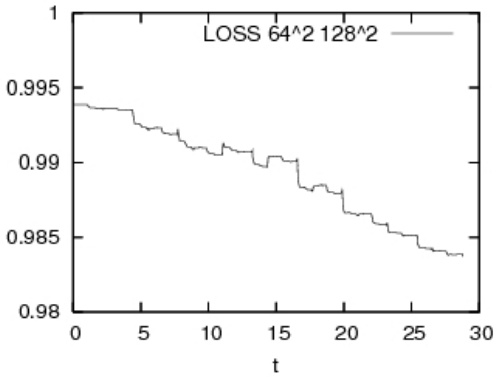

Figure 1: Evolution of the normalized total number of particles

On Figure 2 the evolution of the RMS size and emittance of the beam are represented over almost 30 periods and confirmed the beam is well matched.

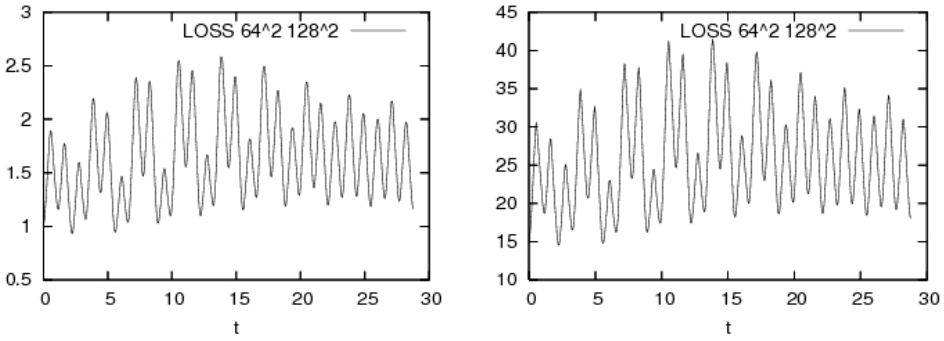

Figure 2: Evolution of x_{rms} and ε_{rms}.

Figure 3 represent the *x-x'* phase space in the focusing part (left) and the defocusing part (right) of the 25th period. They seem to indicate that the beam has relaxed to an equilibrium position. However the smoothness of the contours is certainly linked in part to the dissipativeness of grid interpolation.

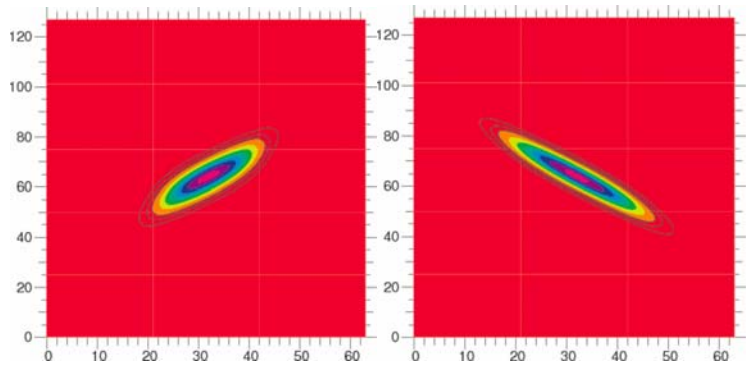

Figure 3: x-x' phase space in the 25th period on $64^2 \times 128^2$ grid

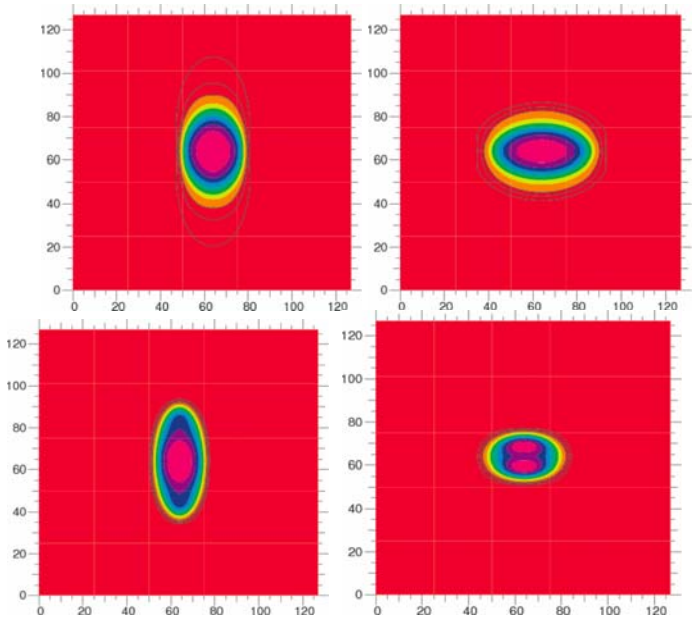

Figure 4: x-y phase space on 128^4 grid, after 4, 4.5, 5 and 5.5 periods

Figures 4 and 5 show the evolution of the *x-y* and *x-x'* phase spaces respectively between the 4th and the 6th period. A space charge wave appears to be propagating leading to the apparition of two density peaks on Figure 4.

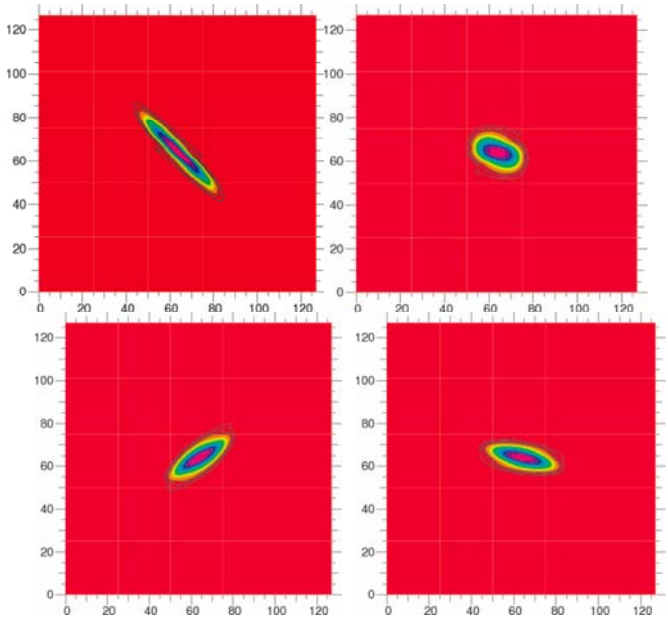

Figure 5: x-x' phase space on 128^4 grid, after 4.75, 5, 5.25 and 5.5 periods

3.3.4.2 Comparison of uniform grid code and adaptive code

The adaptive method we are using does not insure the exact conservation of the number of particles. This feature can be added for a slightly higher computational cost [13]. However, as shown in Figure 6, the lack of conservation is very small and can be made even smaller by setting a lower threshold for discarding the grid points. Note that the total number of particles is computed from the distribution which is known on the grid. And, due to the adaptive, wavelet-based, discarding of grid points positive or negative contributions can be added which can either lead to a numerical increase or decrease of the total number of particles.

The evolution of the x_{RMS} for the two codes is given in Figure 7 and compared to this of a KV beam showing the influence of the nonlinear effects. Both codes give pretty much the same value. Figure 8 displays the influence of the number of grid points on this quantity for the adaptive code.

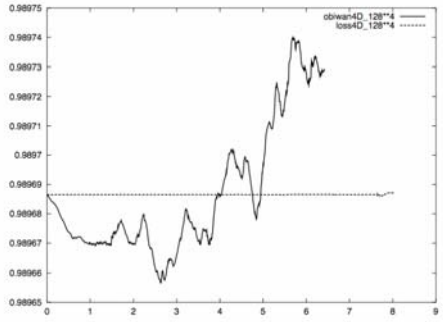

Figure 6: Evolution of normalized total number of particles with uniform and adaptive codes.

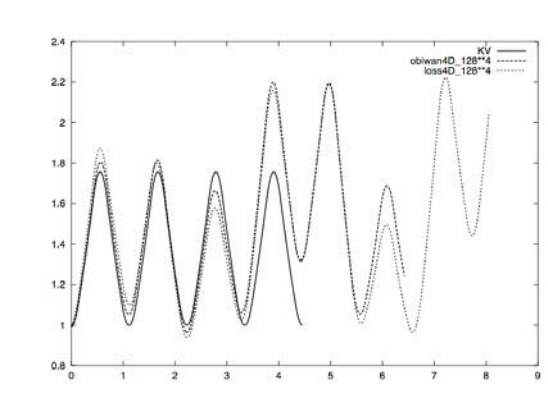

Figure 7: Evolution of x_{rms} for uniform and adaptive code.

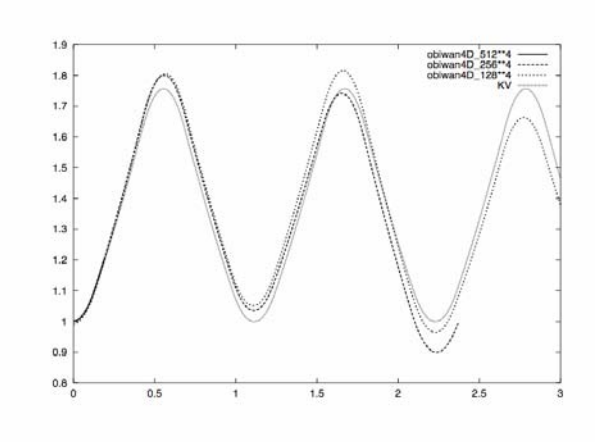

Figure 8: Evolution of x_{rms} at different resolutions with adaptive code.

3.3.4.3 Computational and memory cost

Table 1 below gives the computation time for one time step and the speedup for the two methods on a 64^4 grid. On the one hand, we notice that the computational cost of the two solvers is comparable with a slight advantage for OBIWAN. On the other hand, the speedup of the two methods is quite good, since communication-computation overlapping is performed in the two codes. Note that for finer resolution, as the number of grid points that need to be kept in the adaptive solver is less in percentage, it will always be faster.

Table 1: Computation cost and speedup for uniform and adaptive codes.

Numbers of processors	1	2	4	8
Time (in s.) LOSS/OBI	433/408	226/206	111/105	63/55
Speedup LOSS/OBI	1/1	1.92/1.98	3.9/3.88	6.87/7.41

Table 2 gives the time taken by the different steps of the algorithm for LOSS and in different cases for OBIWAN, on a 128^4 grid with a different number of remaining grid points (which evolves during the simulation). As a splitting scheme is used, the different steps in the algorithm are, the transport in configuration space, the transport in velocity space, the field solve and the diagnostics.

Table 2: Time in seconds for one iteration in 4D simulators on 4 processors (using IBM 16-way nodes of power 5 processors)

	Velocity Space Transport	**Configuration Space Transport**	**Field Solve**	**Diagnostics**	**Total**
LOSS (128^4)	38.1	84.9	1.0	1.0	125.1
OBIWAN (128^4), non-zero=2%, it=1, threshold=10^{-4}	12.4	16.4	0.3	0.4	29.5
OBIWAN (128^4), non-zero=9%, it=750, threshold=10^{-4}	44.1	57.8	0.3	1.0	103.2
OBIWAN (256^4), non-zero=0.75%, threshold=10^{-4}	49.8	70.1	1.1	2.0	123.0

Figure 9 displays the evolution of the number of remaining grid points during the simulation. This number is very small throughout the simulation for our test case.

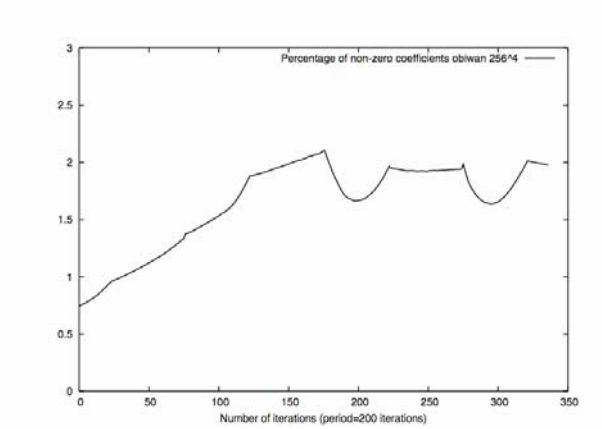

Figure 9: Percentage of remaining grid points in a 256^4 adaptive run.

The memory consumption is reduced considerably with the OBIWAN code versus the LOSS code. For the test case with a 128^4 grid, OBIWAN achieves to use only 0.9 GO memories, whereas LOSS uses 2.8 GO. A grid as large as 256^4 requires 45 GO of available memory for the LOSS code, but only 2.7 GO for OBIWAN.

3.3.5 Conclusion

We have developed two new semi-lagrangian Vlasov solvers based on the direct solution of the Vlasov equation in 4D phase space for numerical simulation of beam transport. They have been validated on the realistic test case of beam transport in a FODO lattice, for which both yield satisfying results. For such cases the adaptive solver

enables to use a very fine resolution with reasonable memory requirements and computing time.

3.3.6 References

1. C.Z. Cheng, G. Knorr, "The integration of the Vlasov equation in configuration space", J. Comput. Phys., 22, p. 330, (1976)
2. N. Crouseilles, G. Latu, E. Sonnendrücker, "Hermite spline interpolation on patches for a parallel solving of the Vlasov-Poisson equation", Research report INRIA Lorraine 5926: http://hal.inria.fr/inria-00078455.
3. F. Filbet, E. Sonnendrücker, "Modeling and numerical simulation of space charge dominated beams in the paraxial approximation", Math. Models Meth. App. Sc., 16, pp.1-29, (2006).
4. E. Sonnendrücker, J. Roche, P. Bertrand, A. Ghizzo, "The semi-Lagrangian method for the numerical resolution of the Vlasov equations", J. Comput. Phys., 149, pp. 201-220, (1999).
5. F. Filbet, E. Sonnendrücker, "Comparison of Eulerian Vlasov solvers", Comput. Phys. Comm., 151, pp. 247-266, (2003).
6. M. Gutnic, M. Haefele, I. Paun, E. Sonnendrücker, "Vlasov simulation on an adaptive phase space grid" , Comput. Phys. Comm., 164, pp. 214-219, (2004).
7. R.C. Davidson, H. Qin, "Physics of Charged Particle Beams in High Energy Accelerators", Imperial College Press, World Scientific, 2001.
8. E. Sonnendrücker, M. Gutnic, M.Haefele, G. Latu, J.-L. Lemaire, " Vlasov simulation of beams and halo", Proc. 21st biennial Particle Accelerator Conference, PAC05, Knoxville TN, 2005.
9. E. Sonnendrücker, M. Gutnic, M.Haefele, J.-L. Lemaire, "Adaptive Vlasov simulations of intense beams", 33rd ICFA Advanced Beam Dynamics Workshop on High Intensity and High Brightness Hadron Beams, 18-22 october 2004, AIP Conference Proceedings 773, pp 154-157 (2005).
10. J.-L. Lemaire, E. Sonnendrücker, "Beam Dynamics Comparisons between Semi-Lagrangian and PIC Techniques for Simulation ot the Propagation of Intense Charged Particle Beams in 2D Channels ", 33rd ICFA Advanced Beam Dynamics Workshop on High Intensity and High Brightness Hadron Beams, 18-22 october 2004, in AIP Conference Proceedings 773, pp 152-154 (2005).
11. F. Filbet, E. Sonnendrücker, P. Bertrand, "Conservative Numerical Schemes for the Vlasov Equation", J. Comput. Phys. 172, no. 1, pp 1-22, (2001).
12. M. Gutnic, G. Latu, E. Sonnendrücker , "Adaptive two-dimensional Vlasov simulation of heavy ion beams". Proceedings 16th International Symposium on Heavy Ion Fusion, Saint-Malo France, to appear in Nucl. Inst. Meth. Phys. Res. A.
13. M. Gutnic, M. Haefele, E. Sonnendrücker, "Moments conservation in adaptive Vlasov solver", Proceedings ICAP 2004 in Nuclear Inst. and Methods in Physics Research, A, 558 (1), pp. 159-162 (2006).

3.4 Benchmark of the IMPACT Code for High Intensity Beam Dynamics Simulation

J. Qiang and R. D. Ryne, LBNL, Berkeley, CA 94720, USA
mail to: jqiang@lbl.gov

3.4.1 Introduction

The IMPACT (Integrated Map and Particle Accelerator Tracking) code was first developed under Computational Grand Challenge project in the mid 1990s [1]. It started as a three-dimensional (3D) data parallel particle-in-cell (PIC) code written in High Performance Fortran. The code used a split-operator based method to solve the Hamiltonian equations of motion. It contained linear transfer maps for drifts, quadrupole magnets and rf cavities. The space-charge forces were calculated using an FFT-based method with 3D open boundary conditions and longitudinal periodic boundary conditions. This code was completely rewritten in the late 1990s based on a message passing parallel programming paradigm using Fortran 90 and MPI following an object-oriented software design. This improved the code's scalability on large parallel computer systems and also gave the code better software maintainability and extensibility [2]. In the following years, under the SciDAC-1 accelerator project, the code was extended to include more accelerating and focusing elements such as DTL, CCL, superconducting linac, solenoid, dipole, multipoles, and others. Besides the original split-operator based integrator, a direct integration of Lorentz equations of motion using a leap-frog algorithm was also added to the IMPACT code to handle arbitrary external nonlinear fields. This integrator can read in 3D electromagnetic fields in a Cartesian grid or in a cylindrical coordinate system. Using the Lorentz integrator, we also extended the original code to handle multiple charge-state beams. The space-charge solvers were also extended to include conducting wall effects for round and rectangular pipes with longitudinal open and periodic boundary conditions. Recently, it has also been extended to handle short-range wake fields (longitudinal monopole and transverse dipole) and longitudinal coherent synchrotron radiation wake fields. Besides the parallel macroparticle tracking code, an rf linac lattice design code, an envelope matching and analysis code, and a number of pre- and post-processing codes were also developed to form the IMPACT code suite. The IMPACT code suite has been used to study beam dynamics in the SNS linac, the J-PARC linac commissioning, the CERN superconducting linac design, the Los Alamos Low Energy Demonstration Accelerator (LEDA) halo experiment, the Rare Isotope Accelerator (RIA) driver linac design, and the FERMI@Elettra FEL linac design [3-8]. It has also been used to study space-charge resonance in anisotropic beams [9-11].

3.4.2 Physical Model and Computational Methods

The IMPACT code assumes a quasi-static model of the beam and calculates space-charge effects self-consistently at each step together with the external acceleration and focusing fields. Here, the longitudinal distance z is used as the independent variable. There are two macroparticle pushers: one is based on transfer maps, another is based on direct integration of the Lorentz equation.

The map based pusher uses a split-operator method to combine the techniques of magnetic optics with those of particle-in-cell simulation. In this approach, the Hamiltonian governing the motion of individual particles in the accelerator is separated into two pieces, $H=H_{ext}+H_{sc}$, where H_{ext} corresponds to externally applied fields and H_{sc} corresponds to space-charge fields. The effect of H_{ext} is treated by using map-based techniques of magnetic optics, while the effect of H_{sc} is treated by using a Poisson solver to find the scalar potential and corresponding space-charge fields that act on the

beam. Let M_{ext} denote the map corresponding to H_{ext} and let M_{sc} denote the map corresponding to H_{sc}. Then the map M corresponding to $H_{ext}+H_{sc}$, accurate through second order in the step size h, is given by:

$$M(h) = M_{ext}(h/2)M_{sc}(h)M_{ext}(h/2) \tag{1}$$

Each complete step involves the following: (1) transport of a numerical distribution of particles through a half step based on M_{ext}, (2) solving Poisson's equation based on the particle positions and performing a space-charge "kick" (i.e. an instantaneous change in momenta, since H_{sc} depends only on coordinates, hence M_{sc} only affects momenta), and (3) performing transport through the remaining half of the step based on M_{ext}. An important feature of this approach is that it enables one to use large step size (i.e. large steps in the independent variable) in the regime of weak or moderate space charge. Essentially, it enables one to decouple the rapid variation of the externally applied fields from the more slowly varying space-charge fields. If more accuracy is required, one can use the fourth-order algorithm of Forest and Ruth [12] or a higher-order algorithm using a method of Yoshida [13].

The pusher based on direct integration solves the Lorentz equation using a leap-frog method. In this method, during each step, particles are drifted a half step following their current momenta, then the momenta are updated using the external fields and the space-charge forces, then the particles are drifted another half step following their new momenta. This pusher can include all details of external nonlinear acceleration and focusing fields without approximation. The disadvantage of this method is that each individual particle has to advance through the external fields with sufficient accuracy. This could result in many tiny steps in order to resolve fast oscillation of the external fields.

The space-charge forces are self-consistently computed at each step by solving the 3D Poisson equation in the beam frame. The resulting electrostatic fields are Lorentz transformed back into the laboratory frame to obtain the space-charge forces of the beam. There are presently six Poisson solvers in the IMPACT code, corresponding to transverse open or closed boundary conditions with round or rectangular shape, and longitudinal open or periodic boundary conditions. These solvers use either a spectral method for closed transverse boundary conditions, or a convolution-based Green function method for open transverse boundary conditions. The convolution for the most widely used open boundary condition Poisson solver is calculated using an FFT with doubled computational domain. The computing time of this solver scales like N·log(N), where N is number of grid points. The parallel implementation is based on a two-dimensional domain decomposition approach for the three-dimensional computational domain.

3.4.3 Verification of the IMPACT Code

To verify the IMPACT code, we have benchmarked this code against a time-dependent PIC code [14]. Here, the time dependent PIC code was tested using two charged particles of identical mass and opposite charges. These two particles are initially placed at the two opposite diagonal corners of a cubic box. The initial speed of the two particles is given by

$$|V| = \sqrt{\frac{q^2}{4\pi\varepsilon_0 mr}} \tag{2}$$

where r is the distance from the corner of the box to the center of the box. Fig. 1 shows the rms value of position and radius of the two particles as a function of time. It is seen that the radius is independent of time since we chose the center of the orbits to be at the origin. With a right initial speed, the centrifugal force should exactly balance the static Coulomb force, and particle radius will stay constant. Using this time dependent code as baseline simulation results, we also performed a multiparticle test in which we compared the beam distribution moments through a periodic transport system of about 10 m. The first order to fourth order moments of the beam distribution together with the maximum amplitude as a function of distance are shown in Fig. 2. In this example, both simulations agree with each other very well.

Besides the above examples, the IMPACT code was also benchmarked with other codes in the European Code Comparison and Benchmarking project [15].

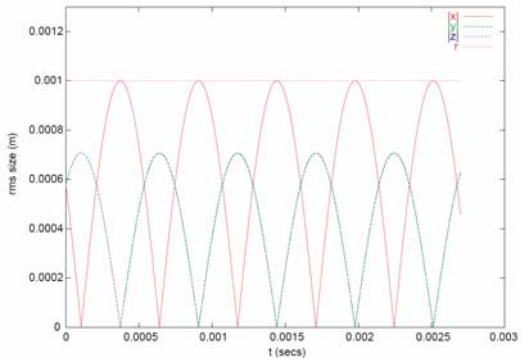

Figure 1: The position and radius of the rotating particle as a function of time.

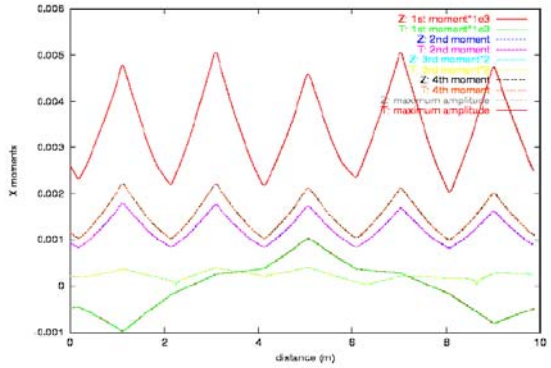

Figure 2: The first four moments and maximum amplitude as a function distance from the time-dependent PIC code and the IMPACT code.

3.4.4 Validation of the IMPACT Code

The IMPACT code was also benchmarked using experimental data involving high intensity beams. Namely, we performed a comparison of simulation results and experimental results from the beam halo experiment, LEDA, at Los Alamos National Laboratory [6]. Fig. 5 shows a schematic plot of the experiment transport system after

the RFQ. It consists of 52 magnetic quadrupoles with alternating polarization to provide transverse strong focusing. The beam current is 75 mA with 6.7 MeV kinetic energy. Fig. 6 shows the transverse rms size at the center of the drift space as a function of distance from the measurements and from the simulations using three types of initial distributions, Waterbag, Gaussian, and simulated RFQ output. The three distributions have the same initial Courant-Snyder parameters and emittances. Small oscillation of the measured rms sizes is reasonably reproduced from the simulation using RFQ output distribution. The emittance was determined from wire scanner measurements and compared with simulations from the IMPACT code. Fig. 7 shows the emittance from the measurements and from the simulations using the RFQ output initial distribution for a set of mismatch factors. The simulations reproduce the measurements at small mismatch factor but under-predict the emittance at large mismatch factor. This discrepancy could be due to the uncertainty of tails in the initial distribution in the experiment as compared with those used in the simulations. It was shown that a larger tail in the initial simulated distribution gives closer agreement with the measured emittance growth.

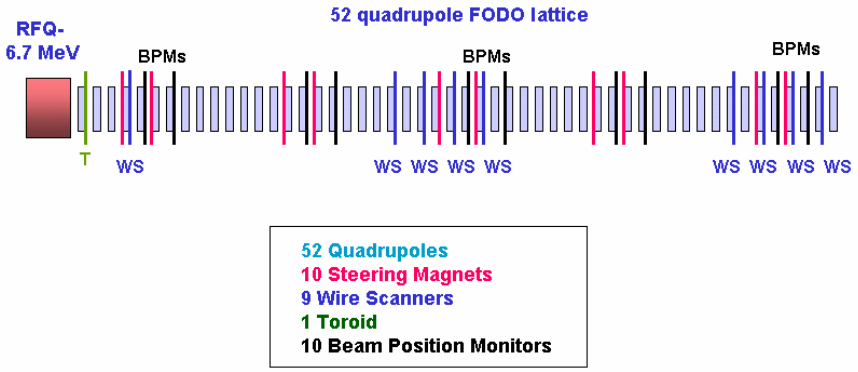

Figure 5: A schematic plot of the LEDA beam halo experiment transport system.

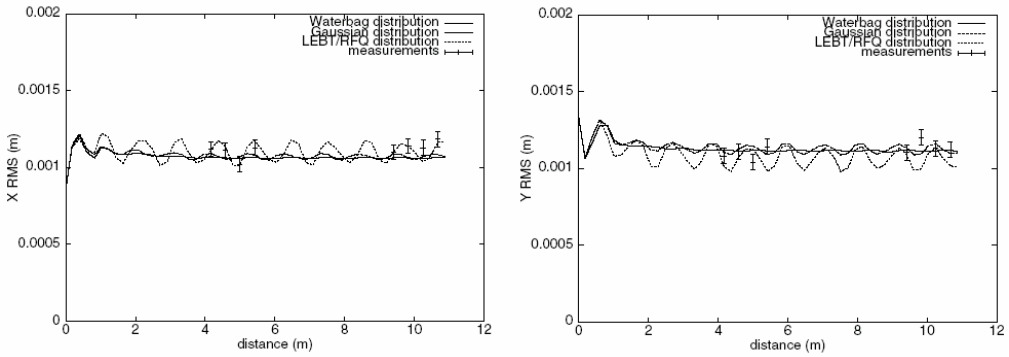

Figure 6: Horizontal and vertical rms sizes as a function of distance from the simulations and from the measurements.

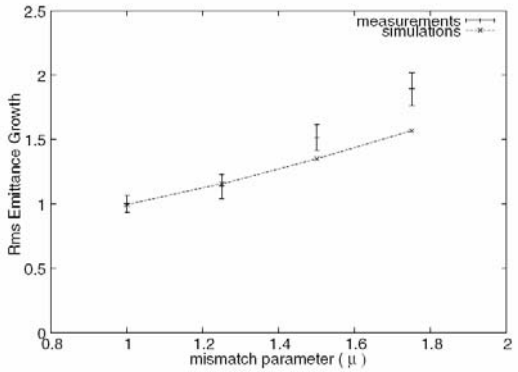

Figure 7: Final emittance growth as a function of mismatch parameter from the simulations and from the measurements.

The IMPACT code was also used to model the beam transport through a section of MEBT at the J-PARC linac [4]. Fig. 8 shows the beam profiles measured with wire scanner 3 located before quadrupole magnet 4 together with simulations from the IMPACT code. The simulated profiles show good agreement with the measured profiles with slightly less peak in the horizontal direction. The agreement in the vertical direction is excellent.

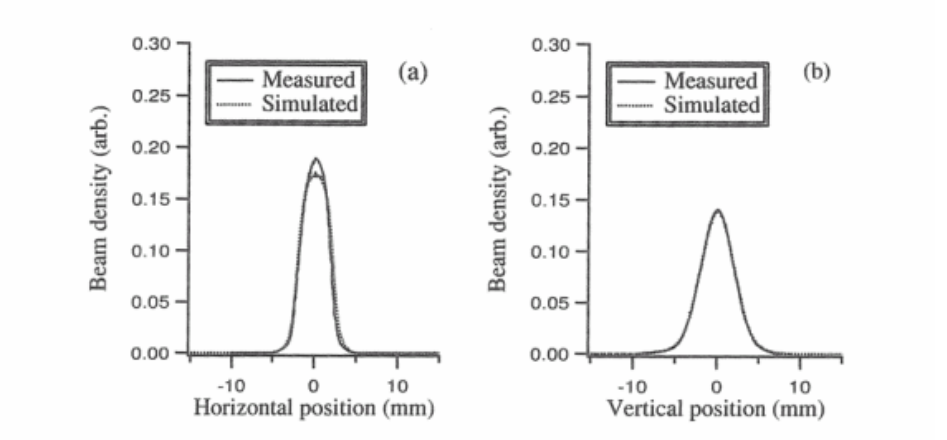

Figure 8: The measured and simulated beam density profiles in the MEBT of J-PARC linac.

3.4.5 Acknowledgements

We would like to thank Dr. S. Habib for helpful discussions during the early development of the IMPACT code, and Dr. V. Decyk for discussions about parallel implementation. We would also like to thank Dr. Tom Wangler for helpful discussions regarding the LEDA experiment, the LEDA experimental team for the validation data, and Dr. M. Ikegami for the J-PARC validation results. This work was supported by the U. S. Department of Energy under Contract no. DE-AC02-05CH11231, and by a Scientific Discovery through Advanced Computing project, ``Advanced Computing for 21st Century Accelerator Science and Technology," which is supported by the US DOE/SC Office of High Energy Physics and the Office of Advanced Scientific

Computing Research. Results presented in this report were obtained using resources of the National Energy Research Scientific Computing Center, which is supported by the Office of Science of the U.S. Department of Energy under Contract No. DE-AC02-05CH11231.

3.4.6 References

1. Robert Ryne, Ji Qiang, and Salman Habib,, "Computational Challenges in High Intensity Ion Beam Physics", in "The Physics of High Brightness Beams", ed. By J. Rosenzweig and L. Serafini, World Scientific (2000).
2. J. Qiang, R. Ryne, S. Habib, V. Decyk, "An Object-Oriented Parallel Particle-In-Cell Code for Beam Dynamics Simulation in Linear Accelerators," J. Comp. Phys. vol. 163, 434, (2000).
3. J. Qiang, R. Ryne, B. Blind, J. Billen, T. Bhatia, R. Garnett, G. Neuschaefer, H. Takeda, "High Resolution Parallel Particle-In- Cell Simulation of Beam Dynamics in the SNS Linac," Nuclear Instruments and Methods in Physics Research - Section A 457, 1, (2001).
4. M. Ikegami, T. Kato, Z. Igarashi, A. Ueno, Y. Kondo, J. Qiang, and R. Ryne, "Comparison of Particle Simulation with J-PARC Linac MEBT Beam Test Results," Proc. HALO'03, May 19-23, Montauk, NY (2003).
5. F. Gerigk, M. Vretenar, R. D. Ryne, "Design of the superconducting section of the SPL linac at CERN," *Proc. PAC01*, p. 3909, (2001).
6. J. Qiang, P. L. Colestock, D. Gilpatrick, H. V. Smith, T. P. Wangler, and M. E. Schulze, "Macroparticle Simulation Studies of a Proton Beam Halo Experiment," Phys. Rev. ST Accel. Beams, Vol 5, 124201.
7. Robert Garnett, James Billen, Thomas Wangler, Peter Ostroumov, Ji Qiang, Robert Ryne, Richard York, Kenneth Crandall, "Advanced Beam-Dynamics Simulation Tools for RIA", *Proc. PAC2005*, Knoxville, Tennessee, May 16-20, p. 4218, (2005).
8. I.V. Pogorelov, J. Qiang, R. Ryne, M. Venturini, A. Zholents, R. Warnock, "Recent developments in IMPACT and application to future light sources," in Proc. ICAP06, Chamonix Mont-Blanc, 2006.
9. I. Hofmann, J. Qiang and R. Ryne, "Collective Resonance Model of Energy Exchange in 3D Nonequipartitioned Beams," Physical Review Letters 86, 2313 (2001).
10. I. Hofmann, G. Franchetti, O. Boine-Frankenheim, J. Qiang, and R. D. Ryne, "Space Charge Resonances in Two and Three Dimensional Anisotropic Beams," Phys. Rev. ST Accel. Beams, Vol 6. 024202 (2003).
11. J. Qiang, R. D. Ryne, I. Hofmann, "Space-charge driven emittance growth in a 3D mismatched anisotropic beam," Phys. Rev. Lett., vol. 92, 174801 (2004).
12. E. Forest and R. Ruth. "Fourth-order symplectic integration," *Physica* **D 43** , p. 105, (1990).
13. H. Yoshida. "Construction of higher order symplectic integrators," *Phys. Lett.* **A 150** , p. 262, (1990).
14. J. Qiang, R. D. Ryne and R. W. Garnett, "Systematic comparison of position and time dependent macroparticle simulations in beam dynamics studies," Phys. Rev. ST - Accel. Beams, vol 5, 064201, (2002).
15. http://www-linux.gsi.de/~franchi/HIPPI/web_code_benchmarking.html.

3.5 CODE BENCHMARKING ON SPACE CHARGE INDUCED PARTICLE TRAPPING

G. Franchetti and I. Hofmann, GSI, 64291 Darmstadt, Germany
S. Machida, CCLRC/RAL/ASTeC, Chilton, Didcot, Oxon, U.K.
mail to: g.franchetti@gsi.de

3.5.1 Introduction

The single particle dynamics in a high intensity bunch stored for long term is challenging especially when the chromaticity is taken into account. The interest in this special operating regime comes from the new generation of high intensity synchrotrons such as the SIS100 for the FAIR project [1]. Several studies of this regime [2, 3] lead to the interpretation that space charge may induce particle trapping into lattice induced resonances via synchrotron motion. The latest results [4, 5] have shown that the combined contribution of space charge and chromaticity enhances the beam loss prediction; for the CERN-PS experiment the prediction of beam loss reaches 16% versus the 32% observed experimentally. Until now all numerical predictions have been made using the MICROMAP library [6], but so far no other code with a frozen space charge model has been applied to particle trapping phenomena. It is therefore necessary to confirm the proposed mechanism by benchmarking different codes on this particular high intensity operating regime.

We present here a comparison between results obtained with MICROMAP and SIMPSONS [7]. The benchmarking is made for the SIS18 synchrotron of GSI. An intensity upgrade for the SIS18 is foreseen which aims at the delivery of 7.5×10^{10} U^{28+} in bunches with emittance of $\varepsilon_{x,2\sigma}=34$, $\varepsilon_{y,2\sigma}=14$ mm mrad with $\Delta Q_x=0.3$. As SIS18 has several significant nonlinear resonances [8], the understanding of beam degradation is essential for the upgrade the operation. The tolerable beam loss should not exceed 1-5% in order to avoid a progressive vacuum degradation. For these reasons an approved experimental campaign, named S317 and consisting of 24 shifts, will start in the near future at the SIS18 for exploring the effect of space charge on beam loss and emittance growth under well-controlled conditions. Consequently we make the code benchmarking for the SIS18 with realistic parameters for the S317 experiment. The SIS18 lattice is taken with the standard triplet configuration typically used at injection energy. The lattice nonlinearities are created by a sextupole magnets in order to excite 3rd order resonances.

3.5.2 The Benchmarking

In Table 1 we report the parameters used in the benchmarking unless otherwise specified. The bunch consists of a 6D matched Gaussian distribution. The space charge is modelled in both codes by an analytic force which is locally matched with the lattice for the Gaussian ellipsoid with rms properties following the exact local beta functions.

3.5.2.1 Step 1: Transverse phase space

The first step of the benchmarking has the purpose of assuring that the transverse Poincare' sections are identical in the two codes. Nonlinearities are excited using the sextupole strength quoted in Table 1. The space charge is absent for the time being. In order to control the phase space topology we take a working point close to the 3rd order resonance at Q_{x0}=4.338,Q_{y0}=3.2

Table 1: Settings for the benchmarking

Parameter	Value	Units
Sextupole strength K_2	0.2	m^{-2}
Maximum tuneshift ΔQ_x	0.1	
Horiz. size X_{rms}	5	mm
Vert. size Y_{rms}	5	mm
Longitudinal size Z_{rms}	40.35	M
Horiz. emittance $(2\sigma_x)$	12.57	mm mrad
Vert. emittance $(2\sigma_y)$	9.30	mm mrad
Turns for 1 synch. oscillation N_{synch}	15000	
Bunch length $(4\sigma_z)$ τ	3472.7	ns
Kinetic energy E_k	11.4	MeV/u
Gamma transition γ_t	5	
$\Delta p/p$ at $3\sigma_z$	$2.5\text{x}10^{-4}$	

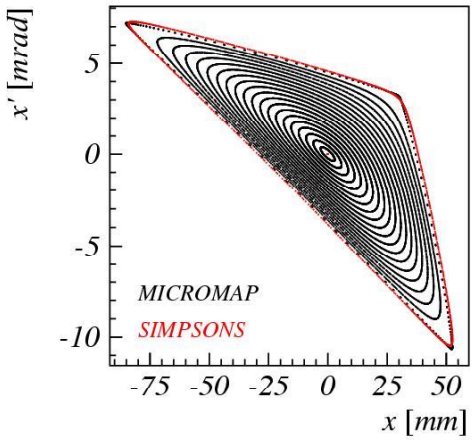

Figure 1: Benchmarking of the phase space without space charge.

In Fig. 1 we show the result of the comparison. The red curve from SIMPSONS is located at the edge of the stability domain: all curves further out are unstable.

3.5.2.2 Step 2: Transverse tune vs. transverse amplitude without sextupole

In this step we control, if the modelling of the frozen space charge has the same impact on the single particle dynamics if the sextupole is deactivated. To this end we compute the nonlinear tune in both transverse planes as a function of the transverse amplitude at z=0. The transverse bare tunes remain as in Step 1 and we take infinitesimal longitudinal oscillations. The tunes are computed with an FFT method in 1024 turns. The results are shown in Fig. 2.

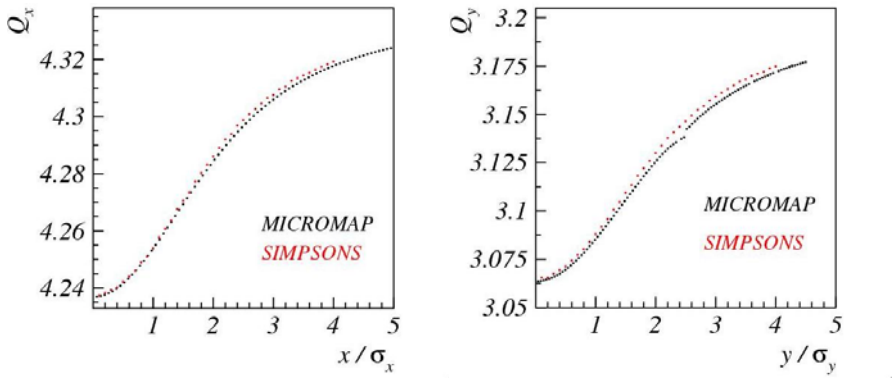

Figure 2: Comparison of a) transverse horizontal and b) vertical tunes.

3.5.2.3 Step 3: Transverse tune vs. transverse amplitude with sextupole

When the sextupole is activated, transverse islands are created at a position controlled by the space charge tune spread ΔQ_x, by the distance of the bare tunes from the resonance, and by the resonance strength. A preliminary test showed that the working point for the steps 1-2 creates islands so far in the phase space to exceed the domain ($\sim 8\sigma_x$) in which the space charge frozen algorithms are applicable. For this reason we move the tunes to Q_{x0}=4.3504,Q_{y0}=3.2 . The dependence of tunes vs. transverse amplitude is shown in Fig. 3.

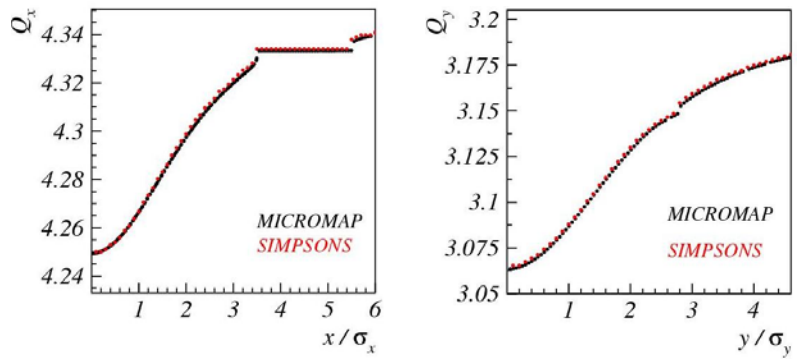

Figure 3: Transverse tunes when the 3rd order resonance is excited.

We find an excellent agreement between SIMPSONS and MICROMAP. This test confirms that in both codes frozen space charge produces the same detuning and the islands are located at the same amplitude (flat between 3.5 and 5.5 s_X in Q_X).

3.5.2.4 Step 4: Phase space with space charge

We compare here the phase space topology in the bunch center at z=0 when sextupole and space charge are present. The results are shown in Fig. 4.

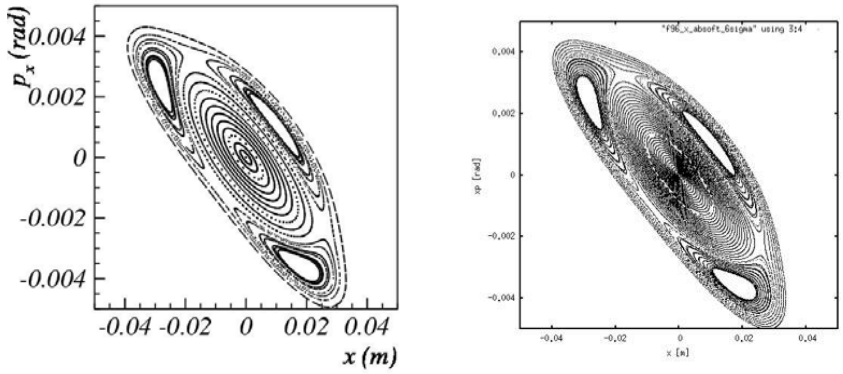

Figure 4: Comparison of phase space when the 3rd order resonance is excited:

a) MICROMAP, b) SIMPSONS .

3.5.2.5 Step 5: Particle trapping

This step benchmarks the full trapping of one test particle during one synchrotron oscillation. The trapping regime is obtained taking a synchrotron tune of $Q_{z0} = 6.6\times10^{-5}$.

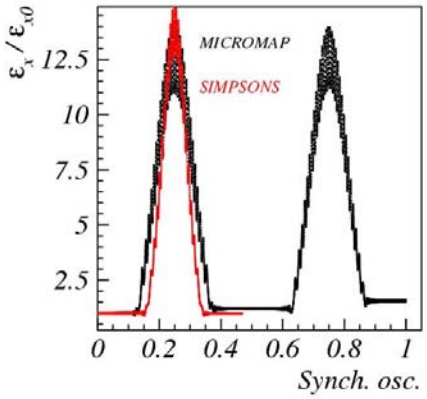

Figure 5: Comparison of single particle invariant in trapping regime.

The parameters of the simulation are those used in the steps 3-4. We take a test particle with coordinates: x=5 mm, x'=y=y'=z'=0, and z=2.5s_z and compute the single

particle invariant. Fig. 5 shows the full trapping. In SIMPSONS, the particle leaves the bucket after the first half synchrotron oscillation. This discrepancy might be due to slight differences in the way the optical elements are represented in the two codes.

3.5.2.6 Step 6: Scattering regime

In this step we compare the effect of the crossing of the 3rd order resonance in 1 synchrotron oscillation for $Q_{z0}=10^{-3}$. Note that the bunch length is now reduced by a factor of 15 in order to keep the momentum spread as for the steps 1-5.

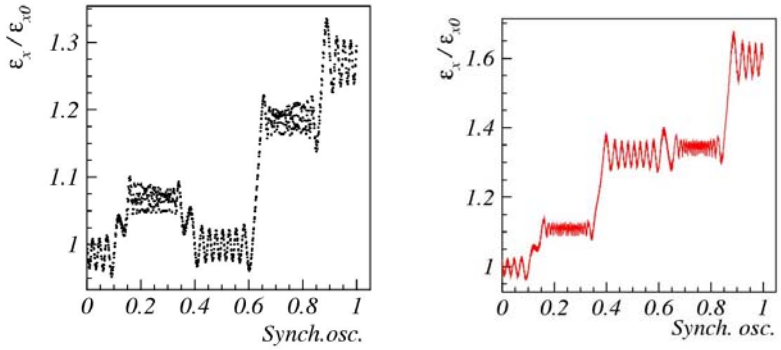

Figure 6: Behaviour of the single particle invariant in 1 synchrotron oscillation:
a) MICROMAP, b) SIMPSONS.

The maximum nominal tune shift in Table 1 is kept also by reducing the number of particles by the same factor. The results are shown in Fig. 6. Note the scatter in the invariant is not equal in both codes as the dynamics is now extremely sensitive to the initial conditions.

3.5.2.7 Step 7: Long term behavior

We compare here the effect of the multiple resonance crossing. The tracking is performed for 200 synchrotron oscillations while all the simulation parameters are as in step 6. The results are shown in Fig. 7. Note the trapping which occurs in a different sequence in a) than in b) due to quasi random process. The maximum value of the invariants does not exceed the outer position of the islands, almost equal in both codes. Note that the results of step 5, $\varepsilon_x/\varepsilon_{x0} \sim 12.5$ do not contradict the actual $\varepsilon_{xmax} / \varepsilon_{x0} = 21$. In step 5 the adiabaticity allows the test particle to remain close to the fixed point, whereas here the particle explores the full area allowed by the islands up to the separatrix because of the scattering regime.

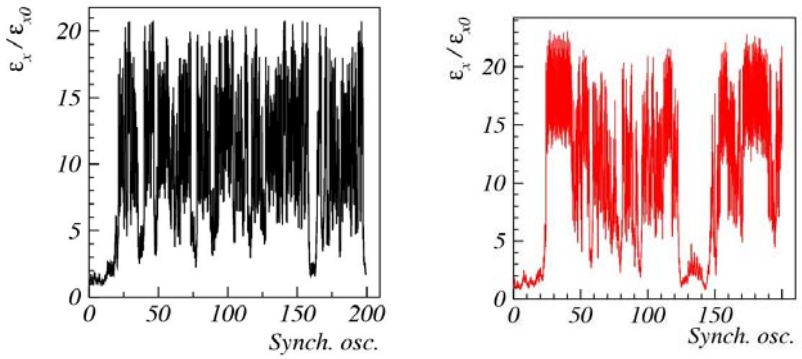

Figure 7: Single particle invariant during long term tracking:
a) MICROMAP, b) SIMPSONS.

3.5.2.8 Step 8: Long term behavior of full bunch

This step benchmarks the transverse emittance evolution of the full bunch of 1000 macro-particles. The number DN_t of particles, which can become trapped, is given by (see [4])

$$\frac{\Delta N_t}{N} \geq \frac{Q_{x0} - Q_{x,res}}{\Delta Q_x} \qquad (1)$$

We improve the statistics in the halo by changing the horizontal tune to Q_{x0}=4.3604 so as to increase the halo density to 27% of the total number of particles. Fig. 8 shows the result of this benchmark.

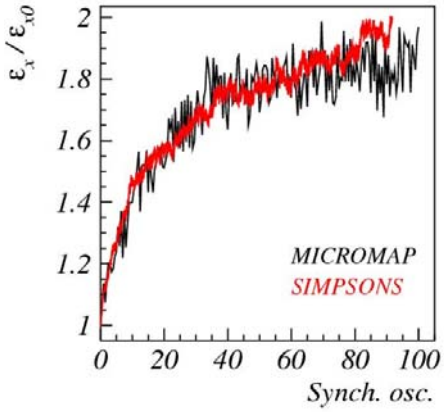

Figure 8: Emittance evolution for the full bunch.

By assuming that all trapped particles are uniformly distributed in the halo we can estimate the asymptotic rms emittance growth as

$$\frac{\tilde{\epsilon}_x}{\tilde{\epsilon}_{x0}} \geq 1 - \frac{\Delta N_t}{N} + \frac{\Delta N_t}{N} \frac{\epsilon_{x,max}}{4\,\tilde{\epsilon}_{x0}}, \tag{2}$$

where $\varepsilon_{x,max}$ is the maximum single particle emittance [4]. Repeating step 7 for Q_{x0}=4.3604 we find $\varepsilon_{x,max}$ / ε_{x0} = 10, which in terms of the rms emittance used here yields $\epsilon_{x,max}/\tilde{\epsilon}_{x0} = 16.5$. By applying Eq. 2 we then find $\tilde{\epsilon}_x/\tilde{\epsilon}_{x0} \geq 1.84$ which is consistent with Fig. 8.

3.5.3 Conclusion

The benchmarking between MICROMAP and SIMPSONS has produced excellent agreement. The trapping and scattering regimes have been found identical for a full ensemble of particles. Obviously, we cannot expect identical orbits for single particle in a chaotic regime, but the agreement is excellent as far as ensemble averages are concerned like rms emittances and halo radii. The comparison of the emittance growth has also shown excellent agreement. A benchmarking on loss prediction and on the contribution of the chromaticity as well as on the effect of self-consistency (update of space charge force) is left for future studies.

3.5.4 References

1. P. Spiller, Proc. 39th ICFA Advanced Beam Dynamics Workshop “HB2006” (Tsukuba, 2006).
2. G. Franchetti, I. Hofmann, M. Giovannozzi, M. Martini, and E. Métral, *Phys. Rev. ST Accel. Beams*, **6**, 124201 (2003).
3. G. Franchetti, I. Hofmann, Proc. 33rd ICFA workshop, AIP **773**, 122.
4. G. Franchetti and I. Hofmann, 39th ICFA Advanced Beam Dynamics Workshop “HB2006” (Tsukuba, 2006).
5. G. Franchetti, I. Hofmann, Nucl. Instr. and Meth. A 561, (2006), 195.
6. G. Franchetti, I. Hofmann, and G. Turchetti, *AIP Conference Proceedings* **448**, 233 (1998).
7. S. Machida, AIP-297,1993.
8. G. Franchetti *et al.* GSI Scientific report 2005, ISSN 0174-0814.

3.6 BENCHMARKING COLLECTIVE EFFECT MODULES IN THE ORBIT SIMULATION CODE

A. Shishlo, S. Cousineau, V. Danilov, J. Galambos, S. Henderson, J. Holmes,
M. Plum, Y. Sato, ORNL, Oak Ridge, Tennessee, USA
mail to: shishlo@ornl.gov

3.6.1 Introduction

ORBIT (Objective Ring Beam Injection and Tracking) began as an “in house” accelerator code for the Spallation Neutron Source (SNS) project in 1997 [1]. ORBIT was designed to accommodate an expandable set of collective effects models such as space charge and wakefields.

We are going to present results of several benchmarking techniques and their combinations for these models: comparison between two computer codes; comparison between simulation and analytic results; and comparison between simulation and real experimental data. Most our benchmarks of experimental data are related to Proton Storage Ring (PSR) at Los Alamos.

3.6.2 Longitudinal Impedance and Longitudinal Space Charge

ORBIT treats longitudinal impedances and/or space charge in a fashion similar to the ESME code [2]. The longitudinal impedance is represented in terms of harmonics of the fundamental ring frequency. Particles are binned longitudinally and the binned distribution is Fourier transformed. The Fourier transformed distribution is multiplied by the impedance to give the longitudinal kicks to the particles. This ORBIT module was successfully benchmarked against the ancestor ESME code and also against experimental data from PSR showing long-lived linac micro-bunch structure during beam storage with no ring rf bunching. Analysis of the experimental data and particle-in-cell ORBIT simulations of the experiments indicated that longitudinal space charge, coupled with energy spread effects, is responsible for the sustained micro-bunch structure [3].

3.6.3 Transverse Impedance Modules

There are two transverse impedance modules in the ORBIT code. The first is based on a frequency domain representation, and the second uses a simple resonance structure in the time domain. The physical approaches implemented in these modules are different, but results of simulations for the same problems agree well.

The frequency domain module implements the same FFT approach as the longitudinal impedance module. The detailed description of the algorithm of this module can be found in the PAC'01 paper [4]. The benchmark of this module has been performed as a comparison between results of simulations and an exactly solvable case of beam dynamics [4]. The case considers an evolution of a coasting beam with Lorentz energy distribution in a constant focusing storage ring with single harmonic impedance. The simulation preserved even small details of an analytic solution, showing the ability of the code to give accurate results [4].

The time domain module uses a wake field of the local element in the lattice to calculate the transverse force kick for each particle in the bunch [5, p.58, formula 2.50].

$$\overline{F}(z_0) = -e \cdot \int_{z_0}^{\infty} j_1(z) \cdot W_1\left(\frac{z - z_0}{\beta \cdot c}\right) \cdot dz \qquad (1)$$

where $\overline{F}$ is the force integrated over the length of the element; j_1 is the line density of the first moment of the bunch; and W_1 is the wake function of the element.

The wake function should satisfy a phasor condition [5]. In this case the effective numerical integration in the formula (1) could be performed over all previous bunch passages through this lattice element. The simplest example of such a function is an RLC resonant element. For this module in ORBIT, the user can specify a transverse impedance element as a sum of any number of RLC elements.

3.6.4 2.5D and 3D Space Charge Modules

Space charge effects are an important factor in determining beam profiles, instabilities and halo generation in high intensity, low-energy storage rings. ORBIT includes two modules to simulate the space charge force in long bunches. The 2.5D Space Charge module uses a simplified approach, but it is far less demanding with respect to computer resources.

The 2.5D space charge model is implemented as a series of transverse momentum kicks separated by other transport operations on the lattice elements. Particles are binned in a 2D rectangular grid using a second order distribution scheme. The potential for the distributed charges is then solved on the transverse grid using a fast FFT solver. Conducting wall (circular, elliptical, or rectangular beam pipe) boundary conditions are then imposed using a method described in Ref. [6]. The particles' kicks are weighted by the local longitudinal density to account for bunch factor effects. This is the reason we call the model 2.5D. This module has been successfully used to explain the beam transverse distribution in the PSR ring [7].

The 3D space charge model is a simple generalization of the 2.5D routine. The 3D rectangular grid is a set of 2D transverse grids. The potential is solved for each 2D grid using the distributed charges and fast Fourier transforms. Particle kicks are obtained by interpolating the potentials in the 3D grid. This module was benchmarked against the 2.5D module and also against analytic models [8].

3.6.5 Electron Cloud Module

The instability caused by an electron cloud effect (ECE) may set an upper limit to the intensity of proton storage rings. This type of instability has been observed in PSR for many years. The electron cloud module of the ORBIT code includes self consistent dynamics of the proton beam and of the electrons including both their space charge interactions and their motion in external electric and magnetic fields.

In the ECE simulation algorithm the ring is covered by a set of Electron Cloud Nodes (ECN). Each node is independent from the others, and calculates momentum kicks induced by the electron cloud upon particles in the bunch. More ECNs imply more realistic simulations, but the calculation time becomes a limiting factor. The details of the EC module implementation have been discussed in Ref. [9].

In each ECN the physical system consists of the proton bunch, electrons inside a special region that is called an electron cloud region, and a perfectly conducting pipe whose surface can be a source of primary or secondary electrons (see Figure 1). The electron dynamics is calculated using time as the independent variable. The changes in proton momentum due to the electron cloud are accumulated as kicks and applied to protons at the end of propagation through ECN.

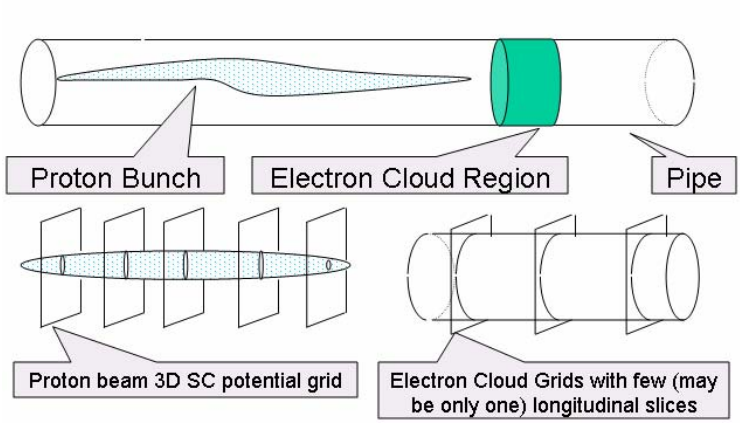

Figure 1: Simulated physical system for the Electron Cloud Node in ORBIT.

The length of each ECN should be short enough to ignore changes in Twiss parameters inside. Each region has its own bunch of electrons with its own unique history and dynamics. The limited length of each ECN creates a technical problem with the electron cloud simulation time. If we cover the whole ring with ECNs the time needed will be unrealistic. To simplify the problem we introduced an effective length of the Electron Cloud Node in ORBIT. This approach gives an overestimation of the electron cloud action on the proton bunch, and it provides a very conservative estimate of the stability limit.

The secondary electron emission processes on the beam pipe surface are simulated by using a modified model of Furman and Pivi [10].

3.6.5.1 Electron Cloud Module Benchmark against Analytic Two-Stream Model

To benchmark ORBIT's EC module, an analytically solvable two-stream model [11] has been used. The model considers a ring filled with two uniform circular bunches with opposite charges. One of bunches moves along the ring, which is an accelerator lattice with constant focusing. The two bunches interact electromagnetically. The analysis in Ref. [11] shows that the system can be unstable with regard to transverse oscillations of bunches. Parameters of the model have been chosen close to the SNS case with nominal proton bunch density and size. To save simulation time only 1/178 part of the SNS ring length has been used. This means that we considered only one wavelength of the dipole instability oscillations. Twenty ECNs were used to cover this part of the ring. The development of the instability has been simulated for different values of the neutralization factor

$$\eta = \rho_e / \rho_p \tag{2}$$

which is the ratio of electron cloud and proton bunch densities. For small values of η (several percent) the ratio between the electron and proton oscillation amplitudes is on the order of one hundred. Small oscillations of the proton bunch are accompanied by significant electron cloud oscillations, which destroy the basic assumption of the model about the uniform covering of the proton bunch by the electron cloud. Therefore, we can not expect exact agreement between the analytic model and the simulation results. A detailed analysis of this benchmark can be found in Ref. [12].

Figure 2 shows the instability growth rate as a function of the neutralization factor for the two-stream model.

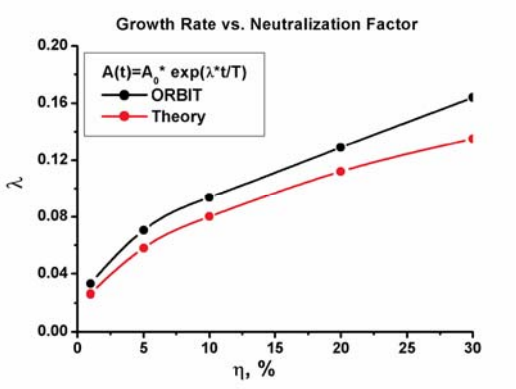

Figure 2: Computational and theoretical growth rates versus neutralization factor [12]. The upper curve is the ORBIT simulation, and the lower curve is the theory prediction.

3.6.5.2 Electron Cloud Module Benchmark against PSR Data

The purpose of this benchmark [13] was to demonstrate that the ORBIT code with the electron-cloud (EC) module can reproduce the main features of electron-cloud driven instabilities in a real machine, namely in the Los Alamos Proton Storage Ring [14]. The benchmark was focused on a limited number of the PSR instability features because of the high computational cost of each simulation. In particular, the following has been demonstrated:

- Existence of the instability.
- The coupling between proton instabilities and electron production. An intense electron flux coincides with high amplitude coherent proton bunch oscillations at the onset of substantial beam losses.
- Agreement with the observed frequency spectrum of the proton bunch oscillation.
- An asymmetry in directions where instabilities occur. The instabilities have been seen mostly in the vertical direction.
- The relationship between the maximum number of protons in the bunch and the threshold rf voltage.

Figure 3 shows that development of the proton bunch instability causes the intensification of the electron production and vice versa. The same effect has been observed in PSR.

When the ECNs were placed only in the drift regions, the simulations showed instabilities in both vertical and horizontal planes. The growth rate of the horizontal oscillations sometimes was bigger than the rate in the vertical plane. After taking account of the electron cloud in the dipole magnets we reversed this situation. This effect can be explained by the fact that electrons inside the dipoles move primarily along the vertical magnetic field, so the horizontal oscillations of the electrons are suppressed.

The use of a realistic distribution of several ECNs in the lattice also predicts the correct frequency of the proton bunch vertical oscillations.

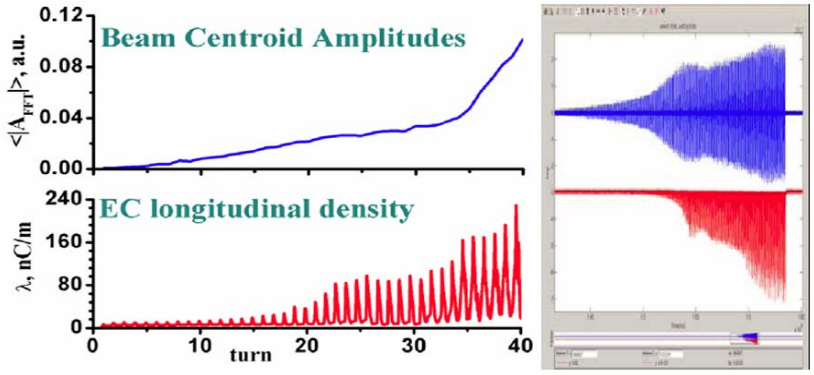

Figure 3: Instability development for one ECN in the PSR lattice. The left half is the simulation results, and the right half is the real PSR data.

In practice, the electron-cloud-related instabilities in the PSR ring are controlled by increasing the voltage to the rf cavities. The higher rf buncher voltage leads to a larger energy spread in the proton bunch which stabilizes the bunch with respect to ECE.

The results of simulations with different rf voltage values clearly demonstrate that instabilities can be suppressed by applying a sufficient rf voltage. Also, with increasing voltage the growth time of instabilities increases from tens to hundreds of turns. These numbers are in good agreement with experimental results.

3.6.6 Conclusions

Many successful benchmarking results have demonstrated that the ORBIT code can be successfully used for the realistic simulation of collective effects in accumulator rings. These effects include impedances, space charge, and electron clouds. The flexible structure of the code allows combining these effects in user defined configurations, and it presents the possibility of further development of ORBIT.

3.6.7 Acknowledgement

This research was carried out in ORNL/SNS which is managed by UT-Battelle, LLC, for the U.S. Department of Energy under contract DE-AC05-00OR22725. We also used resources of the National Energy Research Scientific Computing Center (NERSC), which is supported by the Office of Science of the U.S. Department of Energy under Contract No. DE-AC03-76SF00098.

3.6.8 References

1. J. A. Holmes, S. Cousineau, V.V. Danilov, J. Galambos, A. Shishlo, W. Chou, L. Michelotti, F. Ostiguy, and J. Wei, in Proceedings of the 20th ICFA Advanced Beam Dynamics Workshop on High Intensity and High Brightness Hadron Beams, Fermilab, 2002 (AIP, Melville, NY, 2002); J. A. Holmes, S. Cousineau, V.V. Danilov, S. Henderson, A. Shishlo, Y. Sato, W. Chou, L. Michelotti, and F. Ostiguy, in The ICFA Beam Dynamics

Newsletter, Vol. 30, 2003.
2. J. A. MacLachlan, Longitudinal "Phase Space Tracking with Space Charge and Wall Coupling Impedance," Fermi National Accelerator Laboratory, FN-446, (1987).
3. S. Cousineau,V. Danilov, and J. Holmes, Phys. Rev. ST Accel. Beams 7, 094201 (2004).
4. V.Danilov, J. Galambos, J. Holmes,, "Transverse Impedance Implementation in ORBIT," PAC'01, Chicago, IL, June 2001, p. 1752.
5. A. W. Chao, "Physics of Collective Beam Instabilities in High Energy Accelerators," Wiley, New York, 1993.
6. F. W. Jones, "A Method for Incorporating Image Forces in Multiparticle Tracking with Space Charge," EPAC 2000, Vienna, p. 1381.
7. J. D. Galambos, S. Danilov, D. Jeon, J. A. Holmes, and D. K. Olsen, Phys. Rev. ST Accel. Beams 3, 034201 (2000)
8. J.A. Holmes, V. Danilov, J. Galambos, A. Shishlo, S. Cousineau, W. Chou, L. Michelotti, F. Ostiguy, J. Wei, "Orbit: Beam Dynamics Calculations For High-Intensity Ring," EPAC'02, Paris, June 2002, p. 1022.
9. A. Shishlo, Y. Sato, J. Holmes, S. Danilov, S. Henderson,, "Electron-Cloud Module for the ORBIT Code," in Proceedings of the 20th ICFA Advanced Beam Dynamics Workshop on Electron Cloud Effects ECLOUD'04 (Napa, CA, USA April 2004), p. 241.
10. M.A. Furman and M.T.F. Pivi, Phys. Rev. ST Accel. Beams 5, 124404 (2002).
11. D. Neuffer, E. Colton, D. Fitzgerald, T. Hardek, R. Hutson, R. Macek, M. Plum, H. Thiessen and T.S. Wang, NIM A321, 1-12 (1992).
12. Y. Sato, A. Shishlo, S. Danilov, J. Holmes, S. Henderson,, "Simulation of E-Cloud Using Orbit: Benchmarks and First Application," in Proceedings of the 20th ICFA Advanced Beam Dynamics Workshop on Electron Cloud Effects ECLOUD'04 (Napa, CA, USA April 2004), p. 245.
13. A. Shishlo, Y. Sato, S. Cousineau, V. Danilov, S. Henderson, J. Holmes, R. Macek, S.Y. Lee, "Self-Consistent Electron-Cloud Simulation for Long Proton Bunches," PAC'05, Knoxville, TN 2005, p.722.
14. R. Macek, et al, "Electron proton two-stream instability," PAC'01, Chicago, June 2001, p. 688.

3.7 Benchmarking in the Synergia Framework

Panagiotis Spentzouris, Fermilab, PO Box 500, Batavia, IL 60510
mail to: spentz@fnal.gov

3.7.1 Synergia

Synergia [1] is a parallel, 3D Particle In Cell (PIC) beam dynamics framework, with space-charge and impedance modeling capabilities. Synergia combines newly developed and existing solvers and physics modules (see below) in a fully configurable and extensible framework, with a straightforward, yet powerful, user interface. Figure 1 shows the relationship between Synergia the components, solvers, and the numerical libraries utilized by the framework.

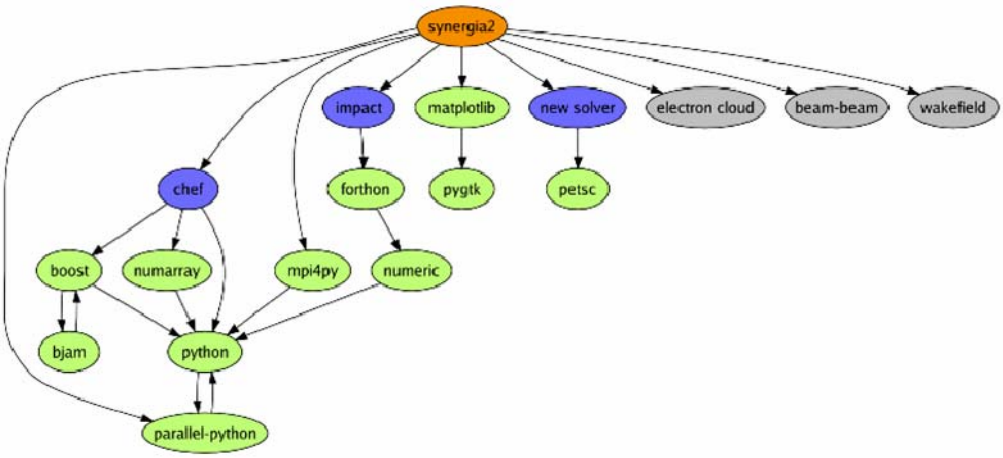

Figure 1: Synergia relations diagram.

Synergia features arbitrary order Lie maps for magnetic optics and it employs multiple Poisson solvers, one FFT based, and one multigrid based for its 3D parallel space-charge physics module. Synergia has unique capabilities for synchrotrons, boosters, and storage rings: multi-bunch, ramping and rf and magnet, multi-turn injection, and active feedback modelling. Synergia has been used extensively to model the FNAL Booster [2]. The simulations have helped provide guidance to accelerator operators to reduce losses and maximize the intensity of the Booster.

3.7.2 Space-Charge Implementation Benchmarking

In order to have confidence in our space-charge simulations, we follow three steps of testing for the validation of our code:

1. Employ a test suite of space-charge problems for code benchmarking [3]. This test suite includes models of several cases simple enough that the solutions are known either analytically or can be found to essentially arbitrary accuracy through numerical means.
2. Compare simulation results with other codes with appropriate model accuracy and level of approximation for the problem at hand.
3. Compare with results of controlled beam experiments.

In the following, we will present a few examples of the application of these three steps for the validation of the Synergia model implementation.

3.7.2.1 Test suite examples

For a K-V distribution the charge density across the beam is constant and the forces associated with space charge vary linearly with the coordinates x and y. The evolution of the beam envelope can be calculated exactly by integrating the envelope equations (see below). As a first check, we compare the evolution of a K-V beam as predicted by Synergia to the solution of the envelope equations:

$$\sigma_x'' + K_x\sigma_x - \frac{\varepsilon_{rms}^2}{\sigma_x^2} = \frac{\xi}{4(\sigma_x + \sigma_y)}$$

and

$$\sigma_y'' + K_y\sigma_y - \frac{\varepsilon_{rms}^2}{\sigma_y^2} = \frac{\xi}{4(\sigma_x + \sigma_y)}, \qquad (1)$$

where $\xi = 4Q^2 r_0 \lambda/(A\beta^2\gamma^3)$, with Q the charge of a beam particle in units of e, r_0 is the classical proton radius, λ is the line charge density, A is the atomic number, $K_{x/y}$ are the focusing strengths, $\sigma_x = \langle x^2\rangle^{1/2}$, $\sigma_y = \langle y^2\rangle^{1/2}$, and ε_{rms} is the unnormalized r.m.s.emittance:

$$\varepsilon_{rms} = \sqrt{\langle x^2\rangle\langle x'^2\rangle - \langle xx'\rangle^2} = \frac{\langle x^2\rangle}{\beta_{Twiss}}. \qquad (2)$$

Note that the r.m.s. value of x in a K-V beam of radius a is given by $\langle x^2\rangle = a^2/4$.

In Figure 2 we compare the numerical solution of Equations (1) to the Synergia result for the FODO channel defined by the following MAD8 [4] file:

```
drs: drift, l=7.44d-2
drl: drift, l=14.88d-2
qd7: quadrupole, l=6.10d-2, k1=-103.11d0
qf7: quadrupole, l=6.10d-2, k1= 103.11d0
channel: line=(drs, qd7, drl, qf7, drs)
```

The file describes a channel consisting of a drift (drs), followed by a quadrupole magnet (qd7), another drift (drl), another quadrupole (qf7) and a copy of the initial drift (drs). The lengths in meters are given by the l parameter. The parameter $k1$ describes the magnetic field gradient in units of meters^{-2} : $k_1 = \frac{1}{(B\rho)}\frac{\partial B_y}{\partial x}$, where $B\rho$ is the ratio of the particle momentum to its charge.

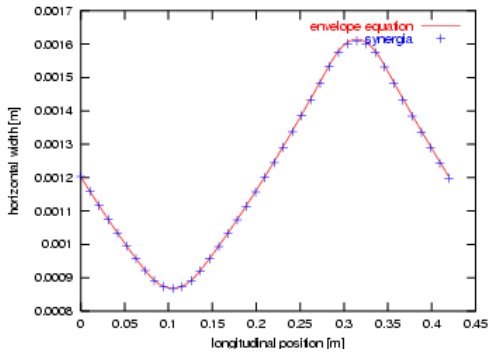

Figure 2: Comparison of the Synergia prediction for the evolution of a 0.5 A beam in the FODO lattice described in the text to the solution of the envelope equations.

For this comparison we used a K-V beam with a kinetic energy 0.0067 GeV and two

dimensional transverse emittance 3.1×10^{-6} m rad in both the horizontal and vertical planes. Figure 2 shows the comparison of the calculated horizontal beam width for a matched beam of 0.5 Amps. Figure 3 shows the effect of taking into account space charge in the matching procedure in the evolution of the horizontal beam width (horizontal beam envelope). The Synergia prediction is consistent with the numerical solution of the envelope equations. The differences between the curves presented in Figure 3 show the magnitude of the space-charge effect.

In the case of a more realistic beam distribution, such as a Gaussian distribution, the envelope equations can model the evolution of the second moments of the beam distribution under the assumption that the emittance evolution is known. In the next comparison presented here we assume that the emittance remains constant. We compare the prediction of Synergia with the prediction of the envelope equations for the evolution of the width of a Gaussian beam in a lattice cell of the FNAL Booster. Here we use a beam that is Gaussian in the transverse coordinates and uniform in the longitudinal coordinate. The results are shown in Figure 4. The current used in this simulation is a typical operating current for the machine (0.420 Amps).

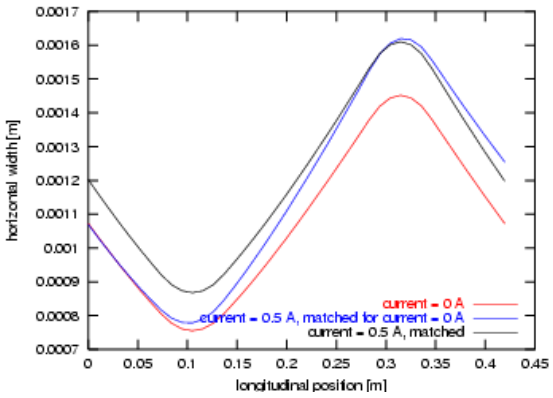

Figure 3: Effect of including space charge in the matching condition, as calculated using Synergia.

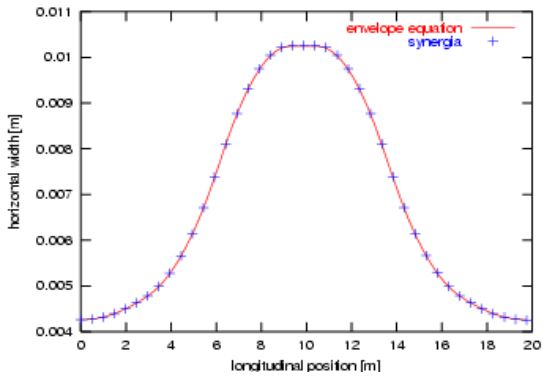

Figure 4: Comparison of the beam width evolution in a FNAL Booster cell as predicted by Synergia and the solution of the envelope equations.

Another simple comparison we can make with analytic calculations is to compare the Laslett tune shift for a K-V beam with results from a Synergia simulation. We use

the formula [5]:

$$\Delta\nu = \frac{-Nr_0}{8\pi\beta^2\gamma^3\varepsilon_{rms}}, \tag{3}$$

where N is the number of particles in the beam, r_0 is the classical proton radius and ε_{rms} is the unnormalized r.m.s. emittance as defined in Equation (2). The Synergia prediction for the tune shift is obtained by taking the peak of the Fourier transform of the horizontal and vertical position of individual particles, as a function of s, sampled each cell (24 times per turn) for 100 turns. Here s is the coordinate along the path of the reference (or design) trajectory. By sampling each cell, we are able to extract the integer portion of the tune. Sampling once per turn is sufficient to extract the fractional tune. Figure 5 shows the comparison between the results from Equation (3) and Synergia for the FNAL Booster (``bare", linear lattice) and for different beam currents. The agreement is very good; we thus conclude that Synergia can reliably reproduce analytical calculations of space-charge effects.

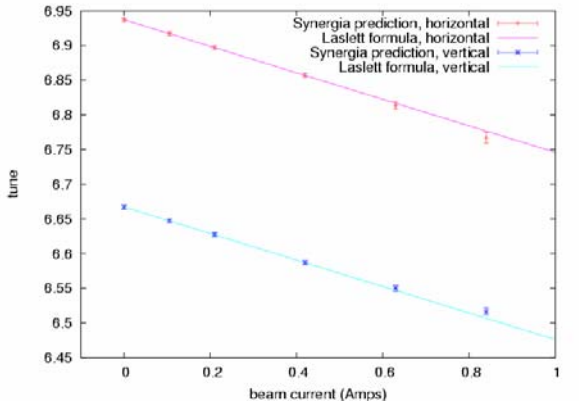

Figure 5: Comparison of the horizontal and vertical tune shifts calculated using Synergia and using equation (3).

3.7.2.2 Comparison with other codes

It is also important to cross-check the results from Synergia with other codes with space charge capabilities. A benchmarking exercise comparing several codes, including Synergia, appears in Ref. [6]. As a simpler test, we include a consistency test comparing Synergia with the MaryLie/IMPACT (ML/I) code [7]. The comparison is done for two cases:

1. the FODO channel described in the previous section, using a 0.5 A matched K-V beam with two-dimensional transverse emittance of 1.0×10^{-6} m rad in both planes.
2. a 0.1 A cold proton beam in a FODO channel with rf cavities.

For each of these comparisons we used a common input file of beam particles for both the Synergia and ML/I simulations. In Figure 6 we show the comparison of the horizontal r.m.s. beam size predictions from the two codes for case 1. The agreement is very good. The difference between the prediction of the two simulations for the r.m.s. width of the beam at the end of the channel is 0.27%. This slight variation in the final

answer is due to minor differences in the implementation of the Poisson solver and differences in the problem description in the simulation, such as the number of slices used in the split-operator particle advance algorithm.

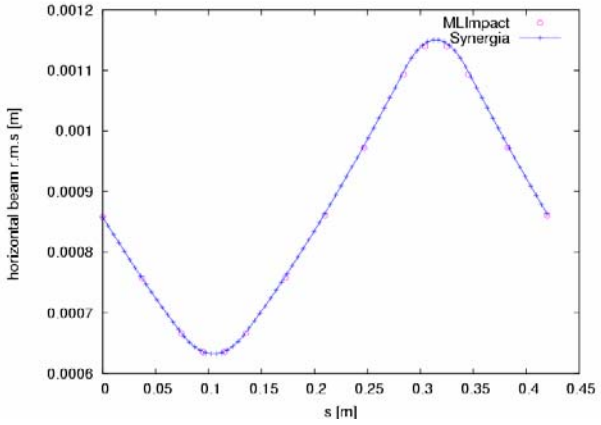

Figure 6: Comparison of the Synergia and MaryLie/IMPACT predictions for the horizontal r.m.s. beam size of a K-V beam propagating in the FODO channel (case 1) described in the text as a function of s.

In Figure 7 we show the results for case 2. The agreement between the two codes and the prediction of the 3D envelope equation [8] is excellent. In this case, we model a cold, uniform density, 100 mA proton beam, with kinetic energy of 250 MeV, in a FODO channel with rf cavities. The channel consists of two 0.15 m focusing quadrupoles (fquad), with a gradient of 6 T/m, a 0.30 m defocusing quadrupole (dquad), with -6 T/m gradient, four 0.10 m drifts (dr), and two 1 m rf cavities (cav), with frequency 700 MHz. The rf cavities are treated by computing the linear transfer maps, including the effects of acceleration, and using numerical integration of the map coefficients. This requires a knowledge of the on-axis electric field and its derivative. For this example, the functional form of the field is given by $E(z) = E_0 \cos(\omega t + \phi)$. The beamline is arranged in the following way: (fquad dr cav dr dquad dr cav dr fquad). The cavity phases have been set so that the first cavity accelerates the beam and the second decelerates it by the same amount. Since the beam is cold, the rms equations describe the problem exactly, as long as the beam remains cold and uniform, so there is a matched condition where the final envelopes are identical to the initial values. We obtained the matched solution by solving the envelope equations in three dimensions [8]. The Synergia toolkit includes envelope equation solvers used to find matched beam parameters. We generated a numerical realization of the matched uniform distribution consisting of 100,000 particles. These particles were used as the input of both Synergia and ML/I.

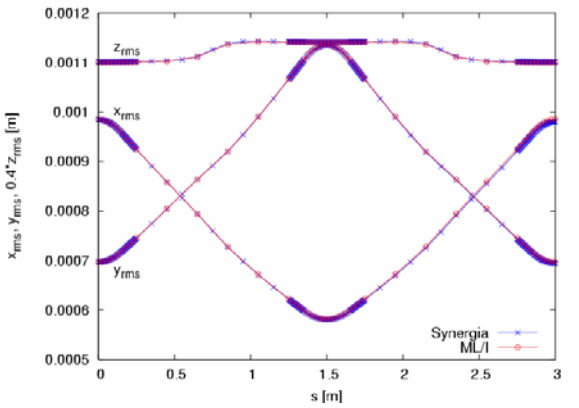

Figure 7: Comparison of the Synergia and MaryLie/IMPACT predictions for the r.m.s. beam envelopes of a cold beam propagating in the FODO channel with rf cavities (case 2) described in the text.

The comparison between the Synergia and ML/I codes demonstrates that both implementations are consistent, and, most importantly, that they are in excellent agreement with the theoretical expectations for the test cases shown. In addition, the small differences in the obtained results demonstrate the level of uncertainty due to different choices of solvers and their parameters.

3.7.2.3 Synergia tests at the Fermilab Booster

The Booster accelerator [2] is the first circular accelerator in FNAL's accelerator chain. It is a synchrotron, i.e the field of its magnets changes with time, as the beam gets accelerated, in order to keep the beam radius constant. The Booster accelerates protons from a kinetic energy of 400 MeV to 8 GeV. It is a rapid-cycling machine, ramping the field of its magnets at 15 Hz. The Booster radius is 75.47 meters and its lattice consists of 24 lattice units or cells. The main components of each cell are four combined function magnets, i.e magnets which combine both quadrupole fields (for focusing) and dipole fields (for bending). The beam is accelerated by seventeen radio-frequency (rf) cavities, with frequency that slews from 37.7 MHz at injection to 52.8 MHz at extraction. The nominal average current immediately after injection is ~420 mA. Typically, the injection process lasts for ten Booster turns. The beam is injected from the FNAL linear accelerator, the linac, and it is a stream of bunches equally spaced at the linac RF frequency of 201.2 MHz. Space-charge effects have long been believed to be responsible for a significant fraction of the observed losses in the Booster during the first 2 ms of the cycle (the injection, capture, and bunching phases).

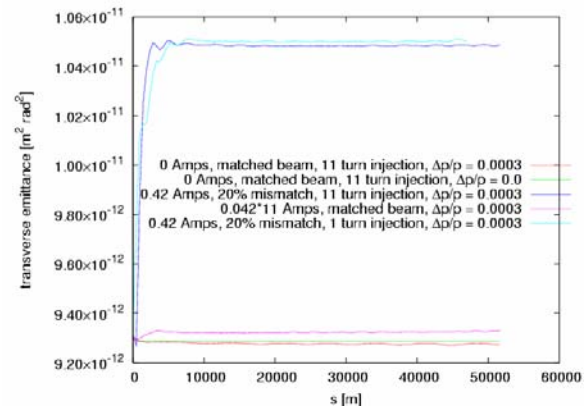

Figure 8: Normalized 4-D transverse emittance in $m^2\ rad^2$ for different initial conditions. The red and green curves correspond to a matched beam, with space-charge effects turned off (0 Amps) with and without a momentum spread of 0.0003, respectively. The purple and light blue curves correspond to a beam of 0.420 Amps total current and momentum spread of 0.0003, matched and mismatched respectively. All of these curves are for 11 turn multi-turn injection (0.038 Amps/turn). The dark blue curve corresponds to a single turn injection simulation of a 0.420 Amp mismatched beam with 0.0003 momentum spread.

The first example of a Synergia test with the Fermilab Booster is an investigation of how space-charge and chromatic effects affect the emittance of the Booster, in the presence of beam envelope parameter injection mismatch, and comparison with model predictions. For this problem, we simulate a coasting beam under a range of initial conditions for matched and unmathed beams, with different intensities and momentum spread. We use 96 space-charge kicks per turn, calculated on a $33\times33\times257$ computational grid with an average of four particles per grid cell. In Figure 8 we plot the normalized 4-D transverse emittance[2] for five different initial beam conditions, described in the caption of the figure. As expected, in the cases where the beam was matched there is no emittance growth. That is the case for both zero and non-zero momentum spread, and for space charge. (Our matching procedure takes into account space-charge effects on the second moments of the beam). In the mismatched cases we observe a 12% increase of the beam emittance during the first 10 to 15 turns after injection. The effect is a combination of chromatic and space-charge effects and it is very similar for both the single- and multi-turn injection cases. The total current is the same, 0.420 Amps, in both cases. The emittance growth can be related to the conversion of beam free energy from mismatch oscillations into thermal energy of the beam, due to the effect of the non-linear space-charge forces [9]. We compare our result with the prediction of the free-energy model for the breathing mode case. In our case, where the space-charge tune shift divided by the tune is small ($\frac{\Delta\nu}{\nu}=-1.15\%$), the free-energy model prediction for emittance growth can be approximated by

$$\frac{\varepsilon_f^T}{\varepsilon_i^T}=1+4\left[(\mu-1)^2-(\mu-1)^3\right]+\mathrm{O}((\mu-1)^4), \qquad (4)$$

[2]The 4-D emittance is the square root of the determinant of the covariance matrix of the transverse phase space.

where μ is the mismatch parameter, and $\varepsilon^T_{f,i}$ are the final (f) and initial (i) 4-D transverse emittances. With a mismatch parameter of 1.2, as in the case of our simulation, the model predicts a 4-D transverse emittance growth $\varepsilon^T_f/\varepsilon^T_i = 1.13$ to be compared with the 1.12 we obtained from the simulation.

For our second Booster example, we compare the Synergia space-charge tune shift prediction for a coasting beam in the Booster with experimental results. The experiment was performed by measuring beam transmission versus machine tune, for different beam intensities. We used a coasting beam with the Booster operating DC (no ramping magnets). The machine tune was changed using the corrector quadrupole circuits. The response of the machine (tune change) to the change of corrector current was calibrated by pinging the beam and directly measuring the tunes with a spectrum analyzer, with one Linac turn injected in the machine. The beam transmission was determined by measuring the beam current at injection and at 2000 turns after injection. The objective was to excite a parametric resonance for cases of different number of Linac turns injected in the Booster. The difference in quadrupole current required to hit the resonace for the runs with higher injection current from the qudrupole current required to excite the resonance in the case of one turn injection provides a measure of the space-charge induced tune shift.

We took data for three different values of the injected beam current 1, 3, and 9 injected Linac turns (approximately 0.042, 0.126, and 0.378 Amps respectively). For each case of different injected beam current we measured the transmission for a range of values of the machine tune, by varying the corrector quadrupole strengths. Resonances were identified by zero transmission; our quadrupole current scan was fine enough to allow to traverse the resonance with multiple data points across its width. We then fit the transmission versus tune curves to obtain the location and width of the resonance, and by subtracting the location of the resonace for the case of one turn injection, extract the space-charge tune shift. In the simulation, we performed an FFT of the beam envelope to extract the tune. Figure 9 shows a comparison of the measured and simulated tune shifts versus the number of turns of injected Linac beam, and the resonance widths. The results are in excellent agreement.

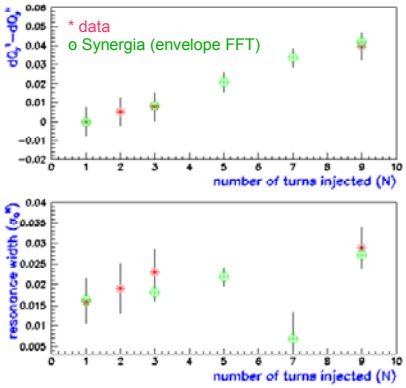

Figure 9: Measured (red) and Synergia calculated (green) space charge tune depression (top) and resonance width (bottom) versus the number of injected turns in the Booster.

3.7.3 References

1. http://cd-amr.fnal.gov/aas/Advanced_Accelerator_Simulation.html; Journal of Computational Physics, Volume 211, Issue 1 , 1 January 2006, Pages 229-248.
2. Booster Staff 1973 Booster Synchrotron ed E L Hubbard Fermi National Accelerator Laboratory Technical Memo TM-405
3. "A test suite of space-charge problems for code benchmarking". J. Amundson, P. Spentzouris, J. Qiang, R.D. Ryne , A. Adelmann. EPAC-2004-WEPLT047, Jul 2004. Presented at the 9th European Particle Accelerator Conference (EPAC 2004), Lucerne, Switzerland, 5-9 Jul 2004.
4. F.Christoph Iselin, ``The MAD program(Methodical Accelerator Design) Version 8.13/8", Physical Methods Manual, CERN/SL/92, 1992.
5. Laslett L.J. 1963 Proceedings of the 1963 Summer Study of Storage Rings, Accelerators and Experimentation at Super-High Energies p. 324
6. I. Hofmann, et al., Proceedings of the PAC05 Particle Accelerator Conference, Knoxville, TN, May 16-20, 2005.
7. http://scidac.nersc.gov/accelerator/mli/manual.pdf
8. R.Ryne 1995, Los Alamos National Laboratory Report No. LA-UR-95-391, e-Print Archive: acc-phys/9502001
9. M. Reiser, Theory and Design of Charged Particle Beams Weiley, N.Y. 1994, pp. 470-473; M. Reiser J. Appl. Phys. 70, 1919, 1991.

3.8 Self-Consistent Simulations of High-Intensity Beams and Electron-Clouds with WARP-POSINST

J.-L. Vay, Lawrence Berkeley National Laboratory, Berkeley, CA, USA
mail to: jlvay@lbl.gov

3.8.1 Introduction

The steadily increasing beam intensity required in operational and upcoming accelerators leads to growing concerns over the degradation of beam emittance due to electron cloud effect and gas pressure rise [1]. Accurate prediction necessitates a detailed understanding of the physical processes at play with a quantification of the relative importance of various effects. To this end, the development of a new generation of computer simulation code is underway, in conjunction with detailed measurements from a heavily diagnosed small dedicated experiment, for extensive benchmarking and code validation. We provide a brief overview of the simulation code and the dedicated experiment, and present recent results, focusing on the dynamics of electrons in a magnetic quadrupole.

3.8.2 A Unique Combination of Simulation and Experimental Tools

3.8.2.1 The WARP-POSINST simulation package

The simulation tool is based on a merge of the Heavy Ion Fusion [2] accelerator code WARP [3] and the High-Energy Physics electron cloud code POSINST [4,5], supplemented by additional modules for gas generation and ionization [6], as well as ion-induced electron emission from Tech-X package TxPhysics [7]. The package allows

for multi-dimensional (2-D or 3-D) modelling of a beam in an accelerator lattice and its interaction with electron clouds generated from photon-induced, ion-induced or electron-induced emission at walls, or from ionization of background and desorbed gas. The generation and tracking of all species (beams particles, ions, electrons, and gas molecules) is performed in a self-consistent manner (the electron, ion and gas distributions can also be prescribed if needed for special study or convenience). The code runs in parallel and benefits from adaptive mesh refinement [8], disparate adaptive time-stepping and a new "drift-Lorentz" particle mover for tracking charged particles in magnetic fields using large time steps [9]. These advanced numerical techniques allow for significant speed-up in computing time (orders of magnitude) relative to brute-force integration techniques.

3.8.2.2 The High Current Experiment

The High Current Experiment [10], located at Lawrence Berkeley National Laboratory, consists of one injector producing singly charged Potassium ion beams (K+) at 1 MeV, followed by a transport lattice made of a matching section, a ten-quadrupole electrostatic section and a four-quadrupole magnetic section. The flat top of the beam pulse reaches 180 mA and its duration is 4 μs (see Fig.1(a)). Note that the tune depression is approximately 0.1.

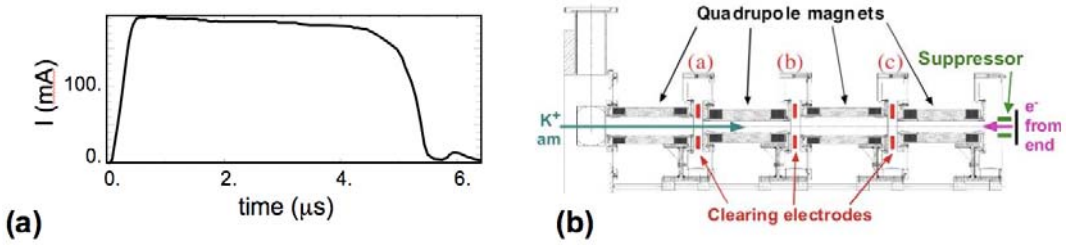

Figure 1: (a) Beam current history recorded from Faraday cup measurement at the exit of the electrostatic section (entrance of the magnetic section), (b) HCX in region of 4 quadrupole magnets, with clearing electrode rings between magnets and a suppressor electrode ring after the last magnet.

We study electron effects in the magnetic section [11,12], shown in Fig.1(b). A suppressor ring electrode, surrounding the beam after it exits the last quadrupole magnet, can be biased to -10kV to prevent ion-induced electron emission off an end wall (a slit plate) from reaching the magnets, or can be left unbiased to allow electrons emitted from the end wall to freely flow upstream into the magnets. There is also a series of three clearing electrodes, labelled (a), (b) and (c) in Fig.1(b), in the drift regions between quadrupole magnets, which can be biased positively to draw off electrons from between any pair of magnets. The current that flows in/out of these clearing electrodes is monitored in the experiment and is compared to simulation results for benchmarking.

3.8.3 Recent Study of Dynamics of Electrons in a Magnetic Quadrupole

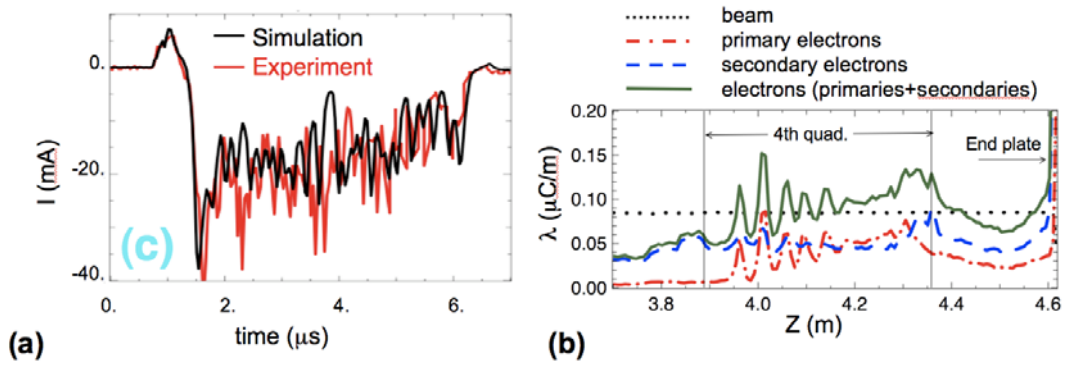

Figure 2: (a) Current history at clearing electrodes (c): red - recorded on HCX experiment, black - WARP-POSINST simulation of HCX, (b) Line charge density λ (absolute value), from WARP-POSINST simulation of HCX at t=3μs.

For convenience, we label the electrons created by the beam hitting the end wall as “primary”, while we label the electrons created by the primary electrons hitting the vacuum pipe surrounding the magnets as ``secondary'' (these encompass any subsequent generation of electrons).

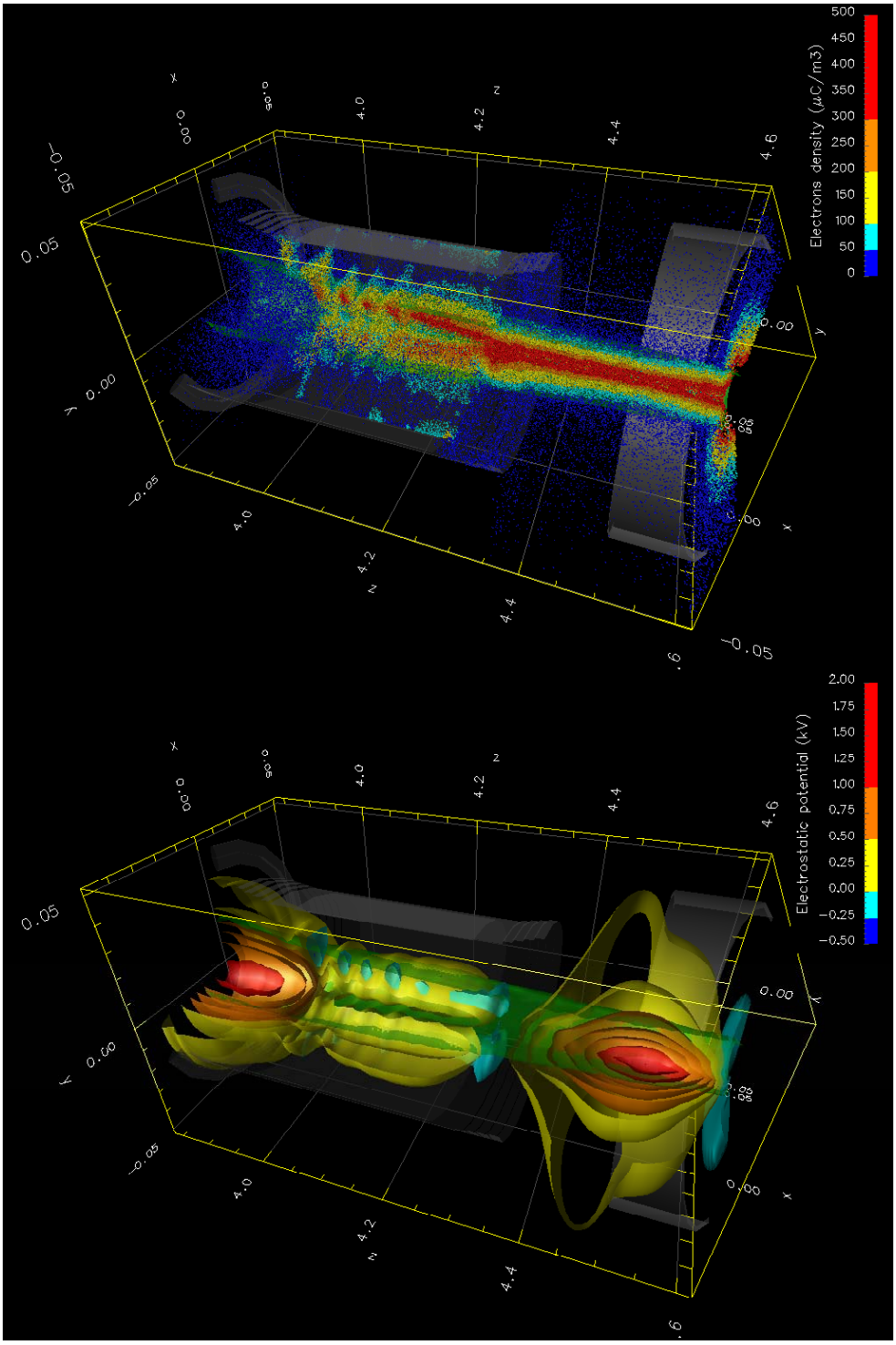

Figure 3: Snapshot of (top) electron macroparticles, colored according to charge density (absolute value), (bottom) equipotential surfaces, from WARP-POSINST simulation of HCX at t=3μs.

The primary electrons created at the end plate and propagating upstream can enter only two quadrants of the fourth (last) magnet, because of the sign of the **E**×**B** drift, and then drift upstream. The current from clearing electrode (c) is compared with simulation in Fig.2(a), in the case where the suppressor ring electrode was left grounded to allow electrons to propagate upstream, and the three clearing electrodes were biased to +9kV. The simulation and experimental results agree on the magnitude and frequency (around 10MHz) of the observed oscillations.

Simulation results reveal that these time-dependent oscillations recorded on clearing electrode (c) are related to bunching of electrons drifting upstream in the fourth magnet. The effect of electrons bunching is revealed on the plot of line charge densities in Fig.2(b), where oscillations of large amplitude and wavelength of approximately 5 cm are observed in the electron density in the fourth magnetic quadrupole. The effect is so pronounced that at the peak the electron line charge density reaches 1.5 times the beam line charge density. The bunching of electrons itself is revealed in Fig.3(top) where electrons bunches are easily observable from the middle of the quadrupole and upstream. The over-neutralization of the beam space-charge by these electron bunches is evident in Fig.3(bottom) where islands of negative potential are formed at the location of the bunches. Although some possible candidate explanations have been eliminated (electron-ion two-stream instability for example) the nature of these oscillations has not yet been firmly identified and other possibilities, such as the Kelvin-Helmholtz instability, are under active investigation.

3.8.4 References

1. Proc. 31st ICFA Advanced Beam Dynamics Workshop on Electron-Cloud Effects (ECLOUD'04), Napa, CA, USA, 19-23 Apr 2004, CERN Report CERN-2005-001 (2005), ISBN 92-9083-241-X, http://icfa-ecloud04.web.cern.ch/icfa-ecloud04/agenda.html
2. G. Logan, et al, Nuclear Fusion 45, 131 (2005).
3. D. P. Grote, A. Friedman, J.-L. Vay. I. Haber, AIP Conf. Proc. 749, 55 (2005).
4. M. A. Furman and G. R. Lambertson, Proc. Intl. Workshop on Multibunch Instabilities in Future Electron and Positron Accelerators ``MBI-97," KEK, p. 170; M. A. Furman, LBNL-41482/LHC Project Report 180, May 20, 1998.
5. M. A. Furman and M. T. F. Pivi, PRSTAB/v5/i12/e124404 (2003).
6. J.-L.Vay, M. Furman, R. H. Cohen, A. Friedman, D. P. Grote,, Proc. 21st Biennial Particle Accelerator Conference, PAC05, Knoxville, TN, (2005).
7. http://www.txcorp.com/technologies/TxPhysics.
8. J.-L. Vay, et al, Phys. of Plasmas 11, 2928 (2004).
9. R. H. Cohen, et al, Phys. of Plasmas 12 (2005) .
10. L. R. Prost, et al, PRSTAB 8, 020101 (2005).
11. A. W. Molvik, et al, PRSTAB 7, 093202 (2004)).
12. A.W. Molvik, et al, Proc. 21st Biennial Particle Accelerator Conference, PAC05, Knoxville, TN, (2005).
13. Benedetto et. al., PRSTAB 8, 124402 (2005)

3.9 Code Web Repository and Benchmarking Effort

Frank Zimmermann, CERN, AB/ABP, 1211 Geneva 23, Switzerland
mail to: frank.zimmermann@cern.ch

3.9.1 Introduction

Recently, a common accelerator physics *code repository* [1] has been constructed in the framework of the "Accelerator Physics and Synchrotron Design" (APD) work package [2] of the CARE [3] network on "High Energy High Brightness Hadron Beams" (HHH) [4].

This code repository provides a platform for ongoing and future *code verification* by mutual comparison and benchmarking against machine experiments, and by centralised documentation, fostering code reliability. It is also meant to support *code extensions* aimed at modelling relevant beam physics and it should help in the implementation of effective procedures for beam measurements, machine protection, background control, and performance optimization. The ultimate goal of the repository and of the parallel benchmarking or development efforts is to enable reliable predictions for, and to boost, the performance of existing and future accelerators. All codes capable of modelling hadron-accelerator features are eligible for inclusion in the repository, even if originally developed for lepton beams.

The CARE-HHH code repository was presented to the community at EPAC'06 [5], where further details can be found. The associated code benchmarking efforts were discussed, with numerous examples, at the ICFA workshop HB'2006 [6,7] and at the ICAP'06 conference [8].

3.9.2 Accelerator Physics Code Web Repository

The code repository web site [1] is dynamically linked to an ORACLE database which allows for search-engine capability, including multiple queries and wildcards, as well as for a standardized format of different code web pages, simple usage, and easy maintenance.

The database contains three main tables where important information is stored: (1) codes identified by names, (2) code categories, e.g., "electron cloud", and sub-categories, e.g., "build up" or "self-consistent", and (3) persons, e.g., authors or contacts. Codes are linked with categories and with persons.

The code repository presently includes close to 40 programmes, ranging from linear and nonlinear optics, over impedance estimates and vacuum, to collective effects, such as conventional instabilities, beam-beam, space charge, ions effects and electron cloud. The distribution of codes among the various categories is illustrated in Fig. 1.

For most codes the following base information is available in a standard format: (1) code name, (2) code purpose, (3) authors, (4) contacts, (5) language, (6) operating system, (7) home page, (8) source code, (9) example inputand output, (10) documentation or manual, (11) list of special model features, (12) accelerators for which this code was or is used, (13) benchmarking exercises against other codes, (14) benchmarking against experiments, (15) special programming features, (16) comments, (17) references, and (18) associated categories. For several codes supplementary web pages with extended links and documentation provide additional information. The

above data were collected via a standard questionnaire sent to about 60 authors and prospective contact persons. About 75% of the contacted colleagues responded positively. As a first spin-off, several code home pages were newly created by the code authors, to the users' benefit.

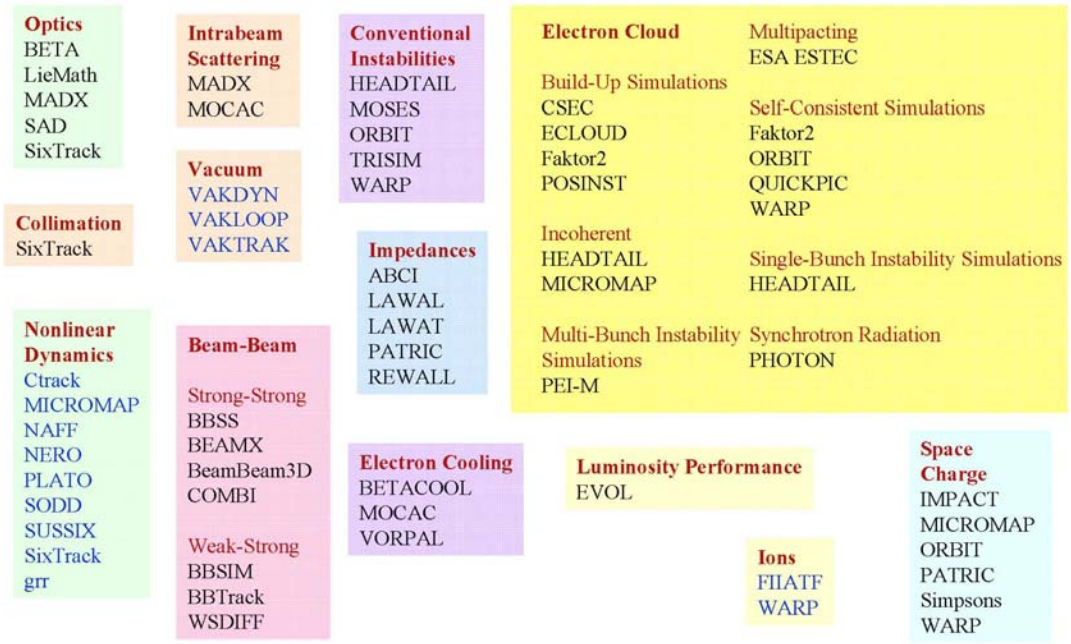

Figure 1: Structure of the accelerator-physics code web repository with presently active categories, sub-categories, and code names (courtesy G. Franchetti [8]).

3.9.3 Code Benchmarking

At HHH-2004, M. Furman pointedly remarked [9] that the term "code benchmarking" may carry a variety of meanings, for example *debugging*, i.e., the code should calculate what it is supposed to calculate; *validation*, i.e., results should agree with established analytic result for specific cases; *comparison*, i.e., two codes should agree if the model is the same; or *verification*, i.e., the code should agree with measurements. The need for debugging is obvious, but validation is often difficult for complex simulations of nonlinear processes. The HHH benchmarking concentrates on the two remaining areas of code comparison and experimental verification.

The present benchmarking worldwide effort seems to focus on simulations of collective effects, in particular beam-beam interaction, space charge and electron cloud. Two reasons for this may be that, first, these phenomena presently limit accelerator performance, and that, second, the more fundamental, and perhaps conceptually simpler, optics design and single-particle nonlinear-dynamics codes were already extensively benchmarked against each other during the past several decades.

Benchmarking studies are supported, and documented, via dedicated links in the code repository, which exist for each category or sub-category. These links point to benchmarking pages for the corresponding code species and to tables comparing the features of codes belonging to each category, respectively. The benchmarking pages

contain the relevant model parameters for comparative simulations or experiments, as well as the corresponding simulation results, where available. Additional links included at the bottom of these pages point to related web sites, articles and papers.

The space-charge benchmarking page documents the extensive simulation work on emittance growth and beam loss in high-intensity proton machines presently underway with a number of codes such as MICROMAP, SIMPSON, and ORBIT. Experimental benchmarking of the space-charge simulations is being conducted in parallel, e.g., at the CERN PS, the LANL PSR, the GSI SIS 18, and the SNS.

The electron-cloud benchmarking page compares results of electron-cloud build-up and single-bunch instability simulations from different codes. This page also indicates that experiments at the CERN SPS were successfully used to benchmark the ECLOUD at the CERN SPS, while POSINST and CSEC were verified with beam observations at the APS and PSR, and the WARP/POSINST simulations with the HCX experiment. Figure 2 shows a more recent comparison of WARP/POSINST and HEADTAIL simulations for a single-bunch instability driven by electron cloud [10]. The results from the two codes are extremely close. Figure 3 displays latest heat-load predictions for the LHC, again from two codes, indicating that equally good agreement is achieved for the electron build up, when a similar model for the secondary emission is assumed [11].

Similar information for beam-beam studies can be found on their associated benchmarking pages, including references to a few dedicated experiments, mostly performed at RHIC.

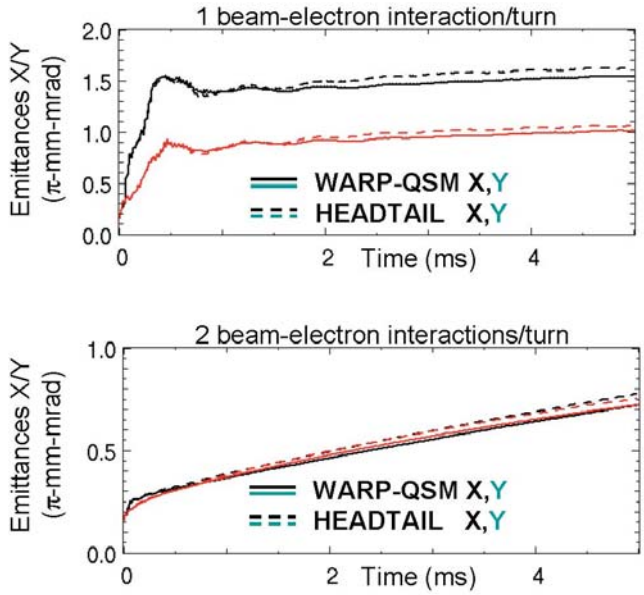

Figure 2: Benchmarking of "quasi-static" WARP/POSINST single-bunch instability simulations and HEADTAIL results with 1 and 2 electron-beam interactions points per turn, for SPS-like proton-beam parameters (courtesy J.-L. Vay [10]).

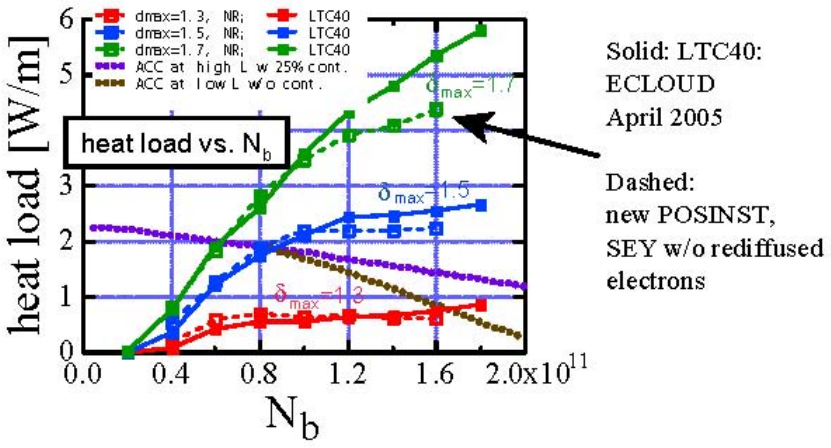

Figure 3: Comparison of electron-cloud heat-load simulations for LHC from the latest version of POSINST with those from ECLOUD; after improvements to the space-charge field calculation, the two codes yield nearly identical results if approximately the same model is used for the secondary emission yield (courtesy M. Furman [11]).

3.9.4 Outlook and Feedback

The recent quantitative experimental confirmation of various predicted instability growth rates in the SNS, a newly built machine, is encouraging [12]. The next large, and even more challenging, accelerator going into operation will be the LHC in 2007. Indeed many of the codes in the repository were originally developed for modeling the LHC, and the LHC commissioning in itself will, therefore, represent some kind of ultimate code benchmarking. The dream goal of code development is to arrive at a complete and reliable simulation tool, providing a self-consistent treatment of the beam evolution, encompassing electron cloud, beam optics, conventional impedance and wake fields, space charge, vacuum, ions, and beam-beam effects [13].

Any feedback from the community on the CARE-HHH code-repository effort and the benchmarking project would be highly appreciated. We welcome, for example, any additional codes to be included – some short answers to the standard questionnaire would be required – any results of code-code or code-experiment benchmarking, or articles describing such results.

3.9.5 Acknowledgements

Francesco Ruggiero has provided initiative and guidance for the CARE-HHH code repository and benchmarking efforts. Romain Basset and Cecile Lapoire have developed the database, collected information, created benchmarking pages, and generated code tables. Dan Abell, Riccardo Bartolini, Giulia Bellodi, Elena Benedetto, Mike Blaskiewicz, Slava Danilov, Ulrich Dorda, Alexei Fedotov, Wolfram Fischer, Giuliano Franchetti, Miguel Furman, Jeff Holmes, Massimo Giovannozzi, Werner Herr, Elias Metral, Kazuhito Ohmi, Yannis Papaphilippou, Tatiana Pieloni, Ji Qiang, Giovanni Rumolo, Frank Schmidt, Tanaji Sen, Ezio Todesco, Jean-Luc Vay, Volker Ziemann, and numerous other colleagues have kindly contributed pertinent pictures and

examples. Ingo Hofmann has encouraged this contribution to the Newsletter. I would like to thank all of them.

This work is supported by the European Community-Research Infrastructure Activity under the FP6 "Structuring the European Research Area" programme (CARE, contract number RII3-CT-2003-506395).

3.9.6 References

1. CARE-HHH-APD Accelerator Physics Code Repository & Benchmarking Web Site *http://oraweb.cern.ch:9000/pls/hhh/code_website.startup*
2. CARE-HHH-APD Web Site *http://care-hhh.web.cern.ch/CARE-HHH/CARE-HHH-APD/*
3. CARE Web Site *http://esgard.lal.in2p3.fr/Project/Activities/Current*
4. CARE-HHH Web Site *http://care-hhh.web.cern.ch/CARE-HHH/*
5. F. Zimmermann et al, "Accelerator Physics Code Web Repository," EPAC'06, WEPCH141. Edinburgh, 26-30 June, 2006.
6. J. Wei et al, "Summary of General Session of Working Groups A+B+D on Code Benchmarking," FRAP08, HB2006 ICFA Workshop, Tsukuba, 29 May- 2 June, 2006.
7. F. Zimmermann, "Electron-Cloud Benchmarking and CARE-HHH Codes," THBW02, HB2006 ICFA Workshop, Tsukuba, 29 May – 2 June, 2006.
8. G. Franchetti, "Towards the Description of Long Term Self Consistent Effects in Space Charge Induced Resonance Trapping," MOA2IS03, ICAP 2006, Chamonix, 2-6 October, 2006
9. M.A. Furman, "Overview of Electron Cloud Simulation Codes," CARE-HHH-APD workshop HHH-2004, Geneva, 8-11 November 2004, CERN-2005-006, p. 297, 2005.
10. J.-L. Vay, "Self-Consistent Simulations of High-Intensity Beams and E-Clouds with WARP POSINST," WEA3MP02, ICAP 2006, Chamonix, 2-6 October, 2006.
11. M. Furman, "E-Cloud in PS2, PS+ and SPS+," CARE-HHH-APD LHC-LUMI-06, Valencia, 2006; Web Site *http://care-hhh.web.cern.ch/CARE-HHH/LUMI-06*
12. V. Danilov and S. Cousineau, "Accumulation of high intensity beam and first observations of instabilities in the SNS accumulator ring," TUAX01, HB2006 ICFA Workshop, Tsukuba, 29 May – 2 June, 2006.
13. F. Zimmermann, "Summary of Panel Discussion 4: Electron Cloud Codes," CARE-HHH-APD workshop HHH-2004, Geneva, 8-11 November 2004, CERN-2005-006, p. 297, 2005.

3.10 Summary of general session of working groups A, B, D on code benchmarking*

J. Wei , Brookhaven National Laboratory, New York, USA
E. Shaposhnikova, F. Zimmermann, CERN, Geneva, Switzerland
I. Hofmann, GSI, Germany
For the working group A, B, and D participants
mail to: jwei@bnl.gov

* Work supported by the auspices of the US Department of Energy. This paper was presented at the ICFA-HB2006 workshop as summary of working groups A, B and D.

3.10.1 Introduction

Computer simulation is an indispensable tool in assisting the design, construction, and operation of accelerators. In particular, computer simulation complements analytical theories and experimental observations in understanding beam dynamics in accelerators. The ultimate function of computer simulation is to study mechanisms that limit the performance of frontier accelerators.

There are four goals for the benchmarking of computer simulation codes, namely debugging, validation, comparison, and verification [1]:

- Debugging: codes should calculate what they are supposed to calculate;
- Validation: results generated by the codes should agree with established analytical results for specific cases;
- Comparison: results from two sets of codes should agree with each other if the models used are the same;
- Verification: results from the codes should agree with experimental measurements.

Adequate debugging is the first goal that established codes should meet. In the following, we summarize the status of validation, comparison, and verification, and provide suggestions for each topic discussed. Speakers in the code benchmarking session were G. Franchetti (GSI), F. Zimmermann (CERN), V. Kornilov (GSI), I. Hofmann (GSI), A. Burov (FNAL), K. Ohmi (KEK), and A. Fedotov (BNL). Authors whose presentations in other sessions are quoted in this summary include V. Danilov (ORNL), S. Cousineau (ORNL), J. Holmes (ORNL), L. Prost (FNAL), J.-L. Vay (LBNL) and E. Benedetto (CERN).

3.10.2 Codes Benchmarking Status

Four topics were covered by this session: space charge, electron cloud, instability driven by external impedances, and electron cooling. Each topic contains one or more tasks for codes benchmarking.

Information on many codes as well as some benchmarking examples can be found in the CARE-HHH accelerator physics code web repository [2].

3.10.3 Space Charge

3.10.3.1 Montague resonance and emittance exchange

The aim is to compare the evolution of horizontal and vertical emittances as the transverse tunes are varied so as to cross the Montague resonance of $2\nu_x - 2\nu_y = 0$.

- Validation with 2D analytical theory is performed for most codes. Validation with 3D theory is performed only for a few cases.
- Comparison is performed [3] between the codes ACCSIM [4], IMPACT [5], MICROMAP [6], ORBIT [7], SIMBAD [8], SIMPSONS [9], and SYNERGIA

[10]. Good agreement is achieved using 2D models, tracking for 10^3 turns, and observing emittance evolution when the transverse tunes are swept to cross the Montague resonance.

- Verification is performed with IMPACT3D [5] against experiments on the CERN PS. When the vertical tune is fixed and various horizontal tunes are selected, the agreement is excellent on resonance but poor off resonance. The agreement is poor when one tune is dynamically varied over a time period of 4×10^4 turns.
- Suggestion: Longitudinal synchrotron motion needs to be added, and lattice nonlinearities need to be included in all simulation codes.

3.10.3.2 Resonance trapping with sextupoles

The present aim is to compare space charge induced trapping of particles in the presence of sextupole magnets during long-term storage. The final aim is to determine halo density and beam loss during long-term storage of high intensity beams.

- No quantitative analytical predictions are available for validation.
- Comparison is performed [11] between codes MICROMAP [6] and SIMPSONS [9]. The comparison is satisfactory on space charge detuning and third-order resonance trapping. However, at the time of the workshop there was about a factor of 2 difference in the full bunch emittance growth for 10^5-turn simulation using 10^3 macroparticles. This factor has recently been resolved and the two codes now are in nearly perfect agreement [12].
- Verification is performed with MICROMAP against experiments on the CERN PS with satisfactory agreement.
- Suggestion: More comparison is needed with fully self-consistent codes like ORBIT [7].

3.10.4 Electron Cloud

3.10.4.1 Electron build-up

The aim is to compare the electron density in the beam and vacuum chamber and the electron flux on the chamber wall under beam induced electron multipacting.

- Validation is limited to some special models of multipacting.
- Comparison is performed [13, 14, 15] between the codes POSINST [16], PEI [17], ECLOUD [18], CLOUDLAND [19], EPI [20], CSEC [21], and MEC [22]. The result is sensitive to often unknown and time dependent surface parameters including the incident angular dependence of secondary emission yield $\delta_{max}(\theta)$ and zero-energy reflectivity R. The agreement is typically within a factor of 2 to 3 in electron density.

- Verification is performed with ECLOUD [18] against SPS experimental data [23]. Fixing the vacuum pressure and using two fitted parameters (δ_{max}=1.35, R=0.3), good agreement is achieved for all measurements (two types of bunch train spacing). Verification is also performed with the codes POSINST [16] against APS and PSR experimental data; good agreement is reached also here using two fitted parameters.
- Suggestion: Benchmarking study on surface scrubbing is needed. More bench measurements are needed on the secondary emission yield and the secondary-electron energy spectrum their dependence on the angle of primary incidence.

3.10.4.2 Multi-bunch instability

The aim is to study multi-bunch instability induced by the electron cloud in a positively charged beam.

- Some model validation is performed against analytical predictions based on simulated wake fields generated by the electron cloud.
- No comparison is performed between codes, since only one code, PEI-M [17, 24], is available.
- Verification is performed with code PEI-M [17] against KEKB experimental data [24]. Qualitative agreement is obtained on the mode frequency. On the other hand, when the solenoid is turned on, a good agreement is obtained only if a factor of 5 adjustment is made on the solenoid field.
- Suggestion: It is preferable to combine multi-bunch electron cloud instability codes with single bunch instability codes. PEI-M [17] is the only example so far.

3.10.4.3 Single bunch instability

The aim is to study single bunch instability induced by electron cloud in a positively charged beam.

- Two-particle and broadband resonator models are used to validate the codes with satisfactory agreement (within about 30% in predicted emittance growth).
- Comparison is performed between the codes PEHT [25], PEHTS [26], HEADTAIL [27], and QUICKPIC [28] with qualitative agreement on the predicted transverse emittance growth [29, 13, 30]. Different from the other codes, PEHT [25] contains a micro-bunch model.
- Verification is performed with the codes PEHTS [26] and HEADTAIL [27] against KEK-B experimental data [25, 31] and with code the ORBIT [7] against SNS experimental data [32]. The intensity threshold for electron-proton instability is correctly predicted for the SNS ring [32]. The upper sideband phenomenon found in KEKB has been understood and reproduced [31] in simulations with PEHTS [25] and HEADTAIL [27].
- Suggestion: Simulations should consider realistic electron distribution.

3.10.4.4 Incoherent effects

The aim is to study incoherent effects related to electron cloud including emittance growth caused by periodic resonance crossing due to electron-cloud induced tune shift and electron-cloud induced resonance trapping or scattering.

- Validation against analytical model is not yet performed.
- Some comparison is performed between codes HEADTAIL [27], Franchetti's codes [12], CLOUD_MAD [33], and PEHTS [26] with qualitative agreements [34].
- Verification is performed with codes HEADTAIL [27] against SPS experiments with good agreement [34].
- Suggestion: KEKB observations below the electron cloud instability threshold need to be bench-marked. Effects due to numerical noise caused by finite number of seed electrons and due to slicing interpolation could further be checked. Analytical estimate needs to be developed for the emittance growth.

3.10.4.5 Self-consistent modelling

The aim is to develop a self-consistent model incorporating both the electron generation and the interaction between electrons and beam particles.

- Analytical validation is not performed.
- No comparison is performed between the available codes: ORBIT [7], WARP/POSINST [35, 16], PARSEC [36], and PEI-M [17].
- Verification is performed with codes WARP/POSINST [35, 16] against experimental observation at HCX [37, 38]. Good agreement is obtained for a "coasting" beam.
- Suggestion: Careful comparison needs to be performed between codes. It is highly desirable to develop self-consistent codes addressing performance limiting mechanisms like transverse emittance growth in LHC, beam losses in RHIC, SPS, PSR, and SNS, and vacuum pressure rise in RHIC.

3.10.5 Instability Driven by External Impedances

3.10.5.1 Transverse instability

The aim is to study the threshold and growth rates of transverse instability induced by external beam coupling impedances.

- An attempt has been made to validate PATRIC [39] with the dispersion relations of Moehl and Laclare [40]. However, large discrepancies are found in the stability area.
- No code comparison has been presented at the workshop. PATRIC [39] and ORBIT [7] are available for such activities.
- Verification is performed with the code ORBIT [7] against experimental observations on the SNS ring [32]. Instabilities due to the resistive wall

impedance and the extraction kicker broadband impedance are predicted at observed intensity thresholds and frequencies.

- Suggestion: Comparison needs to be performed between codes like PATRIC [39] and ORBIT [7]. Codes need to be compared with more comprehensive theories, e.g., one by M. Blaskiewicz [41].

3.10.5.2 Longitudinal instability

The aim is to study the threshold and growth rates of longitudinal instability induced by external beam coupling impedances.

- No validation results have been presented at the workshop.
- No comparison between codes has been presented at the workshop. Codes like ESME [42] and ORBIT [7] are available.
- Verification is performed with ORBIT against observations at PSR [43] and with ESME against observations at SPS [44], in both cases with good agreement.
- Suggestion: Codes for multi-bunch longitudinal instability study are needed.

3.10.6 Electron Cooling Friction Force

The aim is to study the cooling friction force in both magnetized and non-magnetized electron cooling.

- Code VORPAL [45] is validated with Parkhmochuk's expressions for magnetized cooling [46].
- Comparison is performed between codes BETACOOL [47] and VORPAL [45] with good agreement [46].
- Verification is performed with codes BETACOOL [47] and VORPAL [45] against experimental data from CELSIUS for magnetized cooling [48], and with BETACOOL [47] against experimental observations at the FNAL recycler for non-magnetized cooling [48].
- Suggestion: None.

3.10.7 Summary

"Everybody believes in experiments except the experimentalist; nobody believes in simulation except the simulationalist." The recent success at SNS predicting instabilities (resistive wall, broadband, electron-proton) [32] on a newly built machine gives us hope that such rules may be violated!

3.10.8 References

1. M. Furman, HHH-2004 workshop, CERN, Geneva, Session 6B (2004).
2. http://oraweb.cern.ch:9000/pls/hhh/code_website.startup
3. I. Hofmann et al, "Benchmarking of Simulation Codes Based on the Montague Resonance on the CERN Proton Synchrotron," PAC'05 Knoxville (2005).
4. F. W. Jones, G. H. Mackenzie, and H. Schönauer, Part. Accel. **31** (1990) 199.

5. Contact: J. Qiang (LBNL), R. Ryne; J. Qiang et al, J. Comp. Phys. **163** (2000) 434.
6. Contact: G. Franchetti (GSI), S. Rambaldi, G. Turchetti, A. Bazzani, A. Orzhekhovskaya, Web site: http://www-linux.gsi.de/ giuliano/micromap/manmimac_tmp.html
7. Contact: A. Shishlo, J. Holmes, S. Cousineau (ORNL), Web site http://www.ornl.gov/ jzh/JHolmes/ORBIT.html; *ORBIT Users Manual*, J. Galambos, J. Holmes, D. Olsen, A. Luccio, and J. Beebe-Wang, SNS/ORNL/AP TN 0011, (1999), http://www.ornl.gov/sns/APGroup/Codes/ ORBITUserMan1_10.html
8. Contact: A. Luccio and J. Beebe-Wang.
9. Contact: S. Machida (ASTEC), Web site: http://hadron.kek.jp/ machida/simpsons/; S. Machida, Nucl. Instr. Meth. **A 309** (1991) 43.
10. J. Amundson, P. Spentzouris, "SYNERGIA: A Hybrid, Parallel Beam Dynamics Code with 3D Space Charge," PAC 2003 Portland (2003) 3195.
11. http://www-linux.gsi.de/~giuliano/research_activity/trapping_benchmarking/main.html
12. G. Franchetti, S. Machida, I. Hofmann, THBW01, these proceedings.
13. E. Benedetto et al, Proc. EPAC 2004, Lucerne (2004) 2502.
14. G. Bellodi, CARE-HHH-APD HHH-2004 workshop, CERN-2005-006 (2005) 281.
15. http://conf-ecloud02.web.cern.ch/conf-ecloud02/CodeComparison/ecsimbu.htm
16. Contact: M. Pivi (SLAC), M. A. Furman (LBNL), Web site: http://www-project.slac.stanford.edu/ilc/testfac/ecloud/elec_cloud.html; M. A. Furman and M. T. F. Pivi, Phys. Rev. ST-AB, **5** (2003) 124404.
17. Contact: K. Ohmi (KEK); K. Ohmi, Phys. Rev. Lett. **75** (1995) 1526.
18. Contact: F. Zimmermann (CERN), D. Schulte, G. Bellodi, G. Rumolo, O. Bruning, X.-L. Zhang, Web site: http://wwwslap.cern.ch/collective/electron-cloud/Programs/Ecloud/ecloud.html; G. Rumolo, F. Zimmermann, *Practical User Guide for ECloud*, CERN-SL-Note-2002-016 (2002).
19. Contact: L. Wang (SLAC); L. Wang, H. Fukuma, K. Ohmi, et. al., Proc. PAC 2001 (2001) 701.
20. K. Ohmi et al, "Simulation of Ep Instability for a Coasting Beam in Circular Accelerators," EPAC 2004 Lucerne (2004) 2107.
21. Contact: M. Blaskiewicz (BNL).
22. U. Iriso, S. Peggs, "Maps for Fast Electron Cloud Simulations at RHIC," EPAC 2004 Lucerne (2004) 2870.
23. D. Schulte et al, PAC 2005 (2005) 1371.
24. S.S. Win et al, Proc. ECLOUD'02, Geneva, CERN-2002-001 (2002) 199.
25. K. Ohmi, F. Zimmermann, "Head-Tail Instability Caused by Electron Cloud in Positron Storage Rings," Phys. Rev. Lett. **85** (2000) 3821.
26. K. Ohmi, "Particle in Cell Simulation of Beam-Electron Cloud Interactions," PAC 2001 Chicago (2001) 1895.
27. Contact: F. Zimmermann, G. Rumolo (CERN); *Practical User Guide for HEADTAIL*, G. Rumolo and F. Zimmermann, CERN-SL-Note-2002-036 AP (2002)
28. Contact: B. Feng (USC), A. F. Z. Ghalam, C. Huang, V. Decyk.
29. G. Rumolo et al, "Electron Cloud Studies for KEKB," PAC 2001 Chicago (2001) 1889.
30. http://conf-ecloud02.web.cern.ch/conf-ecloud02/CodeComparison/modelinst.htm
31. K. Ohmi, E. Benedetto, J. Flanagan, private communication; and K. Ohmi, HB2006, THBW04 (2006).
32. V. Danilov, S. Cousineau, TUAX01, these proceedings.
33. D. Chen et al, "Single Bunch Electron Cloud Effects in the NLC Beam Delivery System", SLAC-TN-03-051, LCC-0126 (2003).
34. E. Benedetto et al, Phys. Rev. Lett. **97** (2006) 034801.
35. A. Friedman (LBNL), D.P. Grote, J.-L. Vay, Web site: http://hif.lbl.gov/theory/WARP_summary.html
36. Contact: A. Adelmann (LBNL) and M. A. Furman; Proc. PAC 2003 (2003) 3524.

37. J.-L. Vay, HB2006, THAW01 (2006).
38. A. Molvik, HB2006, THAW02 (2006).
39. Contact: O. Boine-Frankenheim (GSI).
40. V. Kornilov, TUBX02, these proceedings.
41. M. Blaskiewicz, Phys. Rev. ST-AB **1** (1998) 044201.
42. Contact: J.A. MacLachlan (FNAL); J.A. MacLachlan, FERMILAB TM-1274 (1984).
43. S. Cousineau, J. Holmes, C. Beltran et al, "Benchmark and Threshold Analysis of Longitudinal Microwave Instability in the PSR", EPAC 2004 Lucerne (2004) 2224.
44. E. Shaposhnikova, TUBX05, these proceedings.
45. Contact: D. Bruhwiler (TX-Corp), C. Nieter, J. Cary, Web site: http://www.txcorp.com/products/VORPAL/ and http://www.txcorp.com/pdf/VORPAL/VORPAL_UsersGuide.pdf; C. Nieter and J. Cary, J. Comp. Physics **196** (2006), 448; D. Bruhwiler et al., AIP Conf. Proceed. **773** (2005), 394.
46. A. Fedotov, WEAY04, these proceedings.
47. Contact: A. Sidorin (JINR), A. Smirnov (JINR), E. Syresin, G. Trubnikov, I. Meshkov, I. Seleznev, Web site: http://lepta.jinr.ru and http://lepta.jinr.ru/betacool/doc.zip; A. Sidorin et al., Nucl. Instru. Methods, **A 558** (2006) 325.
48. A. Fedotov, FRAP05, these proceedings.

4 Activity Reports

4.1 Progress in Commissioning of Indus-2

A.D.Ghodke, Riyasat Husain, Gurnam Singh and Indus-2 Commissioning Team
Raja Ramanna Centre for Advanced Technology (RRCAT), Indore-452 013, India
mail to: ghodke@cat.ernet.in

4.1.1 Introduction

Indus-2 is a 2.5 GeV synchrotron radiation source [1-2] of nearly third generation. It is the second source built in India at Raja Ramanna Centre for Advanced Technology (RRCAT), Indore. First source, a 450 MeV electron storage ring, Indus-1 has been in operation and in use since 1999 [3-5]. Both these sources share a common injector system consisting of a 20 MeV microtron and a booster synchrotron. An electron beam extracted from booster synchrotron is transferred through transfer lines TL-2 and TL-3 into Indus-2 every second till a required beam current is stored

In this article, we discuss the beam dynamics studies and actions taken to reduce the closed orbit distortions and beta beat before the commissioning of Indus-2. The relaxed optics evolved with the objective of making the commissioning easier is also described. The results obtained so far during the commissioning are presented. The commissioning of the storage ring Indus-2 started in August, 2005. In February, 2006 beam accumulation in Indus-2 was achieved at the injection energy of 550 MeV. The beam energy has been ramped from injection energy to 2 GeV successfully. Up to now 38 mA beam current at the injection energy and 26 mA at 2 GeV has been stored in the ring. Horizontal and vertical betatron tunes, closed orbit distortions and beam lifetime has been measured. We present the results obtained so far during the commissioning of TL-3 and Indus-2.

4.1.2 Indus-2 Storage Ring and Injector System

Indus-2 is an electron storage ring of circumference 172.4743 m to accelerate electrons to 2.5 GeV and store them at this energy. It comprises of 8 unit cells of an expanded Chasman Green lattice. Each unit cell has two dipole magnets and nine quadrupoles, (three in achromat part and six in the long straight section) and four sextupoles for chromaticity correction as shown in Fig. 1. Besides these magnets, there 48 horizontal steering magnets and 48 vertical steering magnets for the correction of closed orbit distortion. For correction of coupling, there are 16 skew quadrupole windings mounted on the sextupoles. The ring has eight 4.5 m long straight sections of which two sections are for RF cavities, one for beam injection, in which injection kickers and septa are installed and remaining five for insertion devices. In this way, the ring consists of a total of 16 bending magnets, 72 quadrupoles, 32 sextupoles the power supplies driving these magnets are unipolar in nature, in addition 48 horizontal steering, 40 vertical steering magnets and 16 skew quadrupoles are driven by bipolar power supplies. There are 11 fluorescent beam position monitors (BPMs), one synchrotron light monitor, one wall current monitor(WCM), one DCCT and 56 beam position indicators (BPIs) to measure the closed orbit. There are 6 striplines and 3 scrappers in the ring. The design parameters of Indus-2 are tabulated in Table 1.

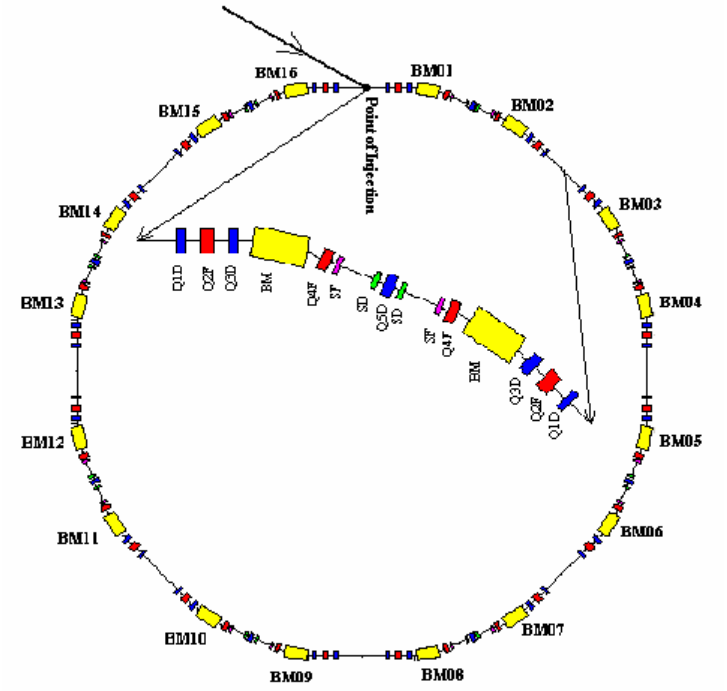

Figure 1: Schematic layout of Indus-2 storage ring

All 16 dipole magnets are connected in series and driven by single power supply. The quadrupoles of the insertion straight sections are driven by 24 power supplies and the quadrupoles of the achromat sections are driven 2 power supplies, so there are 26 power supplies for quadrupoles. There are 2 power supplies, one for focusing and another for defocusing family of the sextupole magnets. Independent power supplies

drive the corrector magnets. The vacuum tube apertures in the horizontal and vertical planes are ± 32 mm and ± 17 mm respectively.

For beam injection in Indus-2, two septum magnets (one thick and other thin) and four kicker magnets are used. These magnets are fast switching magnets. The current pulse shape for these magnets is half sine wave. The thick septum is of pulse width 100 μs and it deflects the beam by 19° whereas thin septum is of 50 μs width and it deflects the beam by 2°. The width of each kicker magnet current pulse is 3 μs. The amplitude of the current pulse of the kicker magnet decides the bump reduction rate.

Table 1: Parameters of Indus-2 Ring

Maximum energy	2.5 GeV
Maximum current	300 mA
Lattice type	Expanded Chasman Green
Superperiods	8
Circumference	172.4743 m
Bending field	1.502 T
Typical tune points	9.3, 5.2
Beam Emittance ε_x ,ε_z	6.10×10^{-8} , 6.10×10^{-9} m-rad
Available straight section for insertion devices	5
Maximum straight length available for insertion devices	4.5 m
Beam sizes σ_x ,σ_z (Centre of bending magnet)	0.247, 0.243 mm
Beam envelope vacuum	$< 1 \times10^{-9}$ mbar
Beam life time	14 hours
RF frequency	505.812 MHz
Critical wavelength	1.98 Å (Bending Magnet) 0.596Å (High Field Wiggler)
Power loss	186.6 kW (Bending magnet)

Indus-1 and Indus-2 have a common injector system consisting of microtron and booster synchrotron. The microtron is designed and optimised to deliver a 20 MeV electron beam with a current of 25 mA in long pulse at a repetition rate of 1-2 Hz. The beam from the microtron is transported to the booster synchrotron through the Transfer Line-1 (TL-1), which has a length of about 14 m. It has 3 quadrupole doublets and one dipole magnet to take care of the beam twiss parameters matching according to the requirement of beam injection in the synchrotron. There are 3 horizontal and 4 vertical steering magnets for centering the beam down the line. The magnetic lattice of the synchrotron consists of 6 superperiods- each consisting of a dipole magnet and a pair of focussing and defocusing quadrupole magnets to achieve the required stability and tuning. The maximum magnetic field of the dipole is 1.32 T. The circumference of the synchrotron is 28.44 m. The electrons are injected into the synchrotron by adopting a multi-turn injection scheme using the electron beam pulse from the microtron at a repetition rate of 1 Hz. A compensated bump producing maximum amplitude near the injection septum is generated with three injection kickers. After injection, the electrons

are accelerated to 550 MeV in nearly 300 ms following a linear ramp using an RF cavity operating at 31.613 MHz. During ramping, the peak accelerating voltage of the cavity is varied from 0.4 kV to 15 kV. The magnetic fields in the dipole, quadrupole and steering magnets are synchronously increased during the acceleration. The harmonic number being three results in three circulating bunches in the synchrotron. The accelerated current is normally few mAs. The accelerated beam is extracted by deflecting it by a fast kicker magnet having a rise time 45 ns. As the separation between two bunches is 32 ns, during the extraction process, one out of three bunches is lost and two bunches are extracted. These two bunches are then transported to Indus-2 through the transfer lines TL-2 which is 20 m long and TL-3 which is 68 m long. TL-2 was already commissioned and has been in use since 1999 for transfer of the beam for injection in Indus-1. TL-3, which is an extended part of TL-2, has recently been commissioned. These transfer lines consist of 4 bending magnets, 24 normal quadrupoles, 14 horizontal steering magnet and 17 vertical steering magnets.

The transfer line TL-3 starts after the second bending magnet of TL-2 and ends at the injection septum of Indus-2. When this bending magnet is kept off, the beam is directed towards TL-3. The length of the line is around 68 m, the optics has been chosen in order to keep the number of magnetic components and their power supplies to a minimum while keeping the beam sizes within acceptable values. This line has 3 bending magnets and 18 quadrupoles. To cover major length of the line with a symmetric structure, a FODO cell is selected as it satisfies all the necessary requirements. Driven by a single power supply, this cell is repeated four and half times. As it is necessary to change the direction of the beam after crossing the wall of the Indus-1 hall and to suppress the dispersion, a double bend achromat is introduced in the line. A bending magnet is also used at the injection point to suppress the dispersion generated by the septum magnet. In order to keep the beam well aligned along the design path, there are 11 horizontal and 12 vertical steering magnets. Besides, the line also has 8 beam position monitors (BPMs) and 4 wall current monitors (WCMs) to observe the beam profile/position and intensity respectively.

4.1.3 Beam Dynamics of Indus-2

4.1.3.1 Trajectory Calculations for Dipoles

In the dipoles, the real magnetic field is not symmetric with respect to their centres along the beam direction and this leads to an asymmetric nature of the trajectory. To minimise the distortion of the orbit in the ring, this effect of asymmetry in the field can be alleviated with longitudinal displacements of the dipoles. Based on the measured dipole field variation in each dipole, a detailed trajectory calculation was carried out for field asymmetry with respect to the dipole centre. In Indus-2 all the 16 dipoles are powered by a single power supply and each dipole is equipped with a secondary coil. The trajectory calculation [6] reveals that an electron of same energy is deflected by different angles in each dipole due to the variation in the field integral. So there is a need to energize the secondary coils to equalize the net field integral of each dipole. Fig. 2 shows the typical behaviour of the trajectory before and after the longitudinal displacement of a dipole at injection energy. The required longitudinal displacements of dipoles at injection energy are shown in Fig. 3.

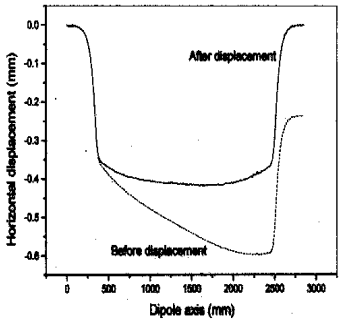

Figure 2: Trajectory before and after longitudinal displacement of dipoles

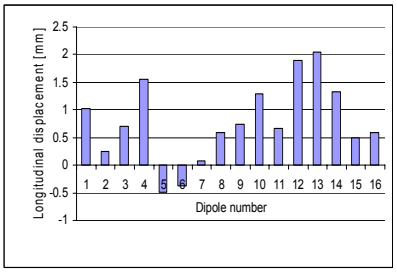

Figure 3: Longitudinal displacements of the of the dipole magnets.

Since the displacement of the trajectory within the dipole is negative (inner side to the nominal trajectory), the total path-length of the ring followed by an electron is shorter than the nominal path-length. As an example, at the injection energy, the path-length is found to be 2.56 mm shorter than the nominal path-length 172.4743 m and is corrected by shifting the dipoles as well as the other magnets in radial direction outward with respect to their reference position. The studies have been carried out at different excitation currents of the dipoles.

4.1.3.2 Sorting of Magnets

The magnet technologies do not produce absolute pure and uniform magnetic fields and there are always deviations from ideal fields. These magnet to magnet field variations and the multipole components produce some unwanted adverse effect on beam dynamical parameters which may degrade the beam quality and even in some cases makes the beam circulation and storage impossible. The disturbing effects of the magnet field errors are unavoidable and can be minimized if these errors are known and if the magnets are placed at the optimized locations. In order to minimize these disturbing effects we define the objective functions which are affected by the errors [7]. The objective function (W) is taken as root mean square of W_i defined by $W_i = \sqrt{A_i^2 + B_i^2}$, where A_i and B_i are constructed at ith observation point. It is known that the dipole errors give rise to a closed orbit distortion (COD). In order to minimize this distortion, the (A, B)-components used in the objective function are defined as $A_i = (\alpha_i x_i + \beta_i x'_i)/\sqrt{\beta_i}$, $B_i = x_i/\sqrt{\beta_i}$ and corresponding Wi is calculated which is known as Courant Snyder invariant. The quadrupole field gradient errors lead to the beating of beta function which in turn leads to change of tune value of the ring. For quadrupole errors, (A, B)-components are defined as $A_i = (\alpha_i \beta_{0i} - \alpha_{0i}\beta_i)/\sqrt{\beta_i \beta_{0i}}$, $B_i = (\beta_i - \beta_{0i})/\sqrt{\beta_i \beta_{0i}}$, where variables with subscript 0 defines undistorted values.

Simulated annealing technique using Metropolis algorithm [8] was applied for this multi-dimensional problem to get a solution close to the global minimum in an acceptable duration. The measured magnet to magnet dipole field errors at 600 MeV, the resulting horizontal closed orbit distortion before and after sorting and effect of sorting at different energy levels are shown in Fig. 4. Similarly, based on the measured magnet to magnet quadrupolar field errors the resulting beta beat before and after

sorting is shown in Fig. 5. By sorting the dipoles and quadrupoles, the closed orbit distortion and the beta beat were reduced to nearly one third of the unsorted values. Finally, the magnets are placed in the ring at the optimized locations [9].

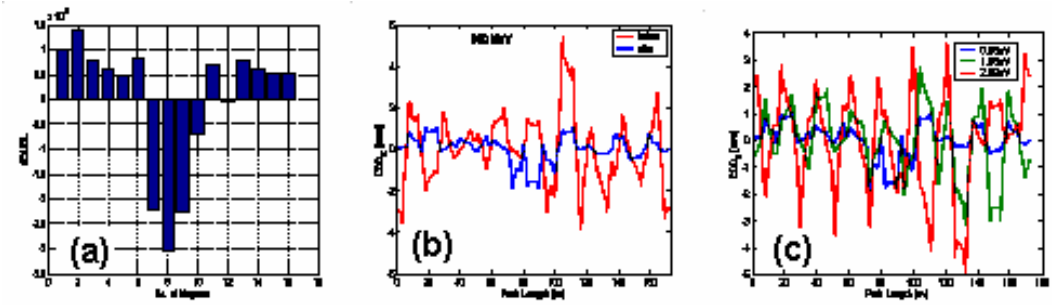

Figure 4: (a): Magnet to magnet field errors in dipoles at 600 MeV; (b): COD before and after sorting the dipole magnets at 600 MeV; (c): COD after sorting at different energy levels

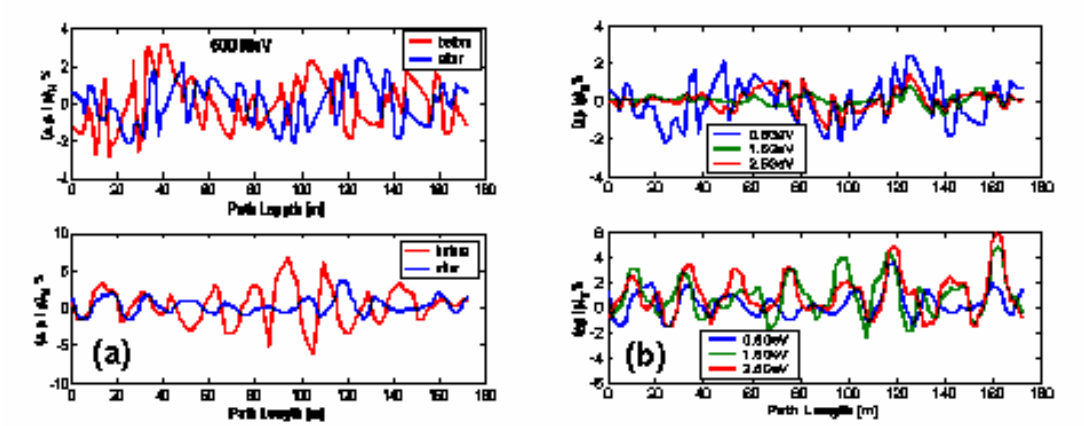

Figure 5: (a): Beta beat before and after sorting the quadrupole magnets at 600 MeV; (b): Beta beat after sorting at different energy levels

4.1.3.3 Nonlinear Beam Dynamics Studies

The tracking studies in presence of all the measured magnetic multipole errors and misalignment errors were done using RACETRACK [10]. The frequency map analysis shows that at design tune (9.3, 5.2), the long term stability is poor and dynamic aperture shrinks rapidly for large number of turns [11]. The simulations were carried out for dynamic aperture at nearby tunes. For this purpose both horizontal and vertical tunes were scanned and for each tune point beam tracking was done for 50 randomly generated machine errors including real measured rms multipole values. In tracking, when linear imperfections, such as quadrupole misalignment, rotation error of the quadrupole, sextupole misalignments were included, the tracking results reveal that during commissioning it might be difficult to operate machine on design optics. Keeping this in view as well as expecting some unforeseen errors during the commissioning, the studies of relaxed (moderate) optics were carried out [12]. These lattices are less prone to misalignment and gradient errors. The studies were carried out for lowering the linear amplification factors of closed obit distortion, beta beat and tune shift due to feed down effects of sextupoles [13].

In addition to linear beam dynamics studies the amplitude dependent tune shifts were derived from canonical perturbation theory considering sextupole field as small perturbations and are expressed as [14]

$$d\nu_x = C_{11} 2J_x + C_{12} 2J_y$$
$$d\nu_y = C_{21} 2J_x + C_{22} 2J_y$$

where $x = \sqrt{(2J_x\beta_x)}\cos(\phi_x)$, $y = \sqrt{(2J_y\beta_y)}\sin(\phi_y)$ and $J_x(J_y)$ denotes the horizontal (vertical) action variables and $\phi_x(\phi_y)$ is the corresponding angle variables. The four coefficients $C_{ij}(i, j = 1,2)$ are expressed in the harmonic expansion. By reducing the $C_{ij}(i, j = 1,2)$ coefficients, the effect of the chromaticity correcting sextupoles is reduced. Based on these studies we found a suitable lattice for the commissioning. In Table 2 the beam parameters of design and moderate optics are listed.

Table 2: Beam parameters at design and moderate optics

Parameters	Design Optics	Moderate Optics
νx, νy	9.3 5.2	9.3 6.2
$X_{co}/\Delta x$, $Y_{co}/\Delta y$	33.41 41.6	36.0 31.4
$\frac{\Delta\beta_x/\beta_x}{\Delta K/K}$, $\frac{\Delta\beta_y/\beta_y}{\Delta K/K}$	24.0 20.8	26.5 14.2
ε@ 2.5 GeV (nm-rad)	58.7	126.
$d\nu_x$	$-75.3x^2 - 315.6y^2$	$-71.7x^2 - 86.1y^2$

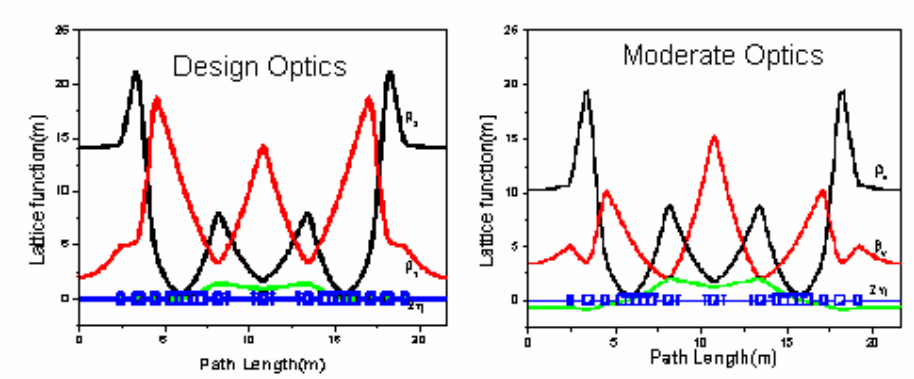

Figure 6: Lattice functions for design and moderate optics

To understand the long term behavior, simulations of beam tracking were done for 200,000 turns. The tracking studies reveal that in the presence of all measured multipole errors and linear imperfections only 2 machines out of 50 random machines are stable at design tune point optics, whereas 47 machines are stable at moderate optics. The lattice functions for two optics are shown in Fig. 6. The dynamic aperture simulation carried

out for on momentum particle for both the lattices with same set of errors for 10,000 turns are shown in Fig. 7.

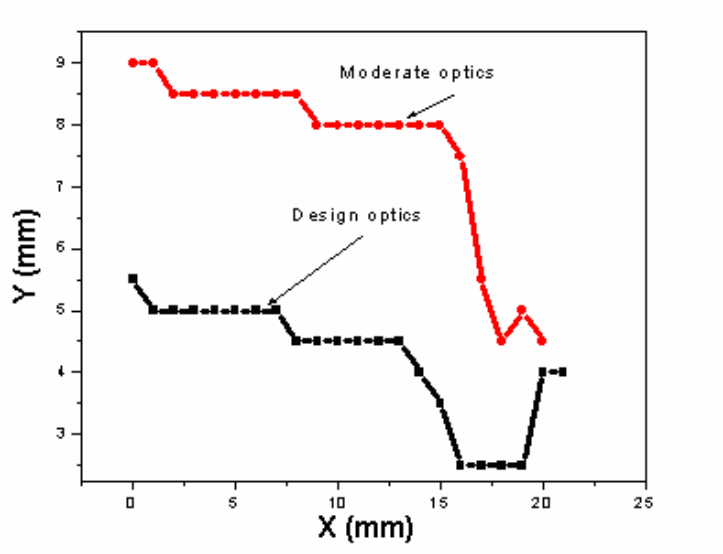

Figure 7: Dynamic aperture for on momentum particle for 10,000 turns

4.1.3.4 Development of GUIs

A graphical user interface (GUI) has been developed for initial commissioning trials and for ramping of the beam energy of the stored beam [15]. For loading optics, 29 magnet power supplies are to be set very precisely. The snapshot of the GUI is shown in Fig. 8. Machine optics is first selected from the off line program and few optics parameters can then be adjusted for the online tuning of the machine. Another GUI is developed for controlling the beam dynamical parameters such as COD, tunes and chromaticities. For orbit correction, this GUI includes various algorithms such as singular value decomposition (SVD), best orbit correctors using SVD, constrained orbit correction, three and four orbit bumps. Efforts are going on to improve the software and add new functionalities for ease in machine operation.

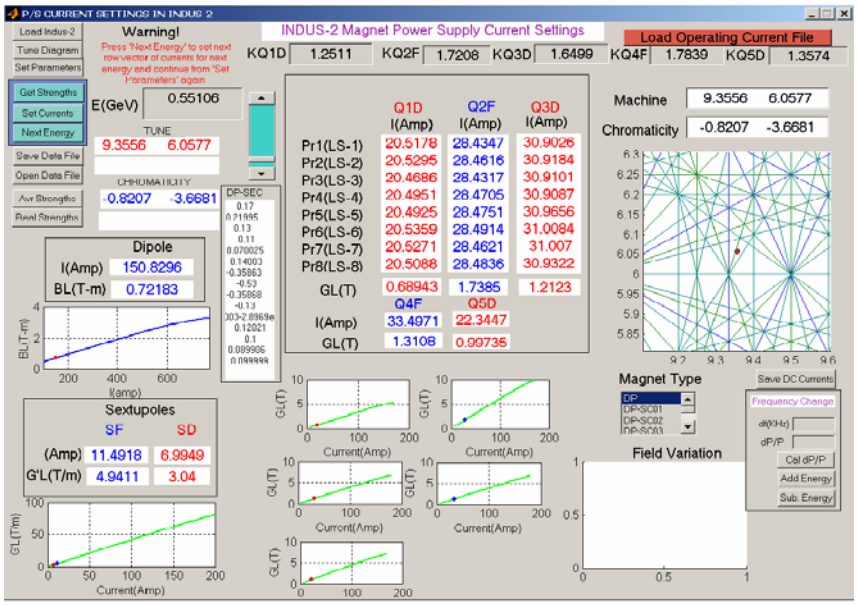

Figure 8: A GUI used for setting of power supplies and for generation of the ramp data

4.1.4 Commissioning of Indus-2

4.1.4.1 Commissioning of TL-3

After installation of all subsystems beam commissioning started. Initial beam transmission trials are carried out at 450 MeV as the synchrotron is routinely delivering the beam to Indus-1 storage ring at this energy. To set the excitation currents of dipole and quadrupole magnets, the measured data has been interpolated employing a cubic spline interpolation technique and magnets are powered corresponding to extracted beam energy 450 MeV from the synchrotron. The beam was successfully transmitted [16] down the line by properly steering or centering the beam on all 8 BPMs using horizontal and vertical steering magnets. The typical estimated beam sizes are shown in Fig. 9. The WCM signals stored on February 23, 2006 are shown in Fig. 10, which shows the good beam transmission through transfer line TL-3.

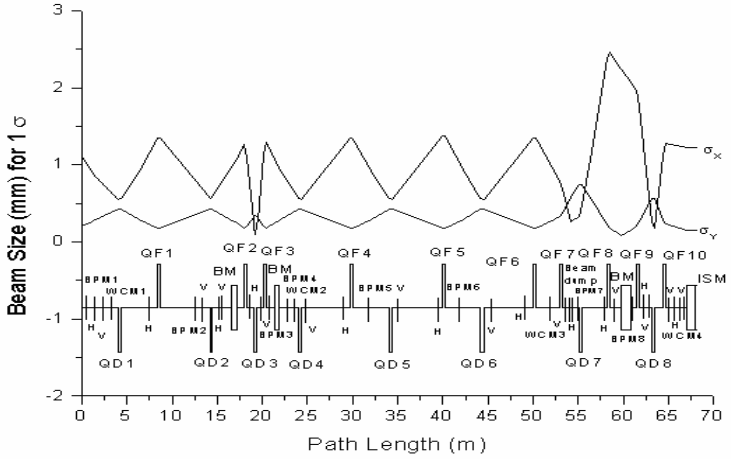

Figure 9: Estimated beam sizes in transfer line TL-3

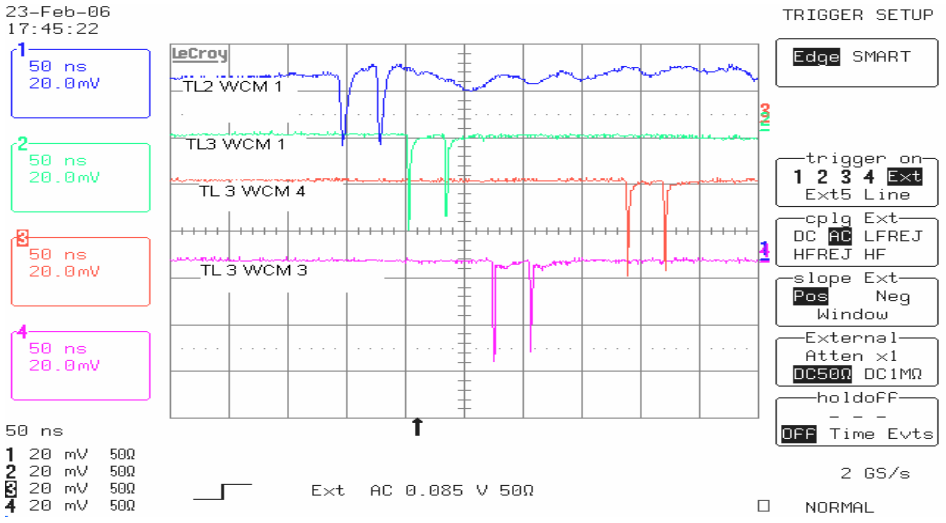

Figure 10: Beam transfer in TL-3; WCM signals TL-3 with respect to signal in TL-2

4.1.4.2 First Turn Circulation

Since the synchrotron routinely delivers the beam to Indus-1 at 450 MeV, initial attempts were made to inject the beam in Indus-2 at this energy. For this, the beam was transported from booster synchrotron to the mouth of injection septum of Indus-2 through TL-3. The first major challenge was to clear the injection septa and to have the beam surviving in the machine for three to four turns. All power supplies in the ring were energized with a proper strengths matching with the synchrotron extracted beam energy. On August 27, 2005, an electron beam was successfully transmitted through both thick and thin septum and seen on beam profile monitor-1 without energizing the kicker power supplies, which were not operational at that time. We observed the beam on all 11 BPMs distributed over the entire ring and the beam positions as well as beam sizes in horizontal and vertical planes were found to be near the expected values calculated from the model. No steering coil was energised during this experiment. In this way beam completed one turn successfully [17]. Subsequently it made four turn circulations in the ring observed on the WCM installed in the 7th short straight section of the ring and its signal is shown in Fig. 11. This has allowed us to complete the very first and important step of beam commissioning. The photographs of the electron beam spot captured at the BPM location in first achromat is shown in Fig. 12.

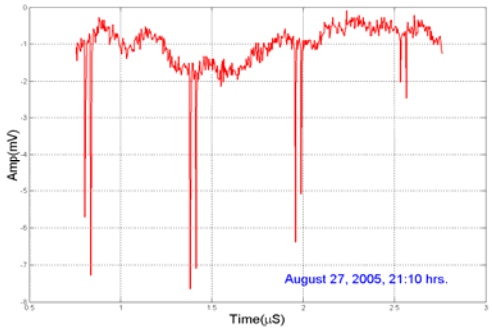

Figure 11: WCM signal showing four turns circulation of electrons at SS-1 BPM

Figure 12: Beam spot taken on 8/27/2005

4.1.4.3 Beam Injection and Accumulation

An injection scheme employing a regulated bump generated by four kickers has been chosen for beam injection to produce required displacement at the septum location. The injection is carried out in the radial plane from the outer side of the ring. Symmetric or asymmetric orbit bump can be used for injection. During beam commissioning, the incoming beam angle is optimized using a GUI developed for regulation of the septa currents such that the injected and stored bunches do not hit the septum magnet or any other part of the vacuum chamber envelope.

The kicker power supplies were ready for operation in November, 2005. By energizing these magnets, one turn beam circulation in ring was achieved on November 22, 2005 with a symmetric bump. On November 28, 2005, beam circulation extending upto 2.1 ms was achieved. On the same day, one RF station was energised with 70 kV peak gap voltage and beam circulation lasting 30 ms was achieved. By optimising the RF cavity gap voltage and its phase, beam circulation up to 200 ms observed and synchrotron light on a synchrotron light monitor was seen. The WCM signal and synchrotron light spot are shown in Fig. 13 and Fig. 14. During this exercise, the synchrotron was operated at the RF frequency of 31.619 MHz. As Indus-2 RF is locked with the synchrotron RF, Indus-2 RF is tuned to 505.904 MHz which is 16 times to that of the synchrotron RF frequency. When Indus-2 RF frequency was changed to its design value i.e. 505.812 MHz, a beam circulation lasting 1 second was obtained.

At 450 MeV beam energy the damping time in horizontal plane is 810 ms, this being comparable to the synchrotron repetition rate, the injected beam oscillations are not fully damped when the next pulse is injected into the ring. So it was decided to inject the beam at higher energy. The energy in synchrotron was then ramped to 550 MeV and the beam at this energy was extracted for injection into Indus-2. At this energy the damping time is 444 ms, therefore, the beam is fully damped when the next pulse arrives after one second. The transmission in transport line TL-2 and TL-3 was once again optimised for this higher beam energy.

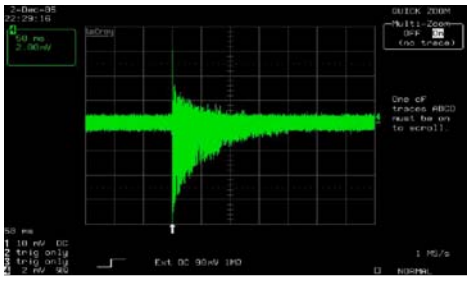

Figure 13: WCM signal indication of survival of the beam upto 200 ms

Figure 14: First synchrotron light observed in of Indus-2

Once the beam was stored for full injection cycle the kickers were adjusted to allow the beam accumulation. At this stage, it was very important to adjust the timing of the kicker pulses. Much time and efforts were spent to ensure that the stored beam traversed kickers at the proper time.

A partial beam loss was observed during initial accumulation trials due to the high value of timing jitter and mismatches between the pulses of the injection kickers. The simulation studies [18] were carried out to understand these effects on the injected and

the stored beam. The beam loss was controlled after reducing the kicker jitter from ±12 ns to ±7 ns. The results of the injection simulation carried out for five turns of injected and stored beams, are shown in Fig. 15 and Fig. 16.

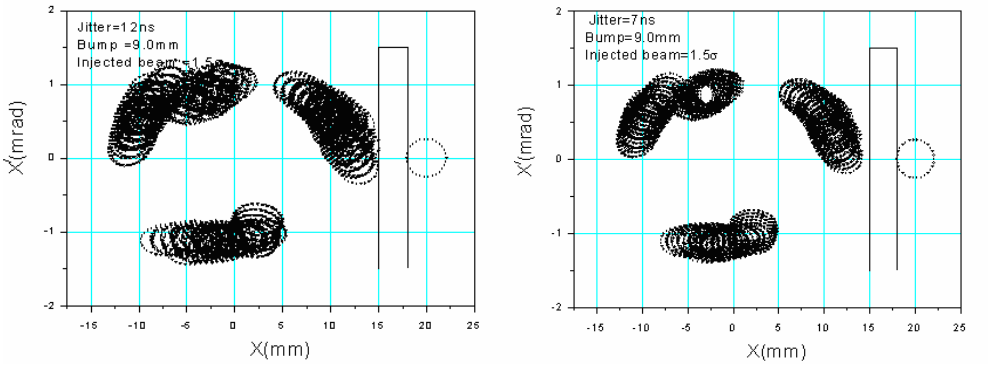

Figure 15: Effect of jitters in timing of kickers on injected beam oscillations

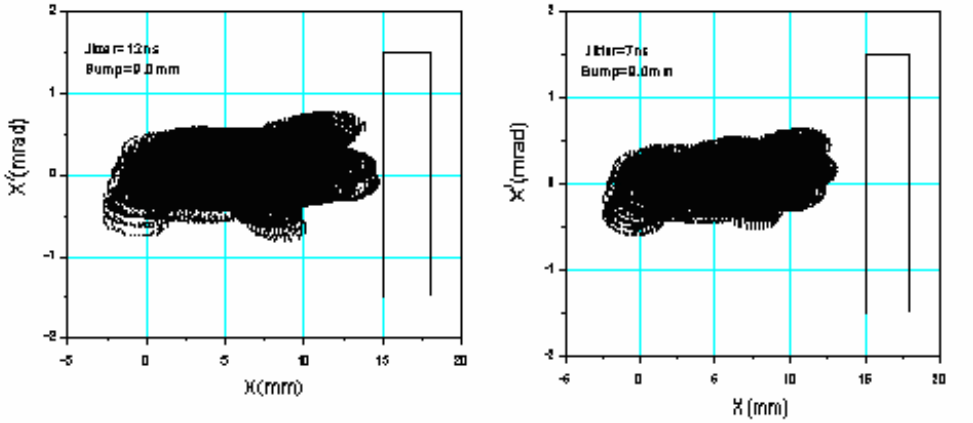

Figure 16: Effect of jitters in timing of kickers on stored beam oscillations

The beam was injected in Indus-2 at design tune (9.3, 5.2), a beam current~2 mA was stored in the ring on February 17, 2006. At this working point, the beam current had reached upto 3.6 mA. The measured lifetime was 8 minutes for 3 mA beam current. The stored current was not increasing further; it was found that at 3.6 mA and at the synchrotron beam current of 1-2 mA, the rate of increase in current was almost equal to the rate of decay. It was decided to operate the ring with the moderate optics which has the tune (9.3,6.2) in May, 2006. So far 38 mA beam current has been stored in the ring and the beam intensity profile recorded using DCCT is shown in Fig. 17.

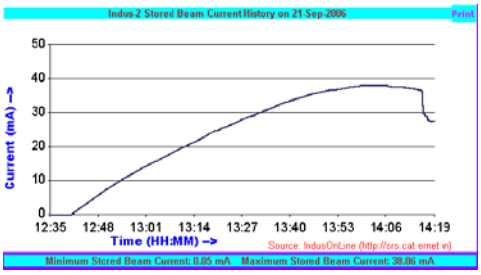

Figure 17: Beam intensity profile with DCCT at injection energy

4.1.4.4 Beam Energy Ramping

The energy ramping can be considered as a process in which the beam energy is increased from the initial energy to final energy in a well defined number of steps by increasing the magnet driving currents in synchronism such that the set tune and chromaticities remain constant. A GUI shown in Fig. 8, has been used for incorporating lattice physics, magnets calibrations and flexible curve fitting to generate necessary magnet power supply waveforms. The dipoles, quadrupoles and sextupoles driven by 1, 26 and 2 power supplies respectively are to be ramped synchronously. The measured dipole current versus magnetic field integral (beam energy) and its first derivative is shown in Fig. 18**.**

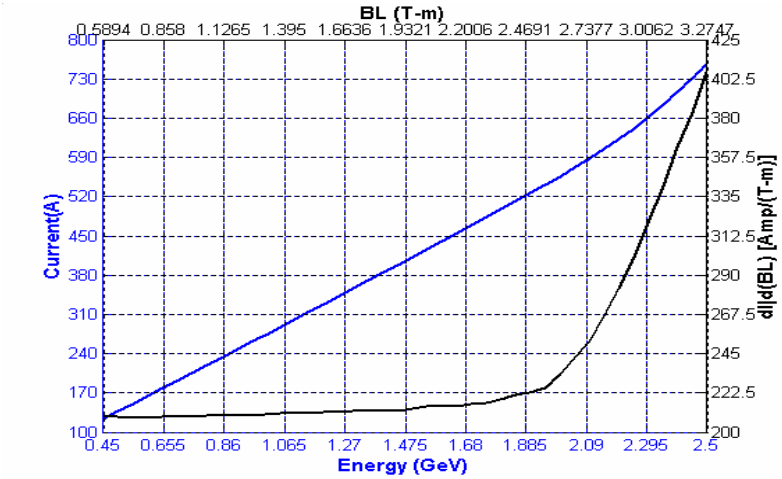

Figure 18: The measured magnetic field integral data of the dipole magnet

It shows that the dipole field integral starts deviating from linearity with respect to the driving current above 1.3 GeV while the quadrupoles and sextupoles almost behave linearly all along the beam energy and this difference in their behaviour may lead to beam loss.

During ramping, the dipole waveform must be synchronized with those of five families of quadrupoles and two families of sextupoles. A look up table for the magnet currents was constructed by interpolating the magnet data using cubic spline interpolation for different energy levels from the injection energy to final energy with coarse steps in linear zone and fine steps in nonlinear zone of the dipole field profile. This table is fed to the hardware, in which the data is further linearly interpolated between every two adjacent energy levels and thus a closely spaced large data set is generated. The ramping speed is decided by the number of data points sent per second which are user defined. On September 13, 2006, in a typical beam energy ramp, 34 mA beam current was accumulated at the beam injection energy and 26 mA beam current remained at 2 GeV [15, 19]. The beam intensity profile during the ramp and stored condition at 2 GeV is shown in Fig. 19. At that time, two RF stations were in operation with gap voltages of 400 kV and 370 kV. The typical time required for ramping beam energy from 550 MeV to 2GeV is 7 minute. Routinely, beam energy ramping is done to 2 GeV. In one of the trials, the beam energy was also ramped to 2.4 GeV.

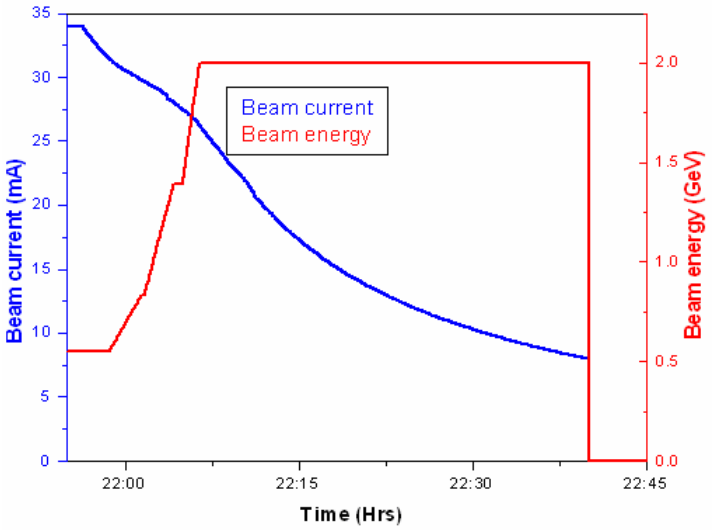

Figure 19: Beam energy ramp to 2GeV on September 13, 2006

4.1.5 Beam Parameter Measurements

4.1.5.1 Closed Orbit Measurement and Correction

56 BPIs are available in the ring for the closed orbit measurement. The closed orbit in horizontal plane has been corrected at the injection energy. In the first trial of orbit correction, out of 48 correctors 16 were identified as the most effective correctors by an SVD of the model response matrix [20]. The uncorrected and corrected closed orbit with these 16 correctors is shown in Fig. 20 .The COD has been reduced from 6.7 mm to 2.8 mm in the first iteration of orbit correction. There is a reduction in the rms, peak to peak and maximum COD values by 58%, 60% and 47% respectively. Further improvement in orbit correction will be tried. The measured closed orbit in vertical plane is shown in Fig. 21. The correction in vertical plane is yet to be tried.

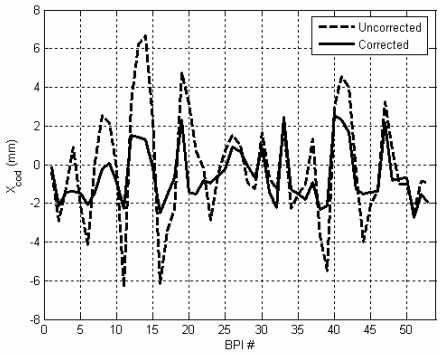

Figure 20: Uncorrected and corrected closed orbit in horizontal plane

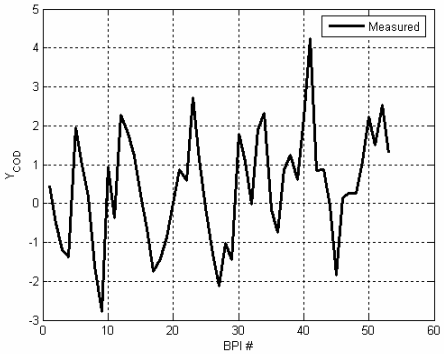

Figure 21: Measured closed orbit in vertical plane

4.1.5.2 Tune measurements

The theoretical betatron tunes estimated by considering magnetic field as per the set current in the magnets and are (9.31, 6.14). The FFT analysis of the measured COD in horizontal and vertical planes is shown in Fig. 22.

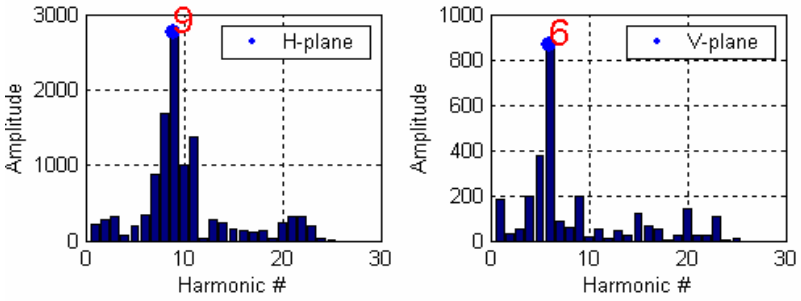

Figure 22: Harmonic contents of the measured COD in horizontal and vertical planes

The larger amplitudes at 9th and 6th harmonics confirm the integer part of the set betatron tune. The fraction part of betatron tune in both transverse planes at the injection energy as well as during ramp was measured on June 16, 2006. The results are summarized in Table 3. The measured tune in horizontal plane is close to the theoretical value, whereas there is a difference in vertical tune of 0.075 at injection energy and by -0.03 at 2 GeV.

Table 3: Measured betatron tunes with beam current at different energy

E(GeV)	I (mA)	νx	νz
0.55	4.3	0.320	0.215
1.0	3.4	0.298	0.135
1.5	2.6	0.303	0.117
2.0	1.7	0.325	0.110

4.1.5.3 Beam Lifetime

The beam lifetime in an electron storage ring is governed by several processes, beam gas scattering from residual gas involving processes such as Bremssstrahlung (inelestic), Coulomb (elastic) from gas nuclei and Touschek effect. Their contributions vary significantly according to the machine operating mode. The dynamic aperture has an important implication for any theoretical estimation of lifetime. Theoretical studies for the overall expected beam lifetime at 550 MeV were carried out assuming a dynamic aperture of 15 mm and 5 mm in horizontal and vertical planes respectively at the injection point for tune point (9.3, 6.2) and all 291 buckets were assumed equally filled for estimation of Touschek lifetime. The electron beam lifetime was measured from the beam current versus time data obtained using a DCCT. The measured lifetime [21] and vacuum pressure variations over the entire ring with the beam current at injection energy are shown in Fig. 23 and Fig. 24.The estimated and measured beam lifetime at 550 MeV are listed in Table 4.

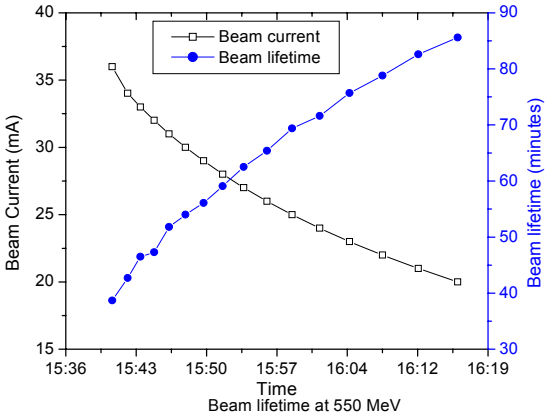

Figure 23: Measured beam lifetime beam at 550 MeV

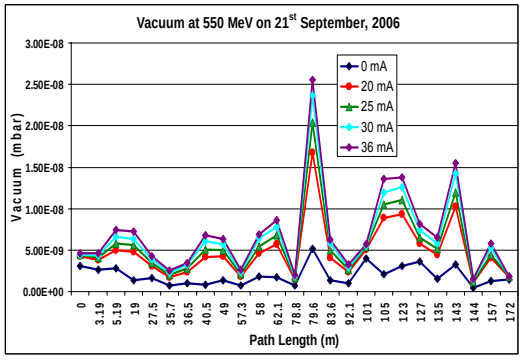

Figure 24: Vacuum for different stored currents at 550 MeV

Table 4: Theoretical and measured beam lifetime at 550 MeV for different stored beam currents

Beam current (mA)	$(\tau_x)_{elastic}$ (hrs)	$(\tau_z)_{elastic}$ (hrs)	$\tau_{inelastic}$ (hrs)	Vacuum lifetime τ_v (hrs)	τ_{tou} (1% coupling) (hrs)	Total τ (1% coupling) (minutes)	Measured lifetime (minutes)
20	5.05	1.70	12.05	1.05	6.88	55	86
25	4.38	1.48	10.48	0.91	6.09	47	69
30	3.87	1.31	9.26	0.81	5.51	43	54
36	3.50	1.19	8.40	0.73	4.99	38	39

The theoretical estimates indicate that the dominant factor in determining the beam lifetime at 550 MeV, is elastic gas scattering that depends on the available aperture and the residual gas pressure throughout the ring. The measured beam lifetime at 2 GeV is shown in Fig. 25 and pressure readings with beam current are shown in Fig. 26. The theoretical estimates of lifetime together with measured one are tabulated in Table 5. The study reveals that here the dominant factor is inelastic gas scattering of electrons with the gas molecules.

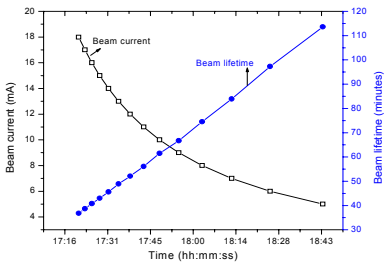

Figure 25: Measured beam lifetime beam at 2 GeV

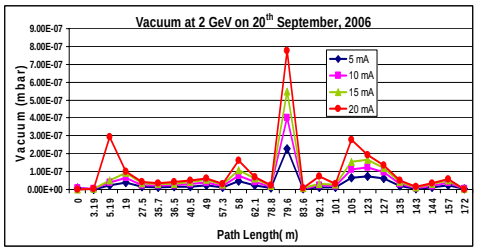

Figure 26: Vacuum for different stored currents at 2 GeV

Table 5: Theoretical and measured beam lifetime at 2 GeV for different stored beam currents

Beam current (mA)	$(\tau_x)_{elastic}$ (hrs)	$(\tau_z)_{elastic}$ (hrs)	$\tau_{inelastic}$ (hrs)	Vacuum lifetime τ_v (hrs)	τ_{tou} (1% coupling) (hrs)	Total τ (1% coupling) (minutes)	Measured lifetime (minutes)
5	12.81	4.59	2.24	0.84	1183	50	113
10	7.67	2.72	1.33	0.50	591	30	61
15	5.73	2.03	0.99	0.37	250	22	43
20	4.04	1.25	0.64	0.24	125	14	38

The discrepancy between theoretical and measured results may be attributed to an uncertainty in finding out the average pressure, as at present the pressures are being monitored at limited locations and also uncertainty in the assumed values of dynamic aperture. Besides, the composition of the gasses is also not included in the calculations.

The accumulated dose of the beam current has reached to 3.0 Ah. Most of the time machine is operated at injection energy level. It seems that at present the beam lifetime is dominated by the vacuum and is limited by the rise in pressure due to the synchrotron radiation induced gas desorption. With the improvement in vacuum, beam lifetime is expected to improve.

4.1.6 Beam Lines

In Indus-2, twenty seven beam lines are proposed for different x-ray applications. One of the beam lines named XRD beam line has been commissioned. For commissioning of this beam line, photon beam was aligned vertically along its design path by generating an angular deflection of about 0.8 mrad in the electron beam path at the center of the dipole magnet (DP-5) from which this line is tapped. With this corrected photon beam position in the beam line, the x-ray diffraction pattern of pyrolytic graphite was obtained.

4.1.7 Conclusion and Future Plans

Indus-2 is presently operated partially for beam physics studies and for further improvements in its performance and partially for the commissioning of the beam lines. So far 38 mA beam current has been stored at the injection energy and 26 mA beam current at 2 GeV. The tune values were measured during the ramp and were found to be closed to the theoretical estimates. The maximum closed orbit distortion has been reduced from 6.7 mm to 2.8 mm in horizontal plane.

Experiments will be carried out soon to increase the beam energy to 2.5 GeV for which, besides increasing the current of the dipoles and quadrupoles to the required values and an accelerating voltage of about 1.5 MV will be required and this voltage will be produced using three or four RF cavities. The orbit correction will be done in both the horizontal and vertical planes as this will also correct the orbit at the points from where the photons beam will be tapped and in addition, this may also improve the injection efficiency. The design optics or another optics providing a low beam emittance will be tried. While doing these studies, detailed studies of lattice parameters will be taken up and experiments will be carried out to optimise the tune point such that

the injection efficiency and beam life time are enhanced. The performance augmentation of the synchrotron is also being tried to provide higher beam currents for injection into Indus-2. Injection and RF parameters will be optimised to increase the stored current in Indus-2. So far, bunch filling pattern is of random nature in Indus-2. Studies will be carried out to achieve bunch filling pattern as per the design of the timing system

4.1.8 Acknowledgement

Authors would like to thank all colleagues involved in the design, construction and installation of Indus-2 for providing full support and for their contributions in the commissioning activities. Authors are grateful to V.C.Sahni, Director RRCAT and S.Kotaiah, Project Manager Indus-2 for their constant guidance and keen involvement in this work.

4.1.9 References

1. G.Singh, G.K.Sahoo, D.Angel, B.Singh, A.D.Ghodke and P.Kant, "Synchrotron radiation source Indus-2", Indian Journal of Applied Physics, Vol. 35, 1 (1997) 183-192.
2. S.Kotaiah et al., "Present status of synchrotron radiation source Indus-2", Proceedings of Indian Particle Accelerator Conference, (2005) 65-68.
3. S.S.Ramamurthi and Gurnam Singh, "Status of the Indus-1 SR source", NIM A, 359(1995) 15-20.
4. D.Angel-Kalinin et al., "Synchrotron radiation source Indus-1", Current Science, Indian Academy of Science, Vol. 82, 3 (2002) 283-290.
5. G. Singh et al., “Status of synchrotron radiation source Indus-1”, Proceedings of Indian Particle Accelerator Conference, (2005) 69-72.
6. Deepak Kumar Vats, Ajay D. Ghodke and G. Singh, "Trajectory calculation for the dipole magnets of Indus-2 storage ring", Proceedings of Indian Particle Accelerator Conference, (2005) 154-155.
7. M.Abo-Bakr & G.Wustfeld, "Sorting of magnets for the BESSY-II booster and storage ring", EPAC (1996) 1341.
8. W.H.Press et al ,"Numerical Recipes in C", Cambridge University Press, Cambridge UK, 2nd Edition, 1992.
9. Riyasat Husain, A.D.Ghodke and Gurnam Singh, “Final placement of the magnets in Indus-2”, CAT Internal Report, CAT\2004-07.
10. A.Wrulich, "RACETRACK; A computer code for the simulation of nonlinear particle motion in accelerators", DESY 84-026 (1984)
11. Ali Akbar Fakhri and Gurnam Singh “Non-linear beam dynamics studies for INDUS-2”, to be published in RRCAT report.
12. Amalendu Sharma, Ajay D. Ghodke and Gurnam Singh, "Relaxed Optics studies for commissioning of Indus-2 ", CAT Internal Report, CAT/2004-05.
13. A.A.Fakhri and Gurnam Singh, "Commissioning optices for Indus-2" to be published in APAC 2007.
14. R.Nagoka et al “Nolinear dynamics with sextupoles in low emittance light source storage ring” NIM A 302 (1991) 9-26.
15. Riyasat Husain, A.D.Ghodke and Gurnam Singh, "Current Setting software for Indus-2", CAT Internal Report, CAT\2005-08.
16. R.S.Sani et al., "Commissioning of transfer line TL-3", CAT Internal Report, CAT\2005-13.

17. V.C.Sahni,"Status of Indus-2", Indian Particle Accelerator Conference, (2006) 1-5.
18. Ali Akbar Fakhri & Gurnam Singh, “Injection optimization for Indus-2” to be published in APAC 2007.
19. Riyasat Husain, A.D.Ghodke and Gurnam Singh, “Beam energy ramping in Indus-2”, to be published in APAC 2007.
20. Riyasat Husain, A.D.Ghodke and Gurnam Singh, "Analysis and Correction of measured COD in Indus-2", to be published in APAC 2007.
21. Pradeep Kumar, Riyasat Husain, A.D.Ghodke and Gurnam Singh, "Beam lifetime in Indus-2", Indian Particle Accelerator Conference, (2006) 217-218.

5 Workshop and Conference Reports

5.1 Report on HB2006 Workshop (the 39th ICFA Advanced Beam Dynamics Workshop on High Intensity, High Brightness Hadron Beams)

Yong Ho Chin, KEK, 1-1 Oho, Tsukuba-shi, Ibaraki-ken, 305-0801, Japan
mail to: yongho.chin@kek.jp

5.1.1 Introduction

The 39th ICFA Advanced Beam Dynamics Workshop on "High Intensity High Brightness Hadron Beams, HB2006" was held at the EPOCAL International Congress Center in Tsukuba City, Japan, near KEK from May 29 to June 2, 2006. This Workshop was co-sponsored by KEK and JAEA (previously JAERI). 135 experts, including 77 from oversees and 58 from Japan, spent pleasant and productive 5 days discussing a wide range of issues associated with high intensity hadron beams. The themes of this workshop follow closely those of the previously held two workshops in the same series: ICFA-HB2002 (April 8-12, 2002 at Fermi-lab, USA) and ICFA-HB2004 (October 18-22, 2004, in Bensheim, Germany). This time, however, since the commissioning of SNS was already started and the construction of J-PARC linac and LHC are nearly completed, more emphasis on J-PARC, SNS and LHC was made as on-going major projects of the hadron machines.

The first and the last days were devoted to the plenary sessions for opening, reviews and working group summaries. The middle three days were dedicated to the working activities. The J-PARC tour was conducted in the afternoon of the last day, which includes the J-PARC linac, RCS, MR and MLF neutron source facility .The subjects of each working group are:

Group A: Beam instabilities and their cures
Group B: Space-charge theory, simulations, and experiments
Group C: Beam diagnostics, collimation, injection / extraction, and targetry
Group D: Beam cooling and intra-beam scattering
Group E: High intensity linacs / Proton drivers

Group F: FFAG and other advanced accelerators and techniques
Group G: Commissioning strategies and procedures

Parallel invited sessions were held in the morning for each topic and were moved to the working sessions for the same topic in the afternoon. The working sessions contained organized discussions as well as contributed papers, which were selected from submitted abstracts by the session conveners. At least 2 hours were dedicated to the discussion time for each topic. About 100 talks were presented all together. Workshop proceedings containing all invited and contributed papers will be published on the JACoW web site, as well as its hard-copies and CD's will be published from KEK.

5.1.2 Plenary Talks

The plenary session of the first day for status and review talks was started with the presentation by Prof. Nagamiya on the J-PARC project. All other talks are:

- Welcome by S. Nagamiya (KEK)
- Approach to a very high intensity beam at J-PARC by Y. Yamazaki (KEK)
- Recent commissioning results of SNS by S. Henderson (ORNL)
- Comparison or survey of proton accelerators for high power applications by B. Weng (BNL)
- Recent progresses on FFAG accelerators by Y. Mori (Kyoto U.)
- ISIS upgrade by D. Findlay (RAL)
- FAIR at GSI by P. Spiller (GSI)
- Upgrade of BNL accelerator facility by A. Ruggiero (BNL)
- Beam intensity upgrade at Fermilab by A. Marchionni (FNAL)
- Status and outlook of high intensity accelerator projects in China by J. Wei (BNL)
- LHC status by R. Schmidt (CERN)
- CARE-HHH activities by F. Zimmermann (CERN)

5.1.3 Working Group Summaries

5.1.3.1 WG A and A+B+D: Beam instabilities and their cures

Convened by A. Burov (FNAL) and F. Zimmerman (CERN)

Most of talks (16 talks) and discussions were centred upon the electron cloud build-up and instabilities.

- There is a growing interest in electron cloud issues in many machines, and a lot of progresses were made in the last few years (PSR e-p feedback, WARP/POSINST self-consistent simulations, HCX experiments, understanding of incoherent e- cloud effects by trapping/scattering & linear instability, KEKB single sideband explained, predictions for future machines).
- But the uncertainty on important surface parameters is still high.

- The electron-cloud is not regarded as limitation for SNS (careful design paid off), and the e-p instabilities are not expected in J-PARC either.
- The electron cloud represents largest "impedance" in many machines.
- The electron cloud is likely a problem for FNAL Main Injector upgrade.
- The main limit for LHC could be electron cloud effects on beam lifetime & emittance rather than the heat load.

5.1.3.2 WG B: Space-Charge Issues

Convened by S. Cousineau (ORNL) and I. Hofmann (GSI)

The highlights of progress (a 10 year perspective) are:

- Simulation codes have made huge progress in terms of modeling real machines. Evident from the now routine success of code benchmarking with experimental data.
- We now place a good deal of faith in the results of our codes, and use them in machine design.
- We are beginning to see benchmarks of real machine beam losses, a "holy grail" of code benchmarking because it relies on high precision modeling, and comprehensive understanding of machine conditions.

The followings may be addressed as remaining challenges:

- We do not yet accurately and reliably predicted experimental beam loss distributions. *Partially due to difficulty in knowing all parameters of the accelerator environment (closed orbit, etc…).*
- We still are not performing self-consistent long-term storage simulations. This is limited by code speed and scalability. Highly scalable codes being developed, but testing against data is sill in progress. Long-term storage simulations will be important for future machines (MR of J-PARC, CERN PS upgrade, FAIR, e-cloud space charge even for LHC, etc…) .
- We still don't have a good handle on simulating, benchmarking, or even knowing the initial beam distribution in linacs. Disproportionately little work has been dedicated to this problem.

5.1.3.3 WG A+B+D: Codes Benchmarking

Convened by I. Hofmann (GSI), E. Shaposhnikova (CERN), F. Zimmermann (CERN) and J. Wei (BNL)

There are four goals of codes benchmarking, namely,

- debugging (code should calculate what is supposed to calculate)
- validation (results should agree with established analytic result for specific cases)
- comparison (two codes should agree if the model is the same)
- verification (code should agree with measurements)

They picked up the following areas to assess the status of the code benchmarking:

- Space charge
- Emittance exchange/Montague resonance; Trapping
- Electron cloud
- Electron build-up; Multi-bunch instability, Single-bunch instability; incoherent effects; self-consistent modeling
- Instability (external impedance)
- Transverse; Longitudinal
- Electron cooling
- Friction force

They found that the space-charge codes in general satisfy the validation and the comparison criteria, but the verification with measurements is poor except the MICROMAP vs. CERN PS, which shows a good agreement. As for the electron build-up, the verification with measurements (ECLOUD vs. SPS and POSINST vs. APS & PSR) scores well. Electron-cloud codes also show relatively good agreements with each other and measurement results as well as in instabilities and incoherent effects categories. There are not many comparison results between different instability codes for external impedance, but some codes show good agreements with measurements such as ORBIT with SNS ring on resistive wall, and kicker impedance or ORBIT vs. PSR and ESME vs. SPS which show good agreements. As for the electron cooling codes, they score very well in all four categories.

5.1.3.4 WG C+G: Beam Diagnostics, Collimation, Injection, Extraction and Targetry

Convened by N. Mokhov (FNAL), M. Tomizawa (KEK), K. Wittenburg (DESY), K. Hasegawa (JAEA), S. Henderson (ORNL) and R. Schmidt (CERN)

They reviewed the recent halo diagnosis and non-destructive beam profile monitoring, beam diagnosis system, detectors and BLM (Beam Loss Mechanizm) system. They also reviewed the collimation and targetry systems of various machines. They addressed the issues of beam accidents and beam-induced damages. They found that all accidents that happened were anlysed in a very detailed way and the causes and consequences are well understood (lot of work). Many weak points were identified (NOT related to the accident) the beam diagnostics system and were fixed. Fast detection of failures is clearly required, in the order of a few turns (the order of ms is not fast enough). Machine protection issues were very much discussed and were issues of common interest for many. They concluded that tools for data recording and analysis are vital (“post mortem”)

5.1.3.5 WG C+G: Accidents, Losses and Commissioning

Many talks on the commissioning strategies and procedures were presented for various machines and the beam accidents that happened in some machines or are worried to happen in coming machines were reported. Discussion were centered upon MPS (Machine Protection System) and commissioning. Main issues were:

- Protection versus Flexibility in early commissioning
- Configuration control of MPS parameters, BLM thresholds
- Bypass capabilities and bypass procedures

- Control of critical parameters (magnet set-points, etc.)
- LHC has stringent requirements on MPS performance very early in commissioning

They also discussed on the online modeling capabilities, essential for rapid beam commissioning progress. The importance of "pre-beam" testing and "dry-runs" of diagnostics systems, applications software, and magnet controls, etc was addressed.

5.1.3.6 WG D: Beam cooling and intra-beam scattering

Convened by A. Fedotov (BNL), I. Meshkov (Dubna) and J. Wei (BNL)

The experimental observation and progresses in the theoretical and computational calculations were presented. They found that surprisingly there are a lot of new and very exciting developments in the (by now mature) field of beam cooling. The "old" applications are being extended, often in an ingenious and sometimes surprising way and new one are coming up. The "cooling business" is very fast and actively developing activity in accelerator technology and beam dynamics.

5.1.3.7 WG E: High intensity linacs / Proton drivers

Convened by R. Garoby (CERN) and B. Weng (BNL)

They found that many new linacs are under design and may be constructed in the near future. The design procedures are well-defined and followed by all of them The error analysis and simulation study of beam dynamics are reliable enough to predict accelerator performance. The degree of maturity of synchrotron design is comparable to that of the linac, but that of FFAG still needs improvements.

The main theme of discussion in Group E was the comparative assessment of the different types of proton drivers: The results can be summarized as the following table:

Table 1: Comparative assessment of the different types of proton drivers.

	LINAC	LINAC + Rings	RCS	CYCLOTRON	FFAG
	CW	Pulsed	Pulsed	CW	CW & pulsed
Status of development	Mature technology	Mature technology	Proven technology	Proven technology	Needs more demonstration
Selling point	Reliability, power efficiency	Flexibility, upgradeability	Proven technology	Cost, reliability, power efficiency	Cost
Pending issues…	How to reduce construction cost ?	Need to study / demonstrate the generation of short bunches	Would benefit from high gradient tunable RF	Possibility to exceed 10 MW?	Design issues for machine and components

5.1.3.8 WG F: FFAG and other advanced accelerators and techniques

Convened by W. Chou (FNAL), S. Koscielniak (TRIUMF) and Y. Mori (Kyoto U.)

They have reviewed the recent progresses on FFAG and other advanced accelerators and technologies and categorized these technologies depending on their maturity. Table 2 shows how mature these technologies are and where their developments are under way:

Table 2: List of advanced accelerator technology hardware R&D and their maturity (Mature=available today, Advanced=available soon, Very advanced=distant horizon).

Technology	Institution
FFAG scaling (Mature)	KEK; Osaka U. (PRISM); Kyoto U.; CEA/Saclay, Kyushu U. (ADS)
FFAG non-scaling (Advanced)	UK (EMMA), Tech-X in US BNL, Electron Energy Corp.; RADIAbeam (LA)
Induction acceleration (Advanced)	KEK
Slip stacking (Mature)	Fermilab
Barrier rf (Advanced)	Fermilab; J-PARC
High intensity short pulse Laser for hadron acceleration	CNRS/LULI; Osaka U.; Livermore; LANL; RAL; Max Planck Inst; Max Born Inst. U. of Nevada; General Atomic; Rochester U.; GSI ;CEA/Bordeaux; JAEA; IENA U., Germany; Imperial College, London; Michigan U.; Etc.
Direct Plasma injection (Mature-almost)	ITEP, Russia; RIKEN, BNL
HEDP, WDM	VNL (PPPL, LBL,LLNL) GSI, ITEP, Russia;IPN, Orsay
SC pulsed magnet (Mature)	GSI; IHEP, JINR (Russia); BNL; CERN; INFN; CEA-Saclay
SC spoke cavity (Mature)	ANL; LANL; IPN-Orsay; Fermilab; Julich
Laser stripping (Advanced)	KEK-BNL;SNS
Adv Cusp ion source	VECC, India; RIKEN, etc

5.1.4 Conclusions

The workshop was concluded with good outcomes and fruitful discussions. It also provided good opportunities for collaboration meetings between labs, which will enrich the hadron community further. During the workshop, the program committee meeting was held to discuss whether and where we will have the next HB workshop,

and it was decided formally that ORNL will host the next HB workshop (HB2008) in 2008.

More information on the HB2006 workshop can be obtained from the workshop home page at http://hb2006.kek.jp/

6 Recent Doctorial Theses

6.1 Beam Halo in High-Intensity Hadron Linacs

Frank Gerigk, CERN, Geneva, Switzerland
mail to: frank.gerigk@cern.ch

Name: Frank Gerigk
University: Technische Universität Berlin, Department of Electrical Engineering
Affiliation: CERN, AB-RF Group
Thesis Title: Beam Halo in High-Intensity Hadron Machines
Graduation date: December, 21st, 2006
Supervisors: Prof. Heino Henke and Prof. Ingo Hofmann

Abstract:

This document aims to cover the most relevant mechanisms for the development of beam halo in high-intensity hadron linacs. The introduction will outline the various applications of high-intensity linacs and it will explain why, in the case of the CERN Superconducting Proton Linac (SPL) study a linac was chosen to provide a high-power beam, rather than a different kind of accelerator. The basic equations, needed for the understanding of halo development will be derived and employed to study the effects of initial and distributed mismatch on high-current beams. The basic concepts of the particle-core model, envelope modes, parametric resonances, the free-energy approach, and the idea of core-core resonances will be introduced and extended to study beams in realistic linac lattices. The approach taken is to study the behavior of beams not only in simplified theoretical focusing structures but to highlight the beam dynamics in realistic accelerators. All effects which are described and derived with simplified analytic models are tested in realistic lattices and are thus related to observable effects in linear accelerators. This approach involves the use of high-performance particle tracking codes, which are needed to simulate the behavior of the outermost particles in distributions of up to 100 million macro particles. In the end a set of design rules will be established and their impact on the design of a typical high-intensity machine, the CERN SPL, will be shown. The examples given in this document mainly refer to two different design evolutions of the SPL study: the first conceptual design report (SPL I) and the second conceptual design report (SPL II).

6.2 Measurement-Based Modeling of Error-Induced Beam Degradations in Fermilab's Accelerators

Phil S. Yoon, Fermilab, Batavia, IL 60510, U.S.A.
mail to: syoon@fnal.gov

Name: Phil S. Yoon
University: University of Rochester
Affiliation: Fermilab, Accelerator Division
Thesis Title: Measurement-Based Modeling of Error-Induced Beam Degradations in Fermilab's Accelerators
Graduation date: February 2007
Supervisor 1: Prof. Arie Bodek, University of Rochester, Rochester NY, U.S.A.
Supervisor 2: Dr. Weiren Chou, Fermilab

Abstract:

In Part I, two independent models are constructed for Fermilab's Booster synchrotron at injection energy.

The first model is a stochastic model. The Ornstein-Uhlenbeck stochastic noise is incorporated into the existing ORBIT-FNAL simulation package. Then, the current ripples and common-mode voltages measured directly from each of four Gradient Magnet Power Supplies (GMPS) are Fourier-analyzed. Based upon the frequency spectra of real noise, the O-U noise model is tuned up, so that the frequency spectra are closely matched between the modelled stochastic noise and real noise. The realistic stochastic noise is then applied to the Booster beam in the presence of the 2.5-D space-charge effects. This modelling, accompanied with a suite of beam diagnostic calculations, manifests that the stochastic noise, impinging upon the beam and coupled to the space-charge effects, can strongly enhance the beam degradation – such as emittance growth and halo formation – during the injection period.

The second model is an alignment model. Employing the latest beamline survey data taken in year 2005, magnet-by-magnet alignment errors of all types – station error, pitch, yaw, roll, twists, etc. – are implemented in the model. The ORBIT-FNAL simulations with the alignment model show that rolled magnets, with 2.5-D space-charge effects included, have noticeable effects on the Booster beam.

In Part II, utilizing the Fermilab's 1-dimensional code ESME, the method of RF-stacking of proton beams is investigated. When the Run2 collider program at Fermilab is terminated in year 2009, the present antiproton source can be available for other purposes. One possible application is to convert the antiproton accumulator to a proton accumulator, so that the beam power from the Main Injector could be greatly enhanced. Given the momentum acceptance available for the Accumulator, the ESME simulation demonstrates that the momentum-stacking of proton beams is attainable with minimum emittance dilution due to the longitudinal space-charge effect.

7 Forthcoming Beam Dynamics Events

7.1 International Workshop on Electron-Cloud Effects "ECLOUD07"

K. Ohmi, National High Energy Accelerator Organization (KEK), Japan
E.S. Kim, Kyungpook National University, Korea
mail to: ohmi@post.kek.jp

Workshop Home page: http://chep.knu.ac.kr/ecloud07
Workshop Contact: ecloud@knu.ac.kr

The International Workshop on Electron-Cloud Effects will be held 9-12 April 2007 at Interburgo Hotel in Deagu, Korea. This workshop will review the experimental and theoretical progress on the electron cloud effect (ECE) since ECLOUD04 workshop, including simulation, analytic theory, surface science, beam observations, mitigation techniques and so on. The workshop will also include ion effects and the incoherent effect of the beam-beam and space charge interaction since they are closely related to the ECE in view of the two-stream interaction.

International Program Committee
Y. Cai (SLAC) W. Chou (FNAL) W. Fischer (BNL) M. Furman (LBNL)
Z. Y. Guo (IHEP) K. Harkay (ANL) S. Henderson (SNS)
R. Macek (LANL) B. Palmer (Cornell) D. Son (KNU)
E. Perevedentsev (BINP) M. Pivi (SLAC) Hong Qin (Princeton)
T. Toyama (J-PARC) R. Wanzenberg (DESY) J. Wei (IHEP, BNL)
A. Wolski(Liverpool) S. Y. Zhang (BNL) F. Zimmermann (CERN)
M. Zobov (LNFN)

Local Organization Committee
Eun San Kim, KNU
He Young Kim (Admin.), KNU
Jung Yun Huang, PAL
Hyoung Suk Kim, KNU
Guinyun Kim, KNU
Hitoshi Fukuma, KEK
Kazuhito Ohmi, KEK

7.2 Beam Dynamics Workshop on Energy Recovery Linacs "ERL07"

Date: May 21-25, 2007
Place: Daresbury Laboratory

The next Beam Dynamics Workshop on Energy Recovery Linacs "ERL07" will be held at the Cockcroft Institute, Daresbury Laboratory, Warrington, UK, from May 21-25, 2007. This follows the successful inaugural Workshop on this topic in March 2005 at Thomas Jefferson Laboratory.

This Workshop is sponsored by ASTeC, the CCLRC Accelerator Centre; Cockcroft Institute; John Adams Institute; Jefferson Laboratory; Brookhaven National Laboratory; Cornell University; ICFA and e2v Ltd. It will address fundamental challenges related to the generation of high brightness and simultaneously high average current electron beams, and its stability and quality preservation during acceleration and energy recovery. Specifically, the Workshop will focus on:

- Design and development of high average current, low emittance, polarized and unpolarized photoinjectors
- Optimized lattice design and start-to-end simulation
- Beam stability and multibunch, multipass instabilities
- Beam halo formation and control of beam loss
- Superconducting RF system optimization for CW, high-current applications
- Higher order mode damping and efficient extraction of higher order mode power
- RF control and stability under the maximum practical Q_L
- Synchronization challenges
- Latest cryogenics techniques
- High current diagnostic and instrumentation techniques.

The program consists of an opening and a closing plenary session and parallel Working Group sessions including the following topics:

1. Electron guns and injector designs
2. Optics and beam transport
3. Superconducting RF and RF system control
4. Synchronization and diagnostics/instrumentation.

The deadline for advanced registration is March 31, 2007. The detailed programme is being finalised and we will be encouraging the submission of contributed papers for the Working Group sessions. Proceedings will be published for both invited and contributed papers. For further information and registration, please visit (end 01/07):

http://www.erl07.dl.ac.uk

Contact: Mike Poole (M.W.Poole@dl.ac.uk) and Susan Smith (S.L.Smith@dl.ac.uk)

8 Announcements of the Beam Dynamics Panel

8.1 ICFA Beam Dynamics Newsletter

8.1.1 Aim of the Newsletter

The ICFA Beam Dynamics Newsletter is intended as a channel for describing unsolved problems and highlighting important ongoing works, and not as a substitute for journal articles and conference proceedings that usually describe completed work. It is published by the ICFA Beam Dynamics Panel, one of whose missions is to encourage international collaboration in beam dynamics.

Normally it is published every April, August and December. The deadlines are 15 March, 15 July and 15 November, respectively.

8.1.2 Categories of Articles

The categories of articles in the newsletter are the following:

1. Announcements from the panel.
2. Reports of beam dynamics activity of a group.
3. Reports on workshops, meetings and other events related to beam dynamics.
4. Announcements of future beam dynamics-related international workshops and meetings.
5. Those who want to use newsletter to announce their workshops are welcome to do so. Articles should typically fit within half a page and include descriptions of the subject, date, place, Web site and other contact information.
6. Review of beam dynamics problems: This is a place to bring attention to unsolved problems and should not be used to report completed work. Clear and short highlights on the problem are encouraged.
7. Letters to the editor: a forum open to everyone. Anybody can express his/her opinion on the beam dynamics and related activities, by sending it to one of the editors. The editors reserve the right to reject contributions they judge to be inappropriate, although they have rarely had cause to do so.
8. Editorial.

The editors may request an article following a recommendation by panel members. However anyone who wishes to submit an article is strongly encouraged to contact any Beam Dynamics Panel member before starting to write.

8.1.3 How to Prepare a Manuscript

Before starting to write, authors should download the template in Microsoft Word format from the Beam Dynamics Panel web site:

http://www-bd.fnal.gov/icfabd/news.html

It will be much easier to guarantee acceptance of the article if the template is used and the instructions included in it are respected. The template and instructions are expected to evolve with time so please make sure always to use the latest versions.

The final Microsoft Word file should be sent to one of the editors, preferably the issue editor, by email.

The editors regret that LaTeX files can no longer be accepted: a majority of contributors now prefer Word and we simply do not have the resources to make the conversions that would be needed. Contributions received in LaTeX will now be returned to the authors for re-formatting.

In cases where an article is composed entirely of straightforward prose (no equations, figures, tables, special symbols, etc.) contributions received in the form of plain text files may be accepted at the discretion of the issue editor.

Each article should include the title, authors' names, affiliations and e-mail addresses.

8.1.4 Distribution

A complete archive of issues of this newsletter from 1995 to the latest issue is available at

http://icfa-usa.jlab.org/archive/newsletter.shtml

This is now intended as the primary method of distribution of the newsletter.

Readers are encouraged to sign-up for electronic mailing list to ensure that they will hear immediately when a new issue is published.

The Panel's Web site provides access to the Newsletters, information about future and past workshops, and other information useful to accelerator physicists. There are links to pages of information of local interest for each of the three ICFA areas.

Printed copies of the ICFA Beam Dynamics Newsletters are also distributed (generally some time after the Web edition appears) through the following distributors:

Weiren Chou	chou@fnal.gov	North and South Americas
Rainer Wanzenberg	rainer.wanzenberg@desy.de	Europe* and Africa
Susumu Kamada	Susumu.Kamada@kek.jp	Asia** and Pacific

* Including former Soviet Union.

** For Mainland China, Jiuqing Wang (wangjq@mail.ihep.ac.cn) takes care of the distribution with Ms. Su Ping, Secretariat of PASC, P.O. Box 918, Beijing 100049, China.

To keep costs down (remember that the Panel has no budget of its own) readers are encouraged to use the Web as much as possible. In particular, if you receive a paper copy that you no longer require, please inform the appropriate distributor.

8.1.5 Regular Correspondents

The Beam Dynamics Newsletter particularly encourages contributions from smaller institutions and countries where the accelerator physics community is small. Since it is

impossible for the editors and panel members to survey all beam dynamics activity worldwide, we have some Regular Correspondents. They are expected to find interesting activities and appropriate persons to report them and/or report them by themselves. We hope that we will have a "compact and complete" list covering all over the world eventually. The present Regular Correspondents are as follows:

Liu Lin	liu@ns.lnls.br	LNLS, Brazil
S. Krishnagopal	skrishna@cat.ernet.in	RRCAT, India
Sameen Ahmed Khan	rohelakhan@yahoo.com	SCOT, Middle East and Africa

We are calling for more volunteers as *Regular Correspondents*.

8.2 ICFA Beam Dynamics Panel Members

Caterina Biscari	caterina.biscari@lnf.infn.it	LNF-INFN, Via E. Fermi 40, C.P. 13, Frascati, Italy
Yunhai Cai	yunhai@slac.stanford.edu	SLAC, 2575 Sand Hill Road, MS 26 Menlo Park, CA 94025, U.S.A.
Swapan Chattopadhyay	swapan@jlab.org	Jefferson Lab, 12000 Jefferson Avenue, Newport News, VA 23606, U.S.A.
Weiren Chou (Chair)	chou@fnal.gov	Fermilab, MS 220, P.O. Box 500, Batavia, IL 60510, U.S.A.
Yoshihiro Funakoshi	yoshihiro.funakoshi@kek.jp	KEK, 1-1 Oho, Tsukuba-shi, Ibaraki-ken, 305-0801, Japan
Miguel Furman	mafurman@lbl.gov	LBL, Building 71, R0259, 1 Cyclotron Road, Berkeley, CA 94720-8211, U.S.A.
Jie Gao	gaoj@ihep.ac.cn.	Institute for High Energy Physics, P.O. Box 918, Beijing 100039, China
Ajay Ghodke	ghodke@cat.ernet.in	RRCAT, ADL Bldg, Indore, Madhya Pradesh, India 452 013
Ingo Hofmann	i.hofmann@gsi.de	GSI, Darmstadt, Planckstr. 1, 64291 Darmstadt, Germany
Sergei Ivanov	ivanov_s@mx.ihep.su	IHEP, Protvino, Moscow Region, 142281 Russia
Kwang-Je Kim	kwangje@aps.anl.gov	Argonne Nat'l Lab, 9700 S. Cass Ave,, Bldg 401, Argonne, IL 60439, U.S.A.
In Soo Ko	isko@postech.ac.kr	Pohang Accelerator Lab, San 31, Hyoja- Dong, Pohang 790-784, South Korea
Alessandra Lombardi	Alessandra.Lombardi@cern.ch	CERN, CH-1211, Geneva 23, Switzerland
Yoshiharu Mori	mori@kl.rri.kyoto-u.ac.jp	Research Reactor Inst., Kyoto Univ. Kumatori, Osaka, 590-0494, Japan
Chris Prior	c.r.prior@rl.ac.uk	ASTeC, Rutherford Appleton Lab, Chilton, Didcot, Oxon OX11 0QX, U.K.
David Rice	dhr1@cornell.edu	Cornell Univ., 271 Wilson Laboratory, Ithaca, NY 14853-8001, U.S.A.
Yuri Shatunov	Yu.M.Shatunov@inp.nsk.su	Acad. Lavrentiev, prospect 11, 630090 Novosibirsk, Russia
Junji Urakawa	junji.urakawa@kek.jp	KEK, 1-1 Oho, Tsukuba-shi, Ibaraki-ken, 305-0801, Japan
Jiuqing Wang	wangjq@mail.ihep.ac.cn	Institute for High Energy Physics, P.O. Box 918, 9-1, Beijing 100039, China
Rainer Wanzenberg	Rainer.wanzenberg@desy.de	DESY, Notkestrasse 85, 22603 Hamburg, Germany
Jie Wei	wei1@bnl.gov	BNL, Bldg. 911, Upton, NY 11973- 5000, U.S.A.